Aus dem Comprehensive Pneumology Center
Institut für Experimentelle Pneumologie der Ludwig-Maximilians-Universität München
und des Helmholtz Zentrums München
Kommissarische Leitung: Dr. rer. nat. Antje Brand
Ehemaliger Direktor: Prof. Dr. med. Oliver Eickelberg
&
Kinderklinik und Kinderpoliklinik des Dr. von Haunerschen Kinderspitals
Ludwig-Maximilians-Universität München
Direktor: Prof. Dr. med. Dr. sci. nat. Christoph Klein

MicroRNA profiling of purified alveolar epithelial type II cells from normal mice

Dissertation
zum Erwerb des Doktorgrades der Medizin
an der Medizinischen Fakultät der
Ludwig-Maximilians-Universität zu München

vorgelegt von
Katharina Julia Singer
aus
München

2018

Mit Genehmigung der Medizinischen Fakultät der

Universität München

Berichterstatterin:	Prof. Dr. med. Susanne Krauss-Etschmann
Mitberichterstatter:	PD Dr. med. Torsten Olszak
	Prof. Dr. med. Andrea Koch
Mitbetreuung durch den promovierten Mitarbeiter:	Dr. rer. nat. Stefan Dehmel
Dekan:	Prof. Dr. med. dent. Reinhard Hickel
Tag der mündlichen Prüfung:	05.07.2018

Für meine Familie

TABLE OF CONTENTS

LIST OF FIGURES

LIST OF TABLES

1 INTRODUCTION

1.1 Alveolar epithelial type II cells

1.1.1 The alveolus

Alveoli are the terminal ends of the respiratory tree and cover a surface of around 70 m^2 (Aumüller et al. 2007). The two major functions of the alveoli are gas exchange and defense against inhaled microorganisms and particles (Mason 2006). Different cell types contribute to this work: these are alveolar epithelial type I (ATI) cells, alveolar epithelial type II (ATII) cells as well as alveolar macrophages on the alveolar side and endothelial cells on the blood side.

ATI and ATII cells differ greatly in their number, morphology and function. ATI cells are thin, squamous cells with fine cytoplasmic extensions. ATI cells constitute only 8% of all lung cells, but account for 93% of the alveolar epithelial surface area in human lungs (Crapo et al. 1982). A fused basement membrane between ATI cells and endothelial cells provides the gas-blood-barrier for gas exchange. ATII cells are cuboidal and smaller in size than ATI cells. They account for 16% of all lung cells. However, only 7% of the alveolar surface area is covered by this cell type (Crapo et al. 1982). Multiple functions have been attributed to ATII cells (as described in 1.1.2).

1.1.2 ATII functions

The wide variety of ATII cell functions early coined the term “defender of the alveolus” (Figure 1) (Mason & Williams 1977) .

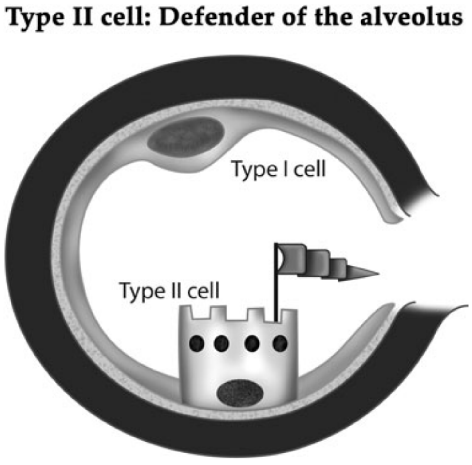

Figure 1. ATII cell as the defender of the alveolus. ATI cells comprise most of the alveolar surface and are responsible for gas exchange. ATII cells are small, cuboidal cells that secure alveolar homeostasis by surfactant production, regulation of immune response, salt and water transport and regeneration into ATI cells upon injury (Mason 2006).

The most studied function of ATII cells is the production of lung surfactant. Surfactant is composed of ~ 90% lipids, mainly phospholipids, and ~ 10% proteins, including the surfactant proteins (SP) SP-A, SP-B, SP-C and SP-D (reviewed in (Griese 1999)). SP-B and SP-C are small hydrophobic proteins, which accelerate the spreading of surfactant phospholipids on the alveolar surface. The hydrophobic monolayer reduces surface tension, thus, preventing alveolar collapse. This is essential for effective gas exchange (Mason 2006).

SP-A and SP-D are large hydrophilic lectins involved in innate host defense. Both proteins can stimulate or suppress the inflammatory response of the lung (Gaunsbaek et al. 2013; Giannoni et al. 2006; Kantyka et al. 2013; Ariki et al. 2012). To further support the immune response, ATII cells secrete additional antimicrobial proteins, transport immunoglobulins to the alveolar surface and produce components of the complement system (Mason 2006).

Apical epithelial sodium channels (ENaCs) and basolateral sodium/potassium adenosine triphosphatase (ATPase) enable transepithelial transport of sodium from the alveolus into the interstitium. By this fine modulation of salt and water transport, ATII cells secure optimal gas exchange (Eaton et al. 2004).

ATII cells have the potential to transform into other cell types. This can be essential for lung repair, but also enhances a risk to develop lung diseases when dysregulated (as described in 1.3.2, page 10). During lung injury, ATII cells have the capability to restore alveolar epithelial cells. Early studies gave evidence that ATII cells were capable of proliferating and differentiating into ATI cells (Evans et al. 1975). Morphologic changes were characterized by an increased surface area, thin cytoplasmic extensions and protruding nuclei (Cheek et al. 1989). Biochemical changes included a decreased expression of SP-C (Fuchs et al. 2003; Demaio et al. 2009) and upregulation of the ATI-expressed proteins caveolin-1 (Fuchs et al. 2003) and T1α (Borok et al. 1998). Recently, lineage tracing studies showed that SP-C^{positive} ATII cells gave rise to ATI cells (Rock et al. 2011), but also replaced ATII cells (Barkauskas et al. 2013). These findings suggest that ATII cells function as stem cells of the alveolar epithelium (Fehrenbach 2001).

The diverse functions of ATII cells illustrate the important role of this cell type in the maintenance of alveolar homeostasis, but also emphasize that injury, loss or dysregulation of ATII cells may result in a pathologic state of the lung.

1.2 MicroRNAs

1.2.1 Small RNAs

Small ribonucleic acids (RNAs) are a subgroup of non-coding RNAs (ncRNAs). NcRNAs are RNAs which are not translated into protein. For a long time, the best-known function of ncRNAs was to support the information transfer from gene to protein. For instance, transfer RNA (tRNA) and ribosomal RNA (rRNA) are involved in translation, small nuclear RNAs (snRNAs) in splicing and small nucleolar RNAs (snoRNAs) in chemical modification of other RNAs (Mattick & Makunin 2006). However, with the discovery of small RNAs an entirely new role of ncRNAs was elucidated.

Small RNAs are RNAs of ~ 20-30 nucleotides (nt) in length and operate together with associated Argonaute (Ago) proteins. By their biogenesis, function and associated Ago protein, they were divided into three main classes: microRNAs (miRNAs), small interfering RNAs (siRNAs) and piwi-interacting RNAs (piRNAs) (V. N. Kim et al. 2009).

The best-characterized class is miRNAs. The first two miRNAs, lin-4 and let-7, were detected in Caenorhabditis elegans as small temporal RNAs involved in timing of larval developmental stages. Both miRNAs showed sequence complementarity to the 3' untranslated region (UTR) of messenger RNAs (mRNAs) suggesting a downregulation of mRNAs by RNA-RNA sequence pairing (Lee et al. 1993; Reinhart et al. 2000). Further RNAs of 21-25 nt were discovered and they were categorized as the miRNA family in 2001 (Lagos-Quintana et al. 2001; Lau et al. 2001; Lee & Ambros 2001). Due to new detection technologies such as small RNA deep sequencing, the number of identified miRNAs has been rapidly expanding in the last years. From 2010 to 2014, the miRBase Sequence Database had nearly doubled from 15172 loci in 142 species (version 16, 2010) to 28645 loci in 223 species (version 21, 2014) (Kozomara & Griffiths-Jones 2014; miRbase 2016). The identified miRNAs were shown to be involved in a great variety of functions such as proliferation, differentiation, development, apoptosis and metabolism (Bartel 2004; He & Hannon 2004).

Another class of small RNA was identified soon and - based on their function - termed siRNAs (Elbashir, Lendeckel, et al. 2001; Elbashir, Harborth, et al. 2001). SiRNAs are double-stranded 19-23 nt long RNAs. It is assumed that the primary function of siRNA is the defense against exogenous nucleic acids and endogenous genomic by-products such as inverted repeat transgenes and abnormal transcription products (Carthew & Sontheimer 2009; Ghildiyal & Zamore 2009; V. N. Kim et al. 2009).

PiRNAs are the third and largest group of small RNAs. They are longer than miRNAs and siRNAs with 24-32 nt in length (Aravin et al. 2006; Girard et al. 2006; Grivna et al.

2006; Lau et al. 2006; Watanabe et al. 2006). For a long time their main function was thought to be the protection of germ cell genome integrity by silencing mRNA of transposable elements, which can interrupt the genome by insertion or transposition (Siomi et al. 2011). However, recent studies have elucidated additional functions in somatic cells, such as genome rearrangement and epigenetic programming (Ross et al. 2014).

Hence, the three different classes of small RNAs are involved in distinct biological functions. Yet, all they have in common is that they operate by gene silencing by small RNA-mRNA sequence pairing with the help of associated Ago proteins: miRNAs in endogenous genes for expression regulation, siRNAs in viral genes and genomic by-products for host defense and piRNAs in transposon genes for maintenance of germline integrity. This mechanism of double-stranded RNA (dsRNA)-mediated mRNA silencing is called RNA interference (RNAi) and has revealed a whole new role of ncRNAs (Fire et al. 1998). In the last decade, the role of ncRNAs in the development of chronic diseases has been more and more elucidated. Thus, ncRNAs have become promising therapeutic targets (Adams et al. 2017).

1.2.2 MiRNA biogenesis

MiRNA biogenesis involves three major steps: miRNA transcription, miRNA maturation and assembly of the miRNA-containing RNA-induced silencing complex (miRISC) (Bartel 2004). The standard pathway of miRNA biogenesis in mammals is depicted in Figure 2, page 5.

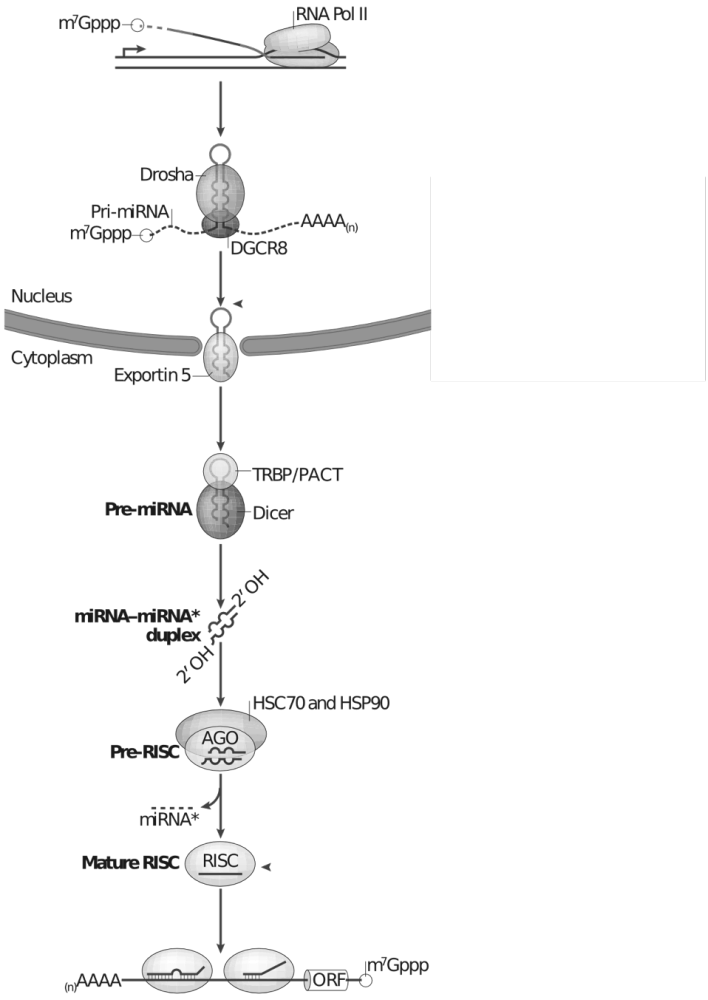

Figure 2. Standard pathway of miRNA biogenesis in mammals. The miRNA gene is transcribed by RNA polymerase (Pol) II. The transcript is cleaved by Drosha in the nucleus and Dicer in the cytoplasm. The miRNA-miRNA* duplex is loaded on the RNA-induced silencing complex (RISC) assembly. One duplex strand is degraded and the survival strand binds to the target mRNA. Alternative pathways for miRNA biogenesis and binding proteins for other animals are not shown (adapted from Ameres and Zamore 2013). m^7Gppp: 7-methylguanosine cap, $AAAA_{(n)}$: 3' poly(A) tail, 2' OH: 2' hydroxyl group, ORF: open reading frame. Other abbreviations are explained in the text below.

MiRNA genes are typically transcribed by Pol II (Lee et al. 2004). However, miRNAs within Alu repetitive elements are transcribed by Pol III (Borchert et al. 2006). The resulting primary miRNA (pri-miRNA) is composed of a ~ 33 nt long double-stranded stem, a terminal hairpin and single-stranded flanking segments (V. N. Kim et al. 2009).

The maturation of miRNAs involves two cleaving steps on the 5' and 3' ends of the double-stranded pri-miRNA. Both steps are performed by ribonuclease (RNase) III enzymes: Drosha in the nucleus and Dicer in the cytoplasm. These dsRNA-specific nucleases operate together with dsRNA-binding proteins to improve substrate restriction, affinity and cleavage site accuracy (Ameres & Zamore 2013). In the first cleavage step, the pri-miRNA is cleaved ~ 22 nt from the loop/stem junction by the

microprocessor complex (Zeng et al. 2005), composed of the nuclear RNAse III Drosha and its dsRNA-binding protein DiGeorge syndrome critical region 8 (DGCR-8) in mammals and Pasha in other animals (Gregory et al. 2004; Landthaler et al. 2004; Denli et al. 2004). DGCR-8 ensures accurate binding and cleavage by recognition of the single-stranded RNA (ssRNA)/dsRNA junction (Han et al. 2004; Han et al. 2006). The resulting small hairpin is ~ 60-70 nt long and it is termed precursor miRNA (pre-miRNA). For further processing, pre-miRNA is actively transported from the nucleus into the cytoplasm by the nuclear export factor Exportin-5 and the ras-related nuclear protein guanosine triphosphate (Ran-GTP) cofactor (Gwizdek et al. 2003).

In the second step of miRNA maturation, the generated pre-miRNA is cleaved near the terminal hairpin by the cytoplasmic RNase III Dicer. This results in a ~ 22 nt long duplex containing the mature miRNA and the fragment of the opposing arm, known as the pre-miRNA* sequence (Bartel 2004). Dicer is associated with Ago proteins and, like Drosha, with dsRNA-binding proteins. In mammals dsRNA-binding proteins are transactivation response RNA binding protein (TRBP) (Chendrimada et al. 2005) and protein kinase R-activating protein (PACT) (Lee et al. 2006).

Dicer, TRBP/PACT and Ago proteins contribute to the formation of the RISC assembly. The miRNA:miRNA* duplex is loaded on the Ago protein assisted by the heat shock cognate protein 70 (HSC70) and the heat shock protein 90 (HSP90) (Ameres & Zamore 2013). A helicase unwinds the duplex and degrades one of the duplex strands, while the surviving strand is retained to the Ago protein (V. N. Kim et al. 2009). The asymmetry theory suggests that the strand with the less extensive base pairing at the 5’ end survives, which is typically the miRNA strand (Schwarz et al. 2003).

The single-stranded miRNA directs the miRISC to recognize complementary mRNAs (Meister et al. 2004). For this process, the two major RNA-binding motifs of the Ago proteins play an essential role: the P-element induced wimpy testis (Piwi) and the Piwi-Argonaute-Zwille (PAZ) domain. With the PAZ domain, Ago binds the miRNA at 3’ end while the 5’ half rests in a pocket in the Piwi domain. Thereby, the miRNA is positioned within the complex such that primarily the bases in position 2-8 of the 5’ end are exposed and able to undergo base pairing (Carthew & Sontheimer 2009). These 7 nt are called the “seed sequence“ of the miRNA and are mainly responsible for target recognition by Watson-Crick base pairing with the mRNA (Huntzinger & Izaurralde 2011).

In recent years, alternative pathways of miRNA maturation have been identified, which are distinct for individual miRNAs (reviewed in (Winter et al. 2009)).

1.2.3 MiRNA function

More than 60% of the protein-coding genes in humans are estimated to be controlled by miRNAs (Friedman et al. 2009). As the short seed sequence of 7 nt is sufficient for complementarity, a single miRNA can regulate several hundreds of mRNAs (Selbach et al. 2008) and one mRNA can be regulated by several miRNAs (Bartel 2009).

The best-characterized mechanism of miRNA-induced gene regulation is gene silencing at the posttranscriptional level. This is achieved by at least two distinct mechanisms: mRNA decay and translational repression. The proportion of sequence complementarity was thought to determine the silencing mechanism with perfect complementarity leading to cleavage and imperfect base pairing resulting in repression. While plant miRNAs show nearly complete base-pairing with the target mRNA, animal miRNAs typically pair the mRNA with mismatches and bulges. Therefore, it was assumed that plant miRNAs degrade and animal miRNAs repress target mRNAs (Bartel 2004; He & Hannon 2004). However, recent studies have shown that there is no clear tendency to one silencing mechanism, neither of plant nor of animal miRNA. Both cause repression and decay (Huntzinger & Izaurralde 2011; Dalmay 2013). Guo and colleagues suggested that decay of mRNAs might actually be the main mechanism of animal miRNA-induced gene silencing. 84% of the measured protein production was associated with decreased mRNA levels (Guo et al. 2010). One pathway by which mRNA decay might be triggered involves GW182, a downstream molecule of AGO proteins. It was demonstrated that GW182 can not only induce repression of translation initiation (Ding & Grosshans 2009), but also recruits CCR4:NOT deadenylation complex (Fabian et al. 2011; Chekulaeva et al. 2011; Braun et al. 2011). CCR4:NOT removes mRNA poly(A) tail, which directs target mRNAs to degradation. Therefore, the role of repression or degradation and the mechanisms that lie behind it remain to be identified.

Controversial data exist on whether miRISC induces repression at translation initiation or post-initiation (Carthew & Sontheimer 2009). Several studies have demonstrated that for miRNA-mediated mRNA repression a 5' 7-methylguanosine cap and 3' poly(A) tail are necessary (Humphreys et al. 2005; Wang et al. 2006; Wakiyama et al. 2007). Ryu and colleagues found that the eukaryotic translation initiation factor 4GI (eIF4GI) supports miRISC binding of 5' cap structure-associated complex (Ryu et al. 2013). These data suggest that miRNA-induced gene silencing is due to repression of translation initiation. Observations that target mRNAs are distributed with polyribosomes, however, indicate that miRNAs repress translation at the post-initiation stage (Nottrott et al. 2006; Petersen et al. 2006; Maroney et al. 2006). Therefore, it is still unclear which or maybe even both mechanisms contribute to mRNA repression.

In recent studies, activation of gene expression has been revealed as another miRNA regulatory mechanism (Iwasaki & Tomari 2009; Vasudevan 2011). Vasudevan and colleagues showed that miRNAs are involved in cell cycle regulation and stimulate translation in quiescent cultured cells (Vasudevan et al. 2007). The highly conserved miRNA-10a was found to enhance protein translation, intriguingly by binding to the 5' UTR of target mRNAs (Ørom et al. 2008). Further, the miRNA-122, which is abundantly expressed in the liver, was demonstrated to bind to the 5' end of Hepatitis C virus (HCV) genome. Likewise to miRNA-10a the binding resulted in an upregulation of HCV translation (Henke et al. 2008; Jopling et al. 2006).

1.2.4 MiRNA organization and regulation

MiRNA genes are localized in intergenic or protein coding regions, mainly introns. Several miRNAs are often located in close proximity within the genome, named miRNA clusters. Further, several miRNAs can share conserved sequences at nt 2-8 of the 5' end of the mature miRNA, a feature which classifies them as miRNA families. MiRNA family members often target overlapping mRNAs sharing similar functions (reviewed in (Ha & Kim 2014)). The miRNA families are highly conserved within different species. Mammals share at least 196 conserved miRNA families (Chiang et al. 2010). This implies a fundamental role of miRNAs in gene regulation. Family members can be located in clusters, but can also have different genomic origins. Further, miRNA cluster members can not only be of one miRNA family, but also have distinct sequences (Natarajan et al. 2013).

Despite the diverse mechanisms miRNAs exert on gene expression, miRNAs themselves are regulated at different levels such as transcription, maturation and turnover. MiRNAs can be transcribed from an intron of a certain gene in response to the same transcription factors as the protein itself (Hammond 2015). This enables a tight regulation of miRNA and protein expression (Bartel 2004; Kim et al. 2005). Further, miRNAs can be controlled by its own promoter and miRNA cluster members can share a polycistronic transcript (Ha & Kim 2014). By conjoint transcription regulation, miRNAs having similar targets in one signaling pathway can enhance the rather small effect of one single miRNA on the overall outcome of the pathway (Inui et al. 2010). Epigenetic mechanisms such as DNA methylation and histone modification additionally alter miRNA gene expression (Liu et al. 2013; Davis-Dusenbery & Hata 2010).

MiRNA maturation and turnover are also thought to be controlled. For instance, let-7g pri-miRNA is expressed at constant levels. However, due to a block at the Drosha cleaving step mature let-7g is found at high levels in mature cells, but not in embryonic

stem cells (Thomson 2006). However, many mechanisms of miRNA regulation still remain elusive (Davis-Dusenbery & Hata 2010; Ha & Kim 2014).

1.3 Epithelial-to-mesenchymal transition

1.3.1 Phenotypic changes in EMT

Epithelial-to-mesenchymal transition (EMT) is a gradual process of epithelial cells changing into mesenchymal cells undergoing intermediate phenotypes (Kalluri & Neilson 2003; Kalluri & Weinberg 2009). The process is reversible, called mesenchymal-to-epithelial transition (MET), and retransformation of mesenchymal cells often coexists with EMT (compare Figure 3) (Li et al. 2010; Samavarchi-Tehrani et al. 2010; Esteban et al. 2012).

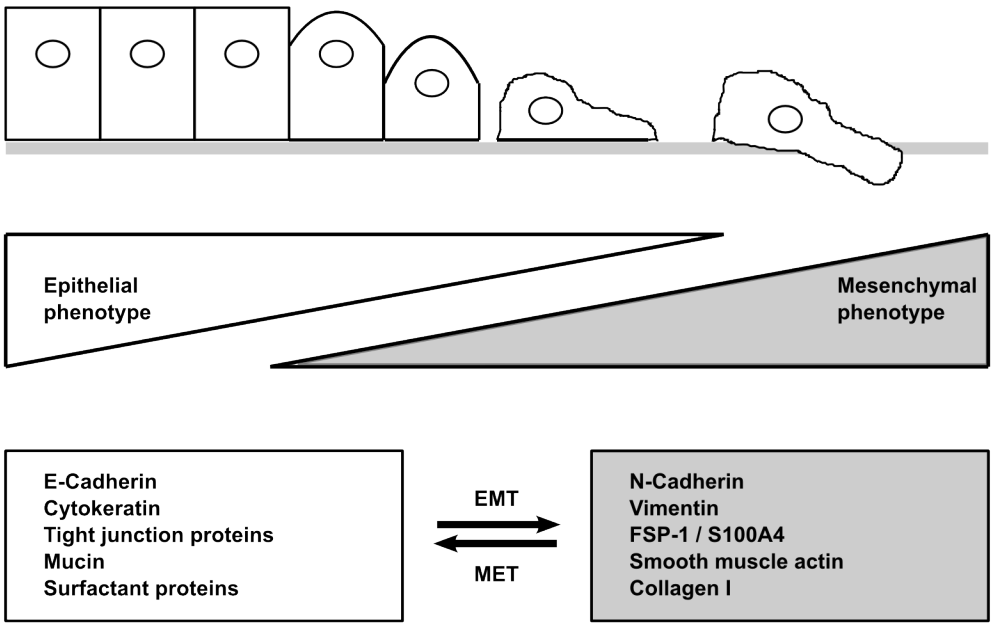

Figure 3. Phenotypic changes in EMT and MET. EMT is a gradual process of downregulation of epithelial markers and upregulation of mesenchymal markers leading to increased cell motility, migration capacity, fibrosis and resistance to senescence and apoptosis. Retransformation of mesenchymal cells, called MET, often coexists (adapted from Bartis et al. 2014). Abbreviations are explained in the text below.

Epithelial cells have an apical-basal polarity, are located on a basement membrane and are connected by cell-cell junctions (Lamouille et al. 2014). The main phenotypic alterations in EMT include change in cell surface proteins with loss of intercellular junctions, reorganization of the cytoskeleton and change of extracellular components. The major element of adherens junctions, epithelial cadherin (E-cadherin), is downregulated while neural cadherin (N-cadherin) is upregulated. The intermediate filaments change from cytokeratin to the fibroblast specific protein 1 (FSP1), also known as S100A4, and to vimentin (Zeisberg & Neilson 2009). Vimentin is expressed in fibroblasts, but also by endothelial cells and hematopoietic cells (Franke et al. 1978;

Dellagi et al. 1983). It is important for cell motility with vimentin-deficient cells showing decreased motility and migration capacity (Eckes et al. 1998). α-smooth muscle actin (α-SMA) is expressed in transformed myofibroblasts (Zeisberg & Neilson 2009). Extracellular components of the basement membrane are degraded (Yilmaz & Christofori 2009) and extracellular matrix components are synthesized by the transformed cells, such as type I collagen (K. K. Kim et al. 2009). Hence, EMT promotes a mesenchymal phenotype with increased cell motility, cell migration capacity, production of extracellular proteins leading to fibrosis and resistance to senescence and apoptosis (Zeisberg & Neilson 2009; Lamouille et al. 2014).

Of note, while for the epithelial phenotype certain markers as E-Cadherin are specific and ubiquitous, mesenchymal markers are nonspecific or only expressed by a subset of mesenchymal cells (Zeisberg & Neilson 2009; Willis & Borok 2007). Therefore, a profile of several markers is necessary to characterize EMT.

1.3.2 ATII cell changes by EMT and its impact on lung diseases

EMT physiologically takes place in embryonic development, during gastrulation and organogenesis, and in repair of epithelial injury. Under pathologic conditions, EMT can induce organ fibrosis as well as cancer development and progression (Thiery et al. 2009; De Craene & Berx 2013; Puisieux et al. 2014). In the lung, various groups of diseases have been discussed to be affected by EMT of ATII cells: developmental disorders, lung malignancies and non-malignant diseases with fibrotic remodeling (Bartis et al. 2014).

Organ fibrosis is currently considered as a pathologic response to organ injury. It can be divided in four phases: the primary injury, activation of effector cells, production and deposition of extracellular matrix (Rockey et al. 2015). In the lung, fibrosis leads to airway remodeling contributing to asthma, chronic obstructive pulmonary disease (COPD) and interstitial lung disease. The effector cells are primarily fibroblasts and myofibroblasts. The origin of mesenchymal cells has been controversially discussed. Numerous studies have suggested that under certain conditions, ATII cells differentiate into mesenchymal cells by EMT. EMT has been documented *in vitro* (Königshoff et al. 2009; Tanjore et al. 2011; Felton et al. 2009) and *in vivo* (Tanjore et al. 2009; Kim et al. 2006; Degryse et al. 2010). However, several lines of evidence support the original concept of ATII cells being the defender of the alveolus (Fehrenbach 2001). An increasing body of literature suggests that apoptosis of ATII cells plus increased proliferation of mesenchymal cells leads to pulmonary fibrosis. Induction of apoptosis in alveolar epithelial cells resulted in pulmonary fibrosis (Hagimoto et al. 1997) and abnormal lung fibroblasts induced apoptosis of alveolar epithelial cells *in vitro* and *in*

vivo (Uhal et al. 1995; Uhal et al. 1998). Lineage trace experiments labeling the endogenous SP-C promoter found no evidence of ATII cells transforming into myofibroblasts *in vivo* (Rock et al. 2011). In the murine kidney, mesenchymal cells originated from local fibroblasts (50%), bone marrow (35%), endothelial-to-mesenchymal transition (10%) and EMT (5%) (LeBleu et al. 2013). These findings suggest that mesenchymal cells might arise from diverse sources. To what extent this can be transferred to the lung is still to be determined (Bartis et al. 2014).

Local tumor invasion and distant metastasizing of epithelial malignancies (carcinomas) have also been contributed to EMT. The loss of cell-cell-adhesion, loss of apical-basal polarity and reorganization of cytoskeleton enables pro-oncogenic migration capacity of epithelial cells. At sites of metastases, regaining epithelial functions of the primary tumor is thought to occur by MET (Hugo et al. 2007). Further, EMT allows tumor cells to acquire stem-cell characteristics (Abell & Johnson 2014). Several studies have correlated lung cancer progression and metastases with EMT (Mittal 2016). EMT transition was shown in specimens of primary non-small cell lung cancer (NSCLC), especially squamous cell carcinoma, and brain metastases showed a decreased epithelial phenotype compared to the primary tumor (Prudkin et al. 2009). At the invasive border of NSCLC, desmoplastic stroma and other markers of EMT were highly expressed (Soltermann 2012). However, it is still highly debated whether EMT actually leads to metastases in humans, mainly because little conclusive data exist on epithelial-mesenchymal changes in the metastatic process *in vivo* (Bastid 2012; Mittal 2016; Brabletz 2012; Bartis et al. 2014).

1.3.3 Molecular changes in EMT: TGF-beta superfamily signaling pathway

Several pathways have been described to promote EMT. Transforming growth factor beta (TGF-beta) superfamily signaling is one of the key pathways (Gordon & Blobe 2008). The TGF-beta superfamily participates in many cellular pathways such as proliferation, differentiation and apoptosis. Thus, it plays an important role in many physiological processes from embryonic development to homeostasis of mature tissue (Massagué 1998).

The TGF-beta superfamily of intercellular signaling mediators consists of more than 30 members in mammals. In addition to the TGF-beta isoforms (TGF-beta 1, TGF-beta 2 and TGF-beta 3), the superfamily comprises bone morphogenetic proteins (BMPs), growth and differentiation factors (GDFs), activins and nodals. The ligands bind to type II transmembrane receptor serine-threonine kinases. This leads to formation of a heteromeric complex with and activation of type I transmembrane receptor serine-threonine kinases by phosphorylation (Weiss & Attisano 2013).

Downstream signaling is primarily mediated by a group of proteins called the SMAD family (depicted in Figure 4), named after the homologous proteins in Caenorhabditis elegans (SMA) and Drosophila melanogaster (mothers against decapentaplegic, MAD). SMA and MAD were the first members of the SMAD family described (Brown 2007; Brushart 2011).

Receptor-regulated SMAD1, 2, 3, 5 and 9 are phosphorylated by the activated type I transmembrane receptor in the cytoplasm. Phosphorylated SMAD proteins form a heteromeric complex with common mediator SMAD protein, SMAD4, and accumulate in the nucleus. SMAD6 and 7 promote negative feedback within the pathway (Weiss & Attisano 2013; Moustakas & Heldin 2009).

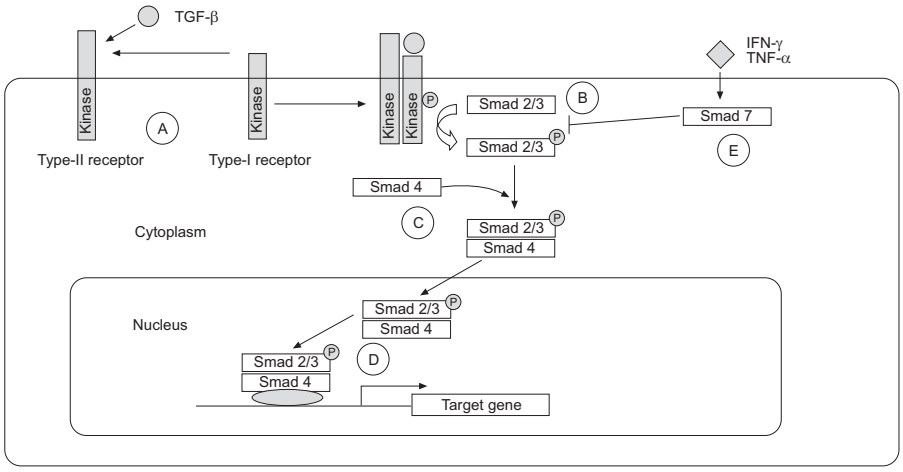

Figure 4. SMAD-dependent TGF-beta superfamily signaling pathway. The TGF-beta superfamily ligands bind to type II transmembrane receptor, which actives type I transmembrane receptor (A). This leads to phosphorylation of SMAD proteins (B). Phosphorylated SMAD proteins form a heteromeric complex with SMAD4 (C). After translocation in the nucleus, the complex associates with transcription factors and binds to promoters. This regulates the expression of target genes (D). SMAD6 and 7 regulate negative feedback. SMAD7 is activated by proinflammatory cytokines such as interferon-γ (INF-γ) and tumor necrosis factor-α (TNF-α) (E) (Zandvoort et al. 2006).

SMAD-dependent signaling is ubiquitous in all cell types studied so far. In addition, cell specific SMAD-independent pathways modulate TGF-beta superfamily signaling in distinct cell types. For EMT, an interplay of SMAD and non-SMAD signaling is necessary. Direct activation of partitioning-defective protein 6 (Par6) by TGF-beta receptors leads to destruction of tight junctions (Ozdamar et al. 2005). However, TGF-beta signaling needs SMAD-mediated transcriptional alteration for the complete process of EMT (Weiss & Attisano 2013; Moustakas & Heldin 2009).

Within the nucleus, the SMAD complex associates with transcription factors. This complex regulates gene expression by binding to promoters (Zandvoort et al. 2006). Depending on the gene context and cellular milieu, TGF-beta signaling can either result in upregulation or suppression of target genes (Massagué 2012). In EMT,

mesenchymal genes are upregulated and epithelial genes are downregulated. In this context, three transcription factor families play an important role in EMT: zinc finger transcription factors of the SNAIL family (SNAIL1 and SNAIL2), zinc-finger E-box binding factor (ZEB1/ZEB2) and basic helix-loop-helix proteins (e.g. TWIST 1, TWIST 2) (Lamouille et al. 2013; Hill et al. 2013). Transcription factors can either activate or downregulate SMAD-induced transcription (Hill et al. 2013). While ZEB1 enhances, ZEB2 downregulates SMAD-induced transcription (Postigo 2003). Further regulation of TGF-beta signaling happens during signal transduction and by epigenetic modulation (Massagué 2012).

MiRNAs are involved in regulation of the TGF-beta signaling pathway on all three levels: signal transduction, transcription and epigenetic modulation (as described in 1.3.4).

1.3.4 MiRNAs in TGF-beta mediated-EMT and its impact on lung diseases

MiRNAs have been shown to be essential regulators of many pathways. For that very reason, dysregulation of miRNAs contributes to multiple pathologic processes such as central nervous system disorders (Jimenez-Mateos & Henshall 2013; Maciotta et al. 2013), cardiovascular diseases (Vickers et al. 2014) and human cancers (Natarajan et al. 2013).

MiRNAs are relevant regulators of the TGF-beta superfamily signaling pathway having targets at different levels. They alter signal transduction by regulation of ligands, receptors and SMAD proteins (Itoh & Itoh 2011). Further, they alter transcription and there are emerging data on miRNAs modifying TGF-beta signaling by epigenetic mechanisms (Butz et al. 2012). Vice versa, the TGF-beta signaling pathway controls miRNA expression. This forms a negative feedback loop of regulation. For instance, the miR-200 family members repress the TGF-beta pathway maintaining an epithelial phenotype, while these miRNAs are downregulated by TGF-beta (B. Wang et al. 2011).

Within the lung, miRNAs play a significant role in lung development and homeostasis. Changes in the fine-tuned miRNA expression levels trigger pulmonary diseases. Numerous dysregulated miRNAs are linked to the TFG-beta superfamily signaling pathway.

Expression profiling of lung tissue from patients with interstitial lung disease compared to controls in two studies revealed 46 and 125 differentially expressed miRNAs, respectively (Pandit et al. 2010; Cho et al. 2011). One of the downregulated miRNAs, let-7d, showed an upstream binding site for SMAD3. TGF-beta 1 reduced let-7d expression *in vitro* and inhibition of let-7d showed EMT-like changes *in vitro* and *in vivo*

(Pandit et al. 2010). Several studies endorsed the important role of miRNAs in the pathogenesis of idiopathic pulmonary fibrosis (IPF) by the TGF-beta signaling pathway. Identified miRNAs were found to function either as inhibitors (Cushing et al. 2011; Yang et al. 2012; Das et al. 2014) or promoters of the TGF-beta signaling pathway (Liu et al. 2010; Yamada et al. 2013).

In asthma, most miRNA studies so far focus on regulation of cytokines and inflammation (Greene & Gaughan 2013). However, it was also shown that miRNAs modulate TGF-beta induced airway remodeling. In human asthmatic airway smooth muscle cells miR-221 is upregulated by TGF-beta leading to increased proliferation and interleukin (IL)-6 production (Perry et al. 2014). MiR-23b inhibited TGF-beta mediated proliferation by suppression of the TGF-beta type II transmembrane receptor in murine airway smooth muscle cells (Chen et al. 2015).

Few studies have traced the role of miRNAs contributing to COPD (Hassan et al. 2012; Sato et al. 2010; Pottelberge et al. 2011). Ezzie et al. explored the relation between miRNAs in COPD and TGF-beta signaling (Ezzie et al. 2012). Seventy miRNAs were found to be differentially expressed in lung tissues from smokers with COPD compared to smokers with no airway obstruction. *In situ* hybridization identified one of the upregulated miRNAs, miR-15b, mainly in bronchial epithelial cells and ATII cells. Interestingly, expression of SMAD7 was decreased in miR-15b expressing cells. SMAD7 is as an inhibitor of TGF-beta signaling and is known to be downregulated in COPD patients compared to healthy controls (Zandvoort et al. 2006). Therefore, miR-15b might serve as an enhancer of TGF-beta signaling.

In lung cancer, miRNAs of TGF-beta mediated pathways can act as tumor suppressors or oncogenes. The loss of miR-200c was correlated with an aggressive, invasive phenotype of NSCLC (Ceppi et al. 2010). MiR-200c represses TGF-beta signaling by downregulation of ZNF217 and ZEB1, two transcriptional activators of the signaling pathway (Bai et al. 2014). In contrast, the oncogenic miR-21 was upregulated in the sputum of patients with lung adenocarcinoma (Yu et al. 2010) and in the plasma of patients with malignant lung cancer compared to healthy controls (Tang et al. 2013). MiR-21 is assumed to play an important role in the TGF-beta signaling pathway. TGF-beta upregulates miR-21 via SMADs by binding the SMAD binding element (SBE) of the pri-miRNA (Davis et al. 2010). In esophageal cancer cells the upregulation of miR-21 by nicotine lead to TGF-beta induced EMT (Y. Zhang et al. 2014).

In summary, EMT is a key mechanism in ATII cells leading to lung disease. TGF-beta signaling pathway is a crucial pathway in EMT with numerous pathway components controlled by miRNAs.

2 AIM AND OBJECTIVES

ATII cells act as progenitors for ATI cells and play a central role in the maintenance of the alveolar homeostasis and local tissue repair.

This present study therefore aimed to identify miRNA-regulated networks which control the homeostasis of murine ATII cells. To achieve this end, three main goals were defined in the project:

1. Establishment of a protocol for the isolation of highly pure and viable "untouched" ATII cells from healthy mice in comparison to a previously published method.
2. Identification of miRNAs expressed by murine ATII cells under normal, non-pathologic conditions defined as a cut-set of miRNAs obtained from ATII cells isolated by two different methods (novel and previously published method) to decrease potential method-related bias due to differences in ATII purity and variation in enrichment of putative ATII subpopulations by different methods.
3. *In silico* identification of potential pathways of ATII cell homeostasis regulated by miRNAs.

3 MATERIAL AND METHODS

3.1 Material

3.1.1 Mice

C57BL/6NCrl mice were obtained from the inhouse breeding facility at Helmholtz Zentrum Munich in Großhadern. Animals were kept under specific pathogen-free (SPF) conditions in individually ventilated cages with a 12/12 hours day/night cycle at constant temperature and humidity and provided with standard rodent chow and water *ad libitum*. For the experiments unchallenged, female, 6 to 12 weeks old mice were used. All experiments were conducted under the federal guidelines for the use and care of laboratory animals.

3.1.2 Chemicals and reagents

Table 1. Chemicals and reagents.

Chemical/reagent	Provider	
Acetone	AppliChem	Darmstadt, DE
Agarose	Invitrogen, Life Technologies	Darmstadt, DE
Bovine serum albumin (BSA)	Sigma-Aldrich	Taufkirchen, DE
D-(+)-Glucose	AppliChem	Darmstadt, DE
Dulbecco's Modified Eagle Medium (DMEM)	Gibco, Life Technologies	Darmstadt, DE
DMEM/F12 (1:1)	Gibco, Life Technologies	Darmstadt, DE
Deoxyribonuclease (DNase) I	AppliChem	Darmstadt, DE
Dispase	BD Pharmingen	Heidelberg, DE
Entellan	Merck Millipore	Darmstadt, DE
Ethanol	Merck Millipore	Darmstadt, DE
Fentanyl	Janssen-Cilag	Neuss, DE
Fetal bovine serum (FBS) Gold	PAA	Cölbe, DE
Hematoxylin solution, Mayer's hemalum solution for microscopy	Merck Millipore	Darmstadt, DE
Heparin	Ratiopharm	Ulm, DE
Lithium carbonate	Sigma-Aldrich	Taufkirchen, DE

Medetomidin	Pfizer	Berlin, DE
Methanol	AppliChem	Darmstadt, DE
Midazolam	Ratiopharm	Ulm, DE
Paraformaldehyde (PFA)	Microcos GmbH	Garching, DE
Penicillin/Streptomycin	PAA	Cölbe, DE
Phosphate buffered saline (PBS)	Gibco, Life Technologies	Darmstadt, DE
Propidium iodide (PI)	Sigma-Aldrich	Taufkirchen, DE
ProLong® Gold antifade reagent with 4',6-diamidino-2-phenylindole (DAPI)	Invitrogen, Life Technologies	Darmstadt, DE
Xylene	AppliChem	Darmstadt, DE

3.1.3 Cell culture media

Table 2. Media for cell separation (medium I) and further processing (medium II).

	Reagent	Volume	Concentration
Medium I	DMEM/F12 (1:1)	500 ml	-
	D-(+)-Glucose	1.8 g	3.6 mg/ml
	Penicillin/Streptomycin	5 ml	1 %
	DNase I	20 mg	0.04 mg/ml
Medium II	DMEM/F12 (1:1)	500 ml	-
	D-(+)-Glucose	1.8 g	3.6 mg/ml
	Penicillin/Streptomycin	5 ml	1 %
	FBS Gold	10 ml	2 %

3.1.4 Antibodies

Immunoglobulins (Igs) used for “panning” are shown in Table 3, page 18. Antibodies and adequate isotype control (ITC) with the fluorochromes allophycocyanin (APC), fluorescein isothiocyanate (FITC) and phycoerythrin (PE) used for cell sorting and flow cytometry are listed in Table 4, page 18. Primary and secondary antibodies used for immunofluorescence staining are listed in Table 5, page 18. Antibodies were obtained from BD Pharmingen (Heidelberg, DE), BioLegend (Fell, DE), Abcam (Cambridge,

UK), Sigma (Munich, Germany), Millipore, Merck Chemicals (Schwalbach, DE) and Invitrogen, Life Technologies (Darmstadt, DE).

Table 3. Antibodies for "panning".

Antigen	Host	Isotype	Clone	Provider	mg/ml
CD45	rat	IgG2b, κ	30-F11	BD Pharmingen	0.5
CD16/32	rat	IgG2b, κ	2.4G2	BD Pharmingen	0.5

Table 4. Antibodies and ITC for cell sorting and flow cytometry.

Antigen	Host	Isotype	Fluorochrome	Clone	Provider	mg/ml	Dilution
CD31	rat	IgG2a, κ	APC	MEC 13.3	BD Pharmingen	0.2	1:10
ITC for CD31	rat	IgG2a, κ	APC	R35-95	BD Pharmingen	0.2	1:10
CD31	rat	IgG2a, κ	PE	390	BioLegend	0.2	1:10
ITC for CD31	rat	IgG2a, κ	PE	RTK2758	BioLegend	0.2	1:10
CD45	rat	IgG2b, κ	APC	30-F11	BD Pharmingen	0.2	1:20
ITC for CD45	rat	IgG2b, κ	APC	A95-1	BD Pharmingen	0.2	1:20
CD74	rat	IgG2b, κ	FITC	In-1	BD Pharmingen	0.5	1:10
ITC for CD74	rat	IgG2b, κ	FITC	A95-1	BD Pharmingen	0.5	1:10

Table 5. Antibodies for immunofluorescence staining.

Primary antibodies for immunofluorescence staining:					
Antigen	**Host**	**Isotype**	**Clone**	**Provider**	**Dilution**
pan-cytokeratin	goat	IgG1	C-11	Abcam	1:500
E-Cadherin	mouse	IgG2a, κ	36/E-Cadherin	BD Pharmingen	1:500
α-SMA	mouse	IgG2a	1A4	Sigma	1:200
CD31	rabbit	IgG	polyclonal	Abcam	1:200
pro-SPC	rabbit	IgG	polyclonal	Chemicon/Millipore	1:100
CCSP	rabbit	IgG	polyclonal	Upstate/Millipore	1:100
CD45	rat	IgG2b, κ	30-F11	BD Pharmingen	1:500
Secondary antibodies for immunofluorescence staining:					
Antigen	**Host**	**Isotype**	**Fluorochrome**	**Provider**	**Dilution**
rabbit-IgG (H+L)	goat	IgG	Alexa Fluor 555	Invitrogen	1:1000

mouse-IgG (H+L)	goat	IgG	Alexa Fluor 555	Invitrogen	1:1000
rat-IgG (H+L)	goat	IgG	Alexa Fluor 555	Invitrogen	1:1000
goat-IgG (H+L)	donkey	IgG	Alexa Fluor 488	Invitrogen	1:1000

3.1.5 Solutions for miRNA profiling

All components of master mixes for reverse transcription (RT), preamplification of complementary DNA (cDNA) and polymerase chain reaction (PCR) were obtained from Applied Biosystems, Life Technologies (Darmstadt, DE) (see 3.1.7, page 21). The TaqMan® microRNA Reverse Transcription Kit contains deoxyribonucleoside triphosphates (dNTPs) with deoxythymidine triphosphate (dTTP), MultiScribe™ Reverse Transcriptase, RT buffer, RNase Inhibitor and nuclease-free water.

Table 6. Composition of master mix for RT.

Reagent	Volume 1x	Volume 6x
MegaPlex™ RT Primers 10x (Pool A or B)	0.80 µl	4.80 µl
dNTPs with dTTP (100 mM)	0.20 µl	1.20 µl
MultiScribe™ Reverse Transcriptase (50 U/µl)	1.50 µl	9.00 µl
RT buffer 10x	0.80 µl	4.80 µl
$MgCl_2$ (25 mM)	0.90 µl	5.40 µl
RNase Inhibitor (20 U/µl)	0.10 µl	0.60 µl
Nuclease-free water	0.20 µl	1.20 µl
Total volume	4.50 µl	27.00 µl

Table 7. Composition of master mix for preamplification of cDNA.

Reagent	Volume 1x	Volume 6x
TaqMan® PreAmp MasterMix 2x	12.5 µl	75.0 µl
MegaPlex™ PreAmp Primers 10x	2.5 µl	15.0 µl
Nuclease-free water	7.5 µl	45.0 µl
Total volume	22.5 µl	135.0 µl

Table 8. Composition of master mix for PCR.

Reagent	Volume
TaqMan® Universal Master Mix II, no UNG	450 µl
Diluted preamplified product	9 µl
Nuclease-free water	441 µl
Total volume	900 µl

3.1.6 Oligonucleotides

Cd74, Pecam1 and Ptprc were designed using Primer-BLAST (see 3.1.10, page 24). The other primers were obtained by the group of Königshoff et al. as previously published: Acta2 (Königshoff et al. 2009), Aqp5 (Königshoff & Eickelberg 2011), Cdh1 (Königshoff & Eickelberg 2011), Hprt (Mutze et al. 2015), Sftpa1 (Mutze et al. 2015), Sftpc (Mutze et al. 2015), Tjp1 (Mutze et al. 2015).

Table 9. Primer sequences for reverse transcription of mRNAs.

Gene symbol	Full name	NCBI GenBank accession	Primer sequences (5'->3')	bp
Acta2	actin, alpha 2, smooth muscle, aorta	NM_ 007392	fwd: GCTGGTGATGATGCTCCCA rev: GCCCATTCCAACCATTACTCC	81
Aqp5	aquaporin 5	NM_ 009701	fwd: CCTTATCCATTGGCTTGTCG rev: CTGAACCGATTCATGACCAC	115
Cd74	CD74 antigen	NM_ 001042605	fwd: GATGGCTACTCCCTTGCTGA rev: TGGGTCATGTTGCCGTACT	93
Cdh1	cadherin 1 (E-cadherin)	NM_ 009864	fwd: CCATCCTCGGAATCCTTGG rev: TTTGACCACCGTTCTCCTCC	89
Hprt	hypoxanthine guanine phosphoribosyl transferase	NM_ 013556	fwd: CCTAAGATGAGCGCAAGTTGAA rev: CCACAGGACTAGAACACCTGCTAA	86
Pecam1	platelet/endothelial cell adhesion molecule 1	NM_ 008816	fwd: ATCGGCAAAGTGGTCAAGAG rev: GGCATGTCCTTTTATGATCTCAG	111

	(protein: CD31)			
Ptprc	protein tyrosine phosphatase, receptor type, C (protein: CD45)	NM_ 001111316	fwd: GTCCCTACTTGCCTATGTCAATG rev: CCGGGAGGTTTTCATTCC	115
Sftpa1	surfactant associated protein A1	NM_ 023134	fwd: GGAGAGCCTGGAGAAAGGGGGC rev: ATCCTTGCAAGCTGAGGACTCCC	124
Sftpc	surfactant associated protein C	NM_ 011359	fwd: AGCAAAGAGGTCCTGATGGA rev: GAGCAGAGCCCCTACAATCA	153
Tjp1	tight junction protein 1	NM_ 009386	fwd: ACGAGATGCTGGGACTGACC rev: AACCGCATTTGGCGTTACAT	112

3.1.7 Commercial kits

Table 10. Commercial kits.

Kit	Provider	
Diff-Quick Staining Set	Medion Diagnostics	Düdingen, CH
IntraPrep™ Permeabilization Reagent	Beckman Coulter	Krefeld, DE
LightCycler® 480 SYBR Green I Master Mix	Roche	Mannheim, DE
Megaplex™ PreAmp Primers, Rodent Pool Set v3.0	Applied Biosystems, Life Technologies	Darmstadt, DE
Megaplex™ RT Primers, Rodent Pool Set v3.0	Applied Biosystems, Life Technologies	Darmstadt, DE
miRNeasy Mini Kit	Qiagen	Hilden, DE
MuLV Reverse Transcriptase	Invitrogen, Life Technologies	Darmstadt, DE
Random Hexamers	Invitrogen, Life Technologies	Darmstadt, DE
TaqMan® Array Rodent MicroRNA A+B Cards Set v3.0	Applied Biosystems, Life Technologies	Darmstadt, DE
TaqMan® microRNA Reverse Transcription Kit	Applied Biosystems, Life Technologies	Darmstadt, DE

TaqMan® PreAmp Master Mix	Applied Biosystems, Life Technologies	Darmstadt, DE
TaqMan® Universal Master Mix II, no UNG	Applied Biosystems, Life Technologies	Darmstadt, DE

3.1.8 Consumables

Table 11. Consumables.

Consumable	Provider	
Cell strainer, BD Falcon, 35 µm: Round-Bottom Tube with Cell-Strainer Cap, Polystyrene, 5ml	BD Biosciences	Heidelberg, DE
Cell strainer, BD Falcon, 40 / 100 µm	BD Biosciences	Heidelberg, DE
Conical tube, BD Falcon, Polypropylene, 15 ml / 50 ml	BD Biosciences	Heidelberg, DE
Culture dish, BD Falcon, 100 x 15 mm	BD Biosciences	Heidelberg, DE
Culture slides, BD Falcon	BD Biosciences	Heidelberg, DE
Eppendorf tube, 5.0 ml	Eppendorf	Hamburg, DE
Needle, BD Microlance 3, 27 gauge x ¾'' / 20 gauge x 1 ½''	BD Biosciences	Heidelberg, DE
Nylon mesh, 10 / 20 / 100 µm	Sefar AG	Heiden, CH
Peripheral venous catheter, Safety IV Catheter with Injection port, 20 gauge x 1 ¼''	Braun	Melsungen, DE
Pipettes, Cellstar, 5 ml / 10 ml	Greiner Bio-One	Frickenhausen, DE
Pipettes, Costar Stripette, 25 / 50 ml	Corning Incorporated	New York, US
Pipette Tips, epT.I.P.S., 0.1-10 / 2-200 / 50-1000 µl	Eppendorf	Hamburg, DE
Round-bottom Tube, BD Falcon, Polystyrene, 5 ml	BD Biosciences	Heidelberg, DE
Syringe, BD Discardit II, 2 ml / 10 ml	BD Biosciences	Heidelberg, DE
Syringe, BD Plastipak, 1 ml	BD Biosciences	Heidelberg, DE

3.1.9 Devices

Table 12. Devices.

Device	Provider	
7900HT Fast Real-Time PCR System	Applied Biosystems, Life Technologies	Darmstadt, DE
BD FACSAria II Cell Sorter	BD Biosciences	Heidelberg, DE
BD LSR II Flow Cytometer	BD Biosciences	Heidelberg, DE
Bioanalyzer, 2100	Agilent Technologies	Stuttgart, DE
Centrifuge, Micro 200R	Hettich	Tuttlingen, DE
Centrifuge, Rotina 420R	Hettich	Tuttlingen, DE
Concentrator plus	Eppendorf	Hamburg, DE
Cytocentrifuge, CytoSpin* 4	Thermo Fisher Scientific	Waltham, US
Refrigerator, ProfiLine	Liebherr	Biberach an der Riss, DE
Freezer - 20°C, Comfort	Liebherr	Biberach an der Riss, DE
Freezer - 80°C, Innova U725-G	New Brunswick Scientific, Eppendorf	Hamburg, DE
LightCycler® 480 II System	Roche	Mannheim, DE
Microscope, Axio Imager.M2	Zeiss	Jena, DE
Pipettes, Eppendorf Research Plus, 2.5 / 10 / 20 / 100 / 200 / 1000 µl	Eppendorf	Hamburg, DE
Pipet-Aid, Eppendorf Easypet	Eppendorf	Hamburg, DE
Pipet-Aid, BD Falcon Express	BD Biosciences	Heidelberg, DE
Spectrophotometer, NanoDrop 1000	Thermo Fisher Scientific	Waltham, US
Thermocycler, peqSTAR 96 Universal Gradient	PEQLAB	Erlangen, DE
Water bath, Aqualine AL 12	Lauda	Lauda-Königshofen, DE

3.1.10 Software

Table 13. Software.

Software	Provider	
AxioVision Release 4.8.1	Zeiss	Jena, DE
DataAssist v3.0	Applied Biosystems, Life Technologies	Darmstadt, DE
FACSDiva Version 7.6.5	BD Biosciences	Heidelberg, DE
FlowJo vX 10.0.6 for Mac	Tree Star	Ashland, US
GraphPad Prism 5	GraphPad Software, Inc.	La Jolla, US
Ingenuity® Software	Ingenuity Systems, Inc.	Redwood City, US
Inkscape X11 for Mac	http://inkscape.org	
Mendeley	Mendeley, Inc.	New York, US
Primer-BLAST	http://www.ncbi.nlm.nih.gov/tools/primer-blast	
Sequence Detection Software (SDS) v2.4	Applied Biosystems, Life Technologies	Darmstadt, DE
SDS RQ Manager 1.2.1	Applied Biosystems, Life Technologies	Darmstadt, DE

3.2 Methods

3.2.1 Workflow

Lung single cell suspensions were prepared from unchallenged, female, 6-12 week old C57BL/6NCrl mice. ATII cells were isolated by Fluorescence Activated Cell Sorting (FACS) (termed sATII) or “panning” (termed pATII). The viability and purity of isolated cells were compared. MiRNA profiles were obtained of both sATII and pATII. MiRNAs with similar expression levels in both preparations were subjected to Ingenuity® pathway enrichment analysis. An overview of the workflow is outlined in Figure 5, page 25.

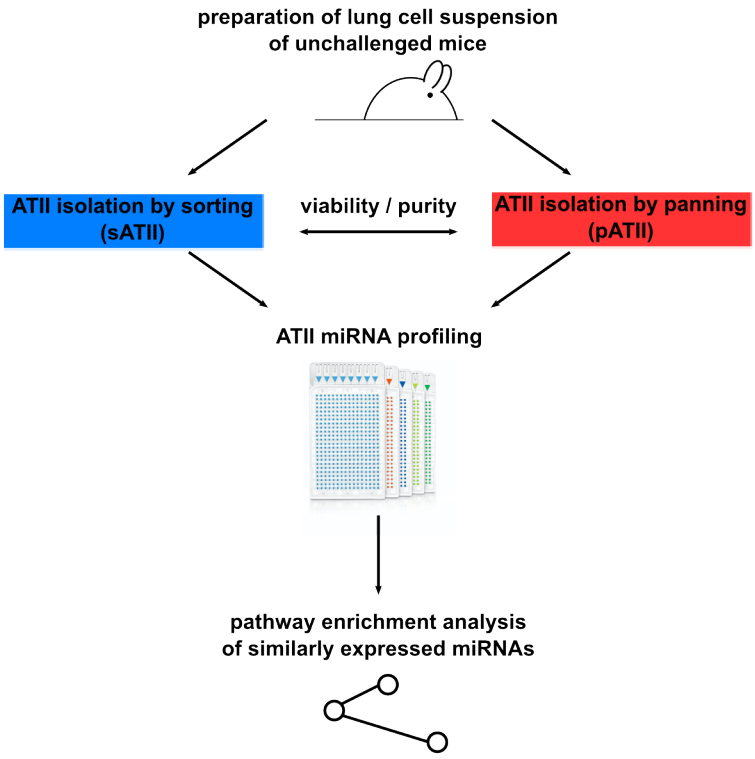

Figure 5. Overview of the workflow. Lung single cell suspensions were prepared from unchallenged mice. ATII cells were isolated by sorting or “panning". The viability and purity were compared. Isolated cells were subjected to miRNA profiling. Similarly expressed miRNAs were used for Ingenuity® pathway enrichment analysis.

3.2.2 Preparation of lung single cell suspensions

Lung single cell suspensions were prepared as previously described with few alterations (Corti et al. 1996; Königshoff 2009; Königshoff et al. 2009). Mice were narcotized with medetomidin 0.5 µg/g, midazolam 5 µg/g and fentanyl 0.5 µg/g and blood coagulation was minimized with heparin 60 µl/mouse (5 IU/µl), both injected intraperitoneally.

Mice were positioned on the back and secured with 20 gauge needles. The skin was disinfected with 70% ethanol. A median incision from the abdomen to the chin was made and the skin and subcutis were dissected to the sides. The trachea was identified, mobilized and a 20 gauge peripheral venous catheter was inserted. The peritoneum was opened and the inferior vena cava was cleaved. A pneumothorax was induced with forceps and the diaphragm was removed (Figure 6 A1-2, page 26). The ribcage was opened and fixed to each side with 20 gauge needles. The lung vessels were perfused via the right ventricle with 10 ml PBS using a 10 ml syringe with a 20 gauge needle until the lung parenchyma appeared exsanguinous (that is white) (Figure 6 B1-2, page 26). The respiratory tract was filled via the tracheal catheter with 1.5 ml dispase (stored at -20°C, defrosted at 4°C overnight), followed by instillation of 0.3 ml

agarose solution (100 mg / 10 ml DMEM, boiled to dissolve, then kept liquid at 45°C in a water bath), both with 2 ml syringes (Figure 6 C1-3). After 2 minutes for agarose gelling, the trachea and esophagus were cut and the lungs were carefully removed (Figure 6 D). Lungs were incubated in 2.5 ml dispase in a 15 ml conical tube for 45 minutes at room temperature.

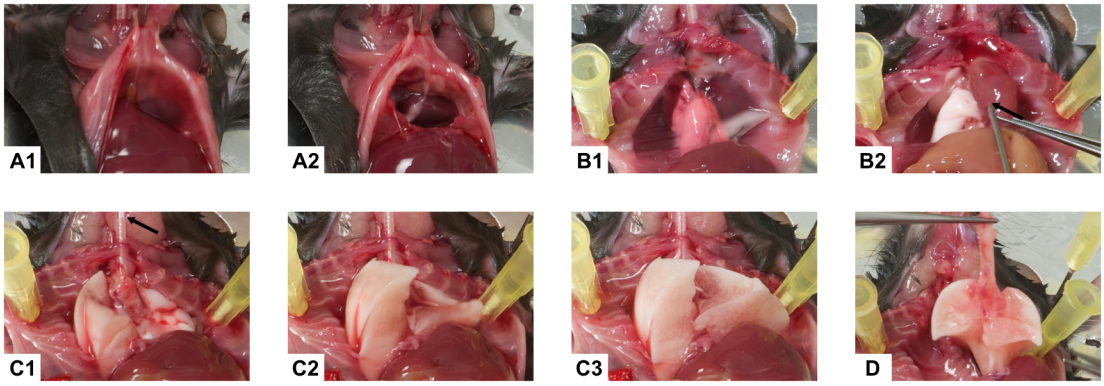

Figure 6. Extraction of murine lungs. A) Diaphragm intact (A1) and after induction of pneumothorax (A2). **B)** Lungs sanguised (B1) and exsanguised after transcardial perfusion (B2, arrow: cannula in right ventricle). **C)** Successive filling of lungs with dispase and agarose (C1-3, arrow: catheter in trachea). **D)** Removal of lungs after gelling of agarose.

For the preparation of single cell suspensions, lungs were consecutively transferred into a culture dish containing 5 ml of medium I (composition as described in Table 2, page 17). Lungs were separated into lobes. The trachea and bronchi were discarded. Lobes were consecutively transferred into a culture dish containing 8 ml of medium I. With one forceps holding the lobar bronchus, cells were detached by gently scraping the tissue with a second curved forceps. The preparation steps are shown in Figure 7. The suspension was aspirated several times with a 10 ml pipette until homogenized. The cell suspension was collected in a 50 ml conical tube and sequentially filtered through 100-, 20- and 10-µm nylon meshes. The filtered suspension was centrifuged at 200g for 10 minutes at 15°C, the supernatant discarded and the pellet resuspended in medium II (composition as described in Table 2, page 17).

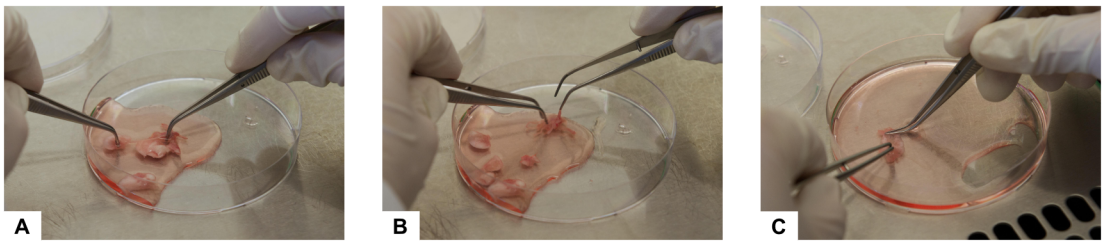

Figure 7. Preparation of single cell suspensions from lungs. A) Lungs were separated into lobes. **B)** Trachea and main bronchi were removed. **C)** Cells were detached by carefully scraping the tissue with a curved forceps.

3.2.3 Fluorescence Activated Cell Sorting

Lung single cell suspensions were obtained as described in 3.2.2, page 25, and pooled from 3-4 mice. Cells were stained with rat anti-mouse CD45-APC (diluted 1:20 in PBS) and rat anti-mouse CD31-APC (diluted 1:10 in PBS) for 20 minutes on ice. Cells were washed with 3 ml of medium II and centrifuged at 200g for 10 minutes at 4°C. The supernatant was discarded and the pellet was resuspended in medium II to a final concentration of 10 x 10^6 / ml. To minimize clumps, the cell suspension was sequentially filtered through 100, 40 and 35 µm cell strainers shortly before sorting.

Cells were sorted by FACS using BD FACSAria II Cell Sorter (Figure 8) and FACSDiva software according to the manufacturer's instructions (BD Biosciences 2009). The most relevant settings are displayed in Table 14.

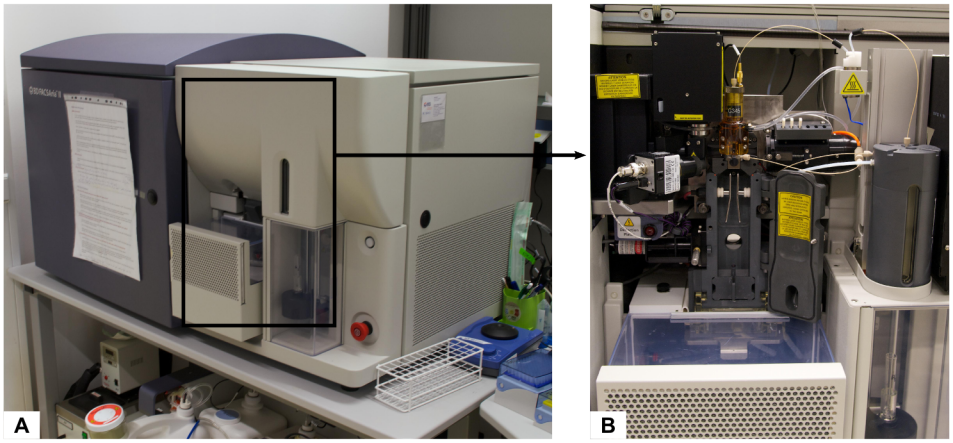

Figure 8. FACSAria II. A) Cell sorter. **B)** Flow cell and sort block with deflection plates.

Table 14. FACSAria II settings for cell sorting.

Parameter	Setting
Nozzle Size	85 µm
Sheath Fluid Pressure	45 PSI
Cell Concentration	10 x 10^6 / ml
Flow Rate	≤ 3 (1.0 -11.0 = ~ 10-80 µl/min)
Event Rate	≤ 10000 evt/s
Precision Mode	Purity
Temperature Sample Chamber / Collection Chamber	4°C

Subsequent gating was performed to sort ATII cells (gates are depicted in Figure 10, page 35, upper row). First, debris and doublets were excluded by using connected

gates on forward scatter (FSC) plots. In the FSC-area (FSC-A) versus (vs.) side scatter-area (SSC-A) dot plot, debris was excluded by low FSC-A and low SSC-A due to the small size. In the FSC-A vs. FSC-height (FSC-H) dot plot, doublets were depleted by a great area to height ratio, because doublets tend to position in the direction of the stream. In the FSC-A vs. FSC-width (FSC-W) dot plot, doublets were excluded by a great width to area ratio, because they take more time to pass through the laser stream equivalent to an increase in width (Houtz et al. 2004).

Second, the ATII cell population was identified by fluorescence parameters. Leukocytes were depleted by the CD45-surface marker and endothelial cells by the CD31-surface marker, both excluded using the APC-channel. The autofluorescence of ATII cells, measured in the FITC-channel, was used to isolate ATII cells from any other contaminating cells. Thus, AT II cells were isolated as the CD45-negative and CD31-negative ($CD45^-CD31^-$) and autofluorescence (FITC-channel)^{high} population. Cells isolated by this procedure were designated as sATII.

Isolated cells were immediately processed for the analysis of purity and viability. For prospective RNA isolation, cells were instantly centrifuged in 5.0 ml Eppendorf tubes at maximum speed for 5 minutes at room temperature. The supernatant was carefully removed and the pellet stored at -80°C until further use.

3.2.4 Isolation of cells by negative selection (“panning”)

Lung single cell suspensions were prepared as described in 3.2.2, page 25, and cells were isolated by “panning” as previously described by Königshoff et al. with few alterations (Königshoff 2009; Königshoff et al. 2009). In summary, culture dishes were coated with CD45 and CD16/32 antibodies (for each culture dish 15 µl of each antibody in 10 ml DMEM) overnight at 4°C. Shortly before isolation, culture dishes were washed twice with 5 ml DMEM. For removal of lymphocytes and macrophages, 5 ml of single cell suspension were incubated on the CD45-CD16/32-coated culture dishes for 35 minutes at 37°C. Unattached cells were collected and incubated on uncoated culture dishes for 35 minutes at 37°C for adherence of fibroblasts. The supernatants were pooled and centrifuged at 200g for 10 minutes at 15°C. Primary ATII cells were resuspended for flow cytometric analysis or pellet stored at -80°C for prospective RNA isolation. ATII cells isolated by this procedure were designated as pATII cells.

3.2.5 Flow cytometric analyses

In order to identify dead cells, PI (2 mg/ml in PBS) was added to the freshly sorted population for 10 minutes at 4°C prior to the analysis.

For the simultaneous staining of extra- and intracellular antigens IntraPrep Kit was used. According to the manufacturer's protocol for intracytoplasmic and membrane staining, cells were stained with a concentration of 1 x 10^5 in 50 µl with the extracellular antibody CD31-PE or adequate ITC (diluted 1:10 in PBS) for 20 minutes on ice protected from light. Cells were fixed with 100 µl IntraPrep Reagent 1 for 15 minutes at room temperature. Cells were washed with PBS and centrifuged at 200 g for 10 minutes at 4°C. The supernatant was discarded and cells were permeabilized with 50 µl IntraPrep Reagent 2 for 5 minutes at room temperature, then the intracellular antibody CD74-FITC or adequate ITC (diluted 1:10 in PBS) was added for 20 minutes on ice. Cells were washed as described above and resuspended in PBS.

Expression markers were analyzed using BD LSR II Flow Cytometer (Figure 9) and FlowJo software. Antibodies and adequate ITC for cell sorting and flow cytometry are listed in Table 4, page 18.

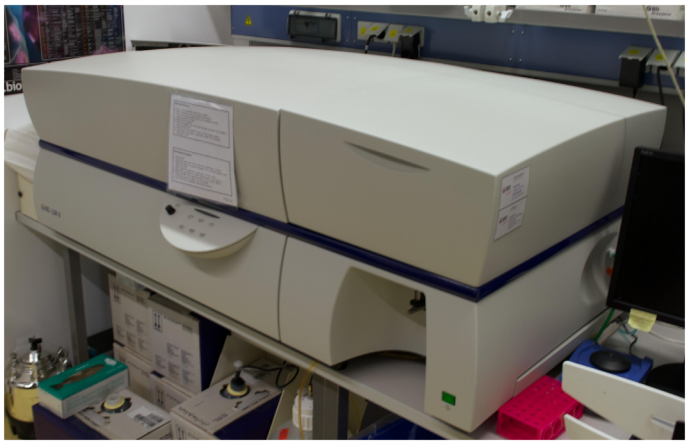

Figure 9. LSR II Flow Cytometer.

3.2.6 Papanicolaou staining

For morphologic identification of ATII cells, inclusion bodies were stained using a modified Papanicolaou staining as described by Dobbs (Dobbs 1990) .

In brief, 1 x 10^5 cells in 200 µl / slide were centrifuged at 400 rpm for 10 minutes on coverslips with CytoSpin* 4 Cytocentrifuge and dried overnight. Cells were stained with hematoxylin solution for 3.5 minutes and rinsed with distilled water. Cells were incubated with lithium carbonate solution (2 ml saturated solution of lithium carbonate in 158 ml distilled water) for 2 minutes and rinsed with water. Cells were stepwise incubated with increasing concentrations of ethanol solutions: 50% ethanol for 1.5 minutes, 80% ethanol for 15 seconds, 95% ethanol for 15 seconds and 100% ethanol for 30 seconds. Then cells were incubated in xylene:ethanol 1:1 for 30 seconds and xylene for 1 minute. Afterwards cells were embedded in Entellan.

3.2.7 Immunofluorescence staining

For immunofluorescence staining 1 x 10^5 cells in 200 µl / chamber were centrifuged at 200 g for 5 minutes at 4°C on culture slides. The supernatant was taken off carefully and slides were fixed with ice-cold acetone:methanol (1:1) for 10 minutes, then blocked with 5% BSA in PBS for 30 minutes and stained with the respective primary and secondary antibodies diluted in 0.1% BSA in PBS for 60 minutes for each antibody. Cells were fixed with 4% PFA for 10 minutes and mounted with ProLong Gold antifade reagent with DAPI. All steps were performed at room temperature, after each step cells were washed three times with 0.1% BSA in PBS. The immunofluorescence expression was analyzed using Axio Imager.M2 and AxioVision software. Primary and secondary antibodies for immunofluorescence staining are listed in Table 5, page 18.

3.2.8 RNA isolation and assessment of RNA integrity and concentration

The total RNA, including miRNAs, was isolated from 5 samples of 2 independent experiments of primary sATII and 2 samples of one experiment of primary pATII stored at -80°C with miRNeasy Mini Kit according to manufacturer's protocol.

In brief, cells were lysed and homogenized in 700 µl QIAzol Lysis Reagent. To separate RNA from DNA and proteins, 140 µl chloroform was added and shaken for 15 seconds. After incubation for 2-3 minutes at room temperature, the suspension was centrifuged at 12000 g for 15 minutes at 4°C. The aqueous phase, containing the RNA, was mixed with 525 µl ethanol, transferred to a RNeasy Mini spin column and centrifuged at ≥ 8000 g for 15 seconds at room temperature, then washed twice by adding 500 µl Buffer RPE and centrifuging at ≥ 8000 g for 15 seconds and 2 minutes at room temperature. The added ethanol enabled binding of RNA molecules from 18 nt and more to the membrane of the RNeasy Mini spin column, while other substances were removed. The RNA was then eluted by addition of 30-50 µl RNase-free water and centrifuging at ≥ 8000 g for 1 minute at room temperature.

RNA concentrations were measured by absorbance at 260 nm in the spectrophotometer. The RNA purity was assessed by 260/280 ratios with values ≥ 1.85 being accepted for further processing. The RNA integrity was analyzed by electrophoresis using an Agilent 2100 bioanalyzer according to the manufacturer's instructions. The RNA Integrity Number (RIN), calculated by a software algorithm, was assessed for each sample with values ranging from 1-10: 1 meaning completely degraded and 10 meaning completely intact (Mueller et al. 2004). Sufficient RNA integrity was defined as RIN ≥ 6.5.

3.2.9 Reverse transcription and quantitative PCR of mRNAs

The synthesis of cDNA was performed with 350 ng total RNA using random hexamers and MuLV reverse transcriptase according to manufacturer's protocol.

The real-time quantitative PCR (RT-qPCR) reaction was conducted with LightCycler® 480 SYBR Green I Master Mix on a LightCycler® 480 II system. Primers are listed in Table 9, page 20. Primer designs for Cd74, Pecam1 and Ptprc were performed using Primer-BLAST with an optimum annealing temperature of 60°C. The melting curve analysis was done to control for primer dimers and unspecific products. To control for contamination by genomic DNA or carry-over cDNA either reverse transcriptase enzyme (reverse transcriptase-controls) or cDNA (no template controls, NTCs) were omitted, respectively. All primers showed an amplification efficiency ≥ 92.5%. Raw cycle threshold (Cq) values > 35 were defined as not expressed.

The relative quantification of mRNA expression was determined using the ΔΔCq method (Livak & Schmittgen 2001). The mean values of four independent experiments and two technical replicates of each sample were used for sATII and pATII, respectively. *Hprt* was used as reference gene and *Sftpc* mRNA expression in sATII was defined as the calibrator. Standard deviation (S) was calculated for each ΔCq value as S = (s_1^2 + s_2^2)^1/2 with s_1 and s_2 being the standard deviations of the Cq(*target*) and Cq(*Hprt*), respectively. Fold changes were calculated as 2^-(ΔΔCq) and the range of values due to sample variation was determined as 2^-(ΔΔCq + S) and 2^-(ΔΔCq - S).

3.2.10 MiRNA profiling of ATII cells by TaqMan® MicroRNA Array

The reverse transcription and quantification of miRNAs were performed with TaqMan® microRNA Reverse Transcription Kit and TaqMan® Array Rodent MicroRNA A+B Cards Set v3.0 according to the manufacturer's protocol. TaqMan® arrays are microfluidic cards including 384 assays per card. Card A and B enable quantification of 641 miRNAs specific to mouse with species-specific endogenous controls and one negative control assay per card (Applied Biosystems Life Technologies 2010). The content for the rodent microRNA assays is based on Sanger miRBase v15 (miRbase 2016), released April 2010, with nearly full coverage.

The miRNA profiling included: reverse transcription with stem-loop primers, an optional preamplification step for small RNA amounts and quantification by real-time PCR.

3.2.10.1 Reverse transcription

The reverse transcription was performed for the synthesis of single-stranded cDNA from miRNA using stem-loop primers. The RNA was concentrated to ~ 45 ng/µl using

Concentrator plus. For each sample ~ 135 ng total RNA in 3 µl and for the NTCs 3 µl of water were used. Master mixes for each Primer Pool (A and B) were prepared as described in Table 6, page 19.

4.5 µl of the RT reaction mix was pipetted in a 0.2 ml PCR Clean tube and 3 µl of total RNA or water for NTC was added to a final volume of 7.5 µl. The samples were incubated for 5 minutes on ice. The RNA was transcribed into cDNA at the thermal-cycling conditions as shown in Table 15.

Table 15. Thermal cycling conditions for reverse transcription.

Cycle	Temperature	Duration
40 cycles	16°C	2 min
	42°C	1 min
	50°C	1 sec
Hold	85°C	5 min
Hold	4°C	∞

3.2.10.2 Preamplification of cDNA

The preamplification reaction was performed due to limited RNA amounts.

Master mixes for each Primer Pool (A and B) were prepared in a 0.5-mL microcentrifuge tube as depicted in Table 7, page 19.

In a 96-well plate, 2.5 µl of each reverse transcription product were pipetted into its corresponding well and dispensed with 22.5 µl of preamplification master mix and incubated for 5 minutes at 4°C. The cDNA was amplified in a thermocycler at the conditions shown in Table 16.

Table 16. Thermal cycling conditions for preamplification of cDNA.

Cycle	Temperature	Duration
Hold	95°C	10 min
Hold	55°C	2 min
Hold	72°C	2 min
12 cycles	95°C	15 sec
	60°C	4 min
Hold	99.9°C	10 min
Hold	4°C	∞

After amplification, 75 µl of 0.1x TE buffer pH 8.0 (1x TE diluted with nuclease-free H_2O) was added to each well and cDNAs were transferred to 0.5 ml PCR Clean tubes.

3.2.10.3 Real-time PCR reaction

The real-time PCR reaction was performed to quantify miRNAs using 641 unique assays. The reaction mix was prepared as shown in Table 8, page 20. TaqMan® Array MicroRNA Cards were loaded with 100 µl of the reaction mix for each port, centrifuged and sealed. The quantitative real-time PCR was performed on a 7900HT Fast Real-Time PCR system.

3.2.10.4 Analysis of real-time PCR microRNA array data

Cq was obtained with automatic settings for baseline and threshold detection using SDS and SDS RQ Manager.

MicroRNA assays with the following characteristics were excluded: 1) Cq differences > 1 between replicates (sATII 1 / 2 and pATII 1 / 2, respectively). 2) Cq > 32 (defined as not detectable). Normalized relative quantities (NRQs) of the remaining miRNAs were calculated using global mean normalization. MiRNAs with |fold difference| < 1.5 between the two different preparation methods (sATII vs. pATII) were defined as equally expressed (termed ATII miRNAs) and used for pathway enrichment analysis. MiRNAs with fold difference ≥ 1.5 were defined as upregulated in sATII and fold difference ≤ -1.5 as upregulated in pATII. MiRNAs with Ct > 32 (defined as not detectable) in one of the preparation methods were named as only expressed in the respective other preparation method.

For volcano plots, the fold difference and statistical significance determined by Benjamini-Hochberg (BH)-correction (BH-adjusted p-value) (Benjamini & Hochberg 1995) were analyzed using DataAssist.

3.2.11 Pathway enrichment analysis by Ingenuity® software

The pathway enrichment analysis was performed using the Ingenuity® Pathway Analysis (IPA) module of the Ingenuity® software (Ingenuity® Systems 2012). IPA is based on the Ingenuity® Knowledge Base which is derived from experimentally demonstrated findings published in peer-reviewed journals, curated knowledge (e.g. pathways) and trusted third party databases. The input data set can be interpreted by analyzing networks and canonical pathways. Networks describe the interaction of the different molecules within the input data set. Canonical pathways reveal the biologic functions affected by the input data within well-established metabolic and signaling pathways based on biomedical literature. Canonical pathways are grouped in pathway categories. They cannot be changed by the input data (Ingenuity® Systems 2012).

The data set of ATII miRNAs was uploaded into IPA. Ingenuity® microRNA target filter was applied to restrict mRNA targets to only experimentally observed miRNA-mRNA interactions. These miRNA-mRNA targets were used for pathway enrichment analysis. MiRNA-mRNA pairs with the mRNA participating in a canonical pathway in the Ingenuity® Knowledge Base were identified. The relevance of the association between the data set and a given canonical pathway was analyzed in two ways by Ingenuity®: 1) A ratio of the number of molecules from the data set that map to the pathway divided by the total number of molecules that map to the canonical pathway was determined. 2) Fisher's exact test was used to calculate a p-value determining the probability that the association between the genes in the data set and the canonical pathway is explained by chance alone. The adjustment to multiple testing was performed using BH-correction (BH-adjusted p-value) (Benjamini & Hochberg 1995). An enrichment of target mRNAs in a canonical pathway with BH-adjusted p-values < 0.001 was regarded as significant.

3.2.12 Literature research on autofluorescence based ATII isolation

The following search terms were used to inquire about previous work on autofluorescence based isolation of ATII cells in PubMed (NCBI 2016).

Syntax:

AECII OR AEC2 OR ATII OR AT2 OR alveolar epithelial type II OR alveolar epithelial type 2 OR type II pneumocytes OR type 2 pneumocytes AND autofluorescence.

AECII OR AEC2 OR ATII OR AT2 OR alveolar epithelial type II OR alveolar epithelial type 2 OR type II pneumocytes OR type 2 pneumocytes AND natural fluorescence.

13 scientific articles were found, however, none of these articles reported about autofluorescence based isolation (Rochat et al. 1988; Baker et al. 1992; Pataki et al. 1996; Agarwal et al. 2001; Griese et al. 2001; Kotton et al. 2005; Zander et al. 2006; Loh et al. 2006; Davies et al. 2007; Ravasio et al. 2010; Wu et al. 2013; Xu et al. 2014; Lee et al. 2015).

The last search was performed in July 2016.

4 RESULTS

4.1 Isolation of primary murine ATII cells by sorting

4.1.1 Fluorescence Activated Cell Sorting

Based on previous reports showing autofluorescence of ATII cells (Kim et al. 2005; Cunningham et al. 1994), a method was established to isolate “untouched” ATII cells taking advantage of their autofluorescence characteristic.

Lung single cell suspensions from healthy mice (preparation see 3.2.2, page 25) were subjected to FACS. After exclusion of debris and doublets, the population for sorting was defined as CD45/CD31-APC^{negative} and autofluorescence-FITC^{high} (gating strategy described in 3.2.3, page 27, and shown in Figure 10, upper row). In brief, leukocytes were excluded by CD45- and endothelial cells by CD31-surface markers using the APC-channel for both cell types. ATII cells were isolated from any other contaminating cell types based on their autofluorescence in the FITC-channel.

The reanalysis of the sorted cells showed a homogeneous CD45/CD31^{negative} cell population with high residual autofluorescence (displayed in Figure 10, lower row).

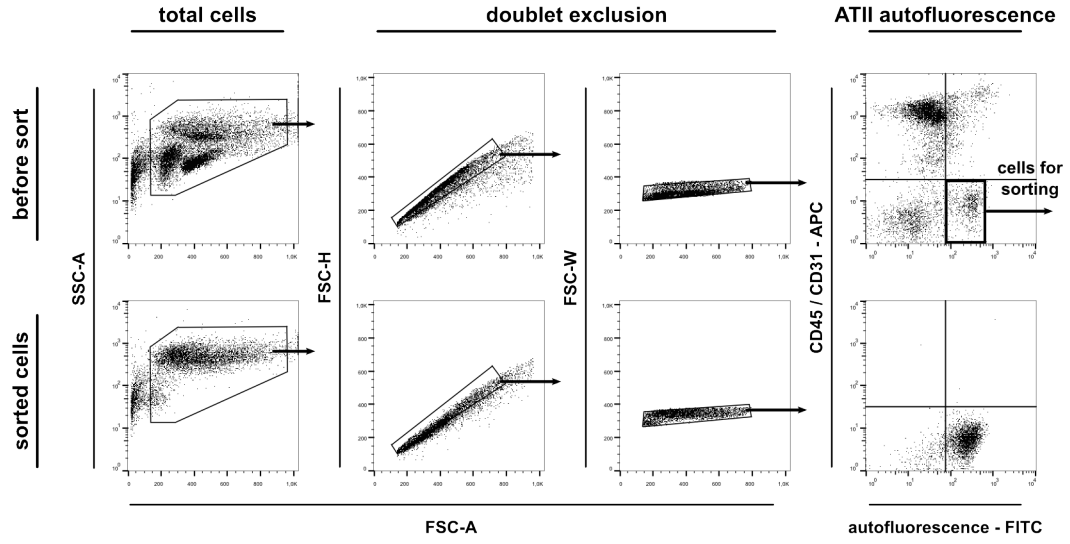

Figure 10. Gating strategy for FACS. Debris was excluded in the FSC-A vs. SSC-A dot plot. Doublets were excluded by increased FSC-A to FSC-H and FSC-W to FSC-A ratio. Population for sorting was defined as high in autofluorescence (measured in the FITC channel) and negative for the surface markers CD45 and CD31 (both measured in the APC-channel). The gating strategy is shown in the upper row. The sorted cell population was reanalyzed with the same settings as illustrated in the lower row. All dot plots are representative of four independent experiments. Each subsequent dot plot only displays cells that have been gated in the previous dot plot.

4.1.2 Confirmation of epithelial and ATII phenotype of sorted primary cells

ATII cells can be distinguished from other cell types within the lung by dark blue inclusion bodies using modified Papanicolaou staining (Dobbs 1990). To confirm ATII phenotype of the isolated cells, modified Papanicolaou staining of cytospin slides was performed. Sorted cells uniformly showed dark blue inclusion bodies characteristic for ATII cell phenotype (Figure 11, right image).

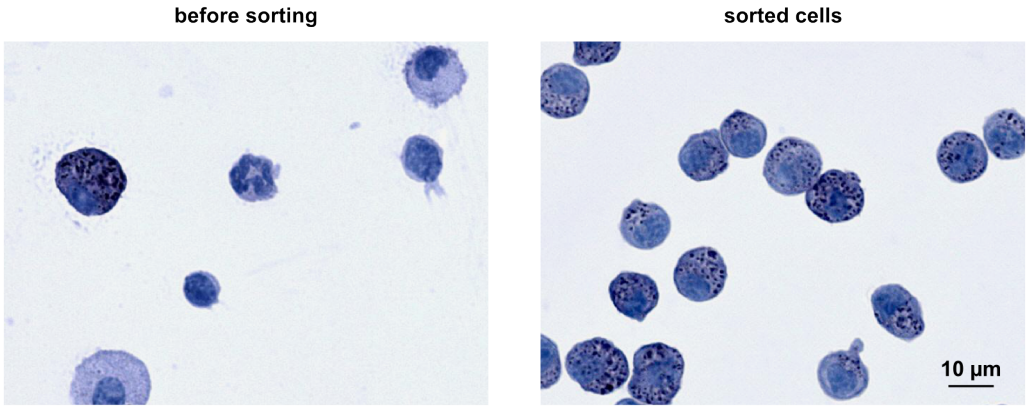

Figure 11. Modified Papanicolaou staining of cytospin prepared slides of whole lung suspension cells (before sorting) and sorted cells. ATII cells were identified by characteristic dark blue inclusion bodies in the cytoplasm. Light microscopic images.

To further certify ATII phenotype, biochemical markers for ATII and non-ATII cells were assessed by immunocytochemistry of cytospin preparations of sorted cells in comparison to whole lung suspension cells. The ATII cell-specific marker prosurfactant protein C (proSP-C) as well as the epithelial cell markers E-Cadherin and pan-cytokeratin were highly expressed in sorted cells (Figure 12 A, lower row, page 37). The leukocyte marker CD45, endothelial cell marker CD31 and mesenchymal cell marker α-SMA were not detectable after sorting. Very few sorted cells were positive for the club cell secretory protein (CCSP) (Figure 12 B, lower row, page 37).

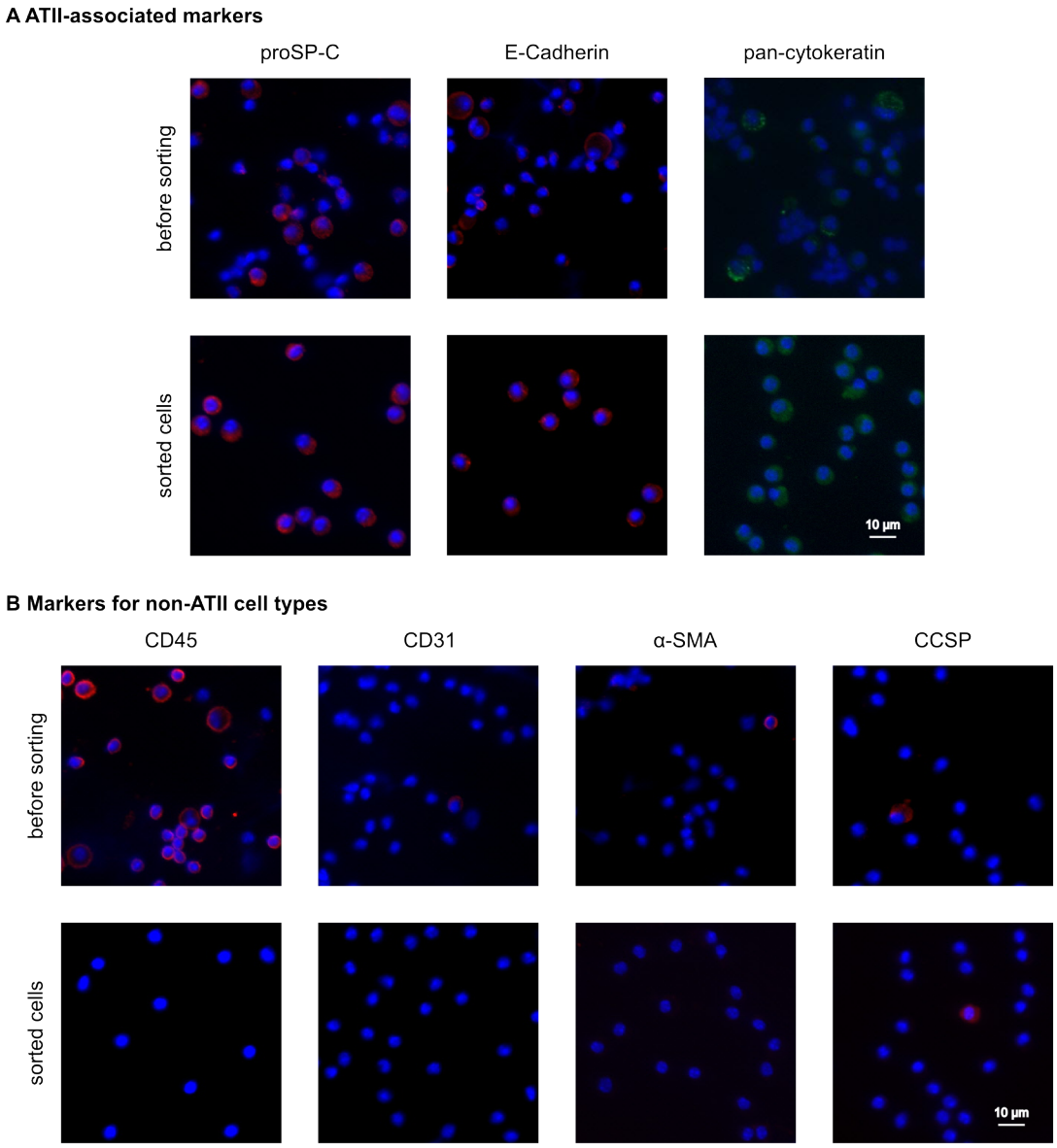

Figure 12. Immunocytochemical staining for ATII-associated and non-ATII phenotypic markers in whole lung suspension cells (before sorting) and sorted cells. A) Cytocentrifuged preparations of whole lung suspension cells and sorted cells were stained with an ATII cell-marker (proSP-C, red fluorescent) and epithelial cell markers (E-Cadherin, red fluorescent, and pan-cytokeratin, green fluorescent). **B)** Cytocentrifuged cells of whole lung suspension cells and sorted cells were tested for markers of the non-ATII cell types leukocytes (CD45, red fluorescent), endothelial cells (CD31, red fluorescent), smooth muscle cells (α-SMA, red fluorescent) and club cells (CCSP, red fluorescent).

4.2 Comparison of primary ATII cells isolated by sorting vs. “panning”

Based on cell morphology and immunocytochemistry the isolated sATII population showed epithelial and ATII phenotypes. In order to determine the advantages and limitations of the newly developed isolation protocol, sATII were compared with an already published isolation method by “panning” (pATII) (Königshoff et al. 2009). PATII have been described to be positive for pan-cytokeratin and SP-C and negative for α-SMA and CD45 (Königshoff et al. 2009).

The two isolation methods were compared based on following criteria: 1) viability and 2) purity. Viability was assessed by PI exclusion from viable cells analyzed by flow cytometry. Purity was compared by two quantitative methods: 1) expression of phenotypic markers examined by flow cytometry and 2) expression of mRNA of phenotypic markers analyzed by RT-qPCR.

4.2.1 Viability of isolated cells

After debris and doublets were eliminated (Figure 13 A, page 39), viable cells were identified as PI negative by flow cytometry (Figure 13 B and C, page 39).

Before isolation, lung single cell suspensions had an average viability above 98%. After isolation, sATII and pATII demonstrated viabilities higher than 95%. The average viability in pATII was slightly higher (96.7%) than in sATII (96.2%).

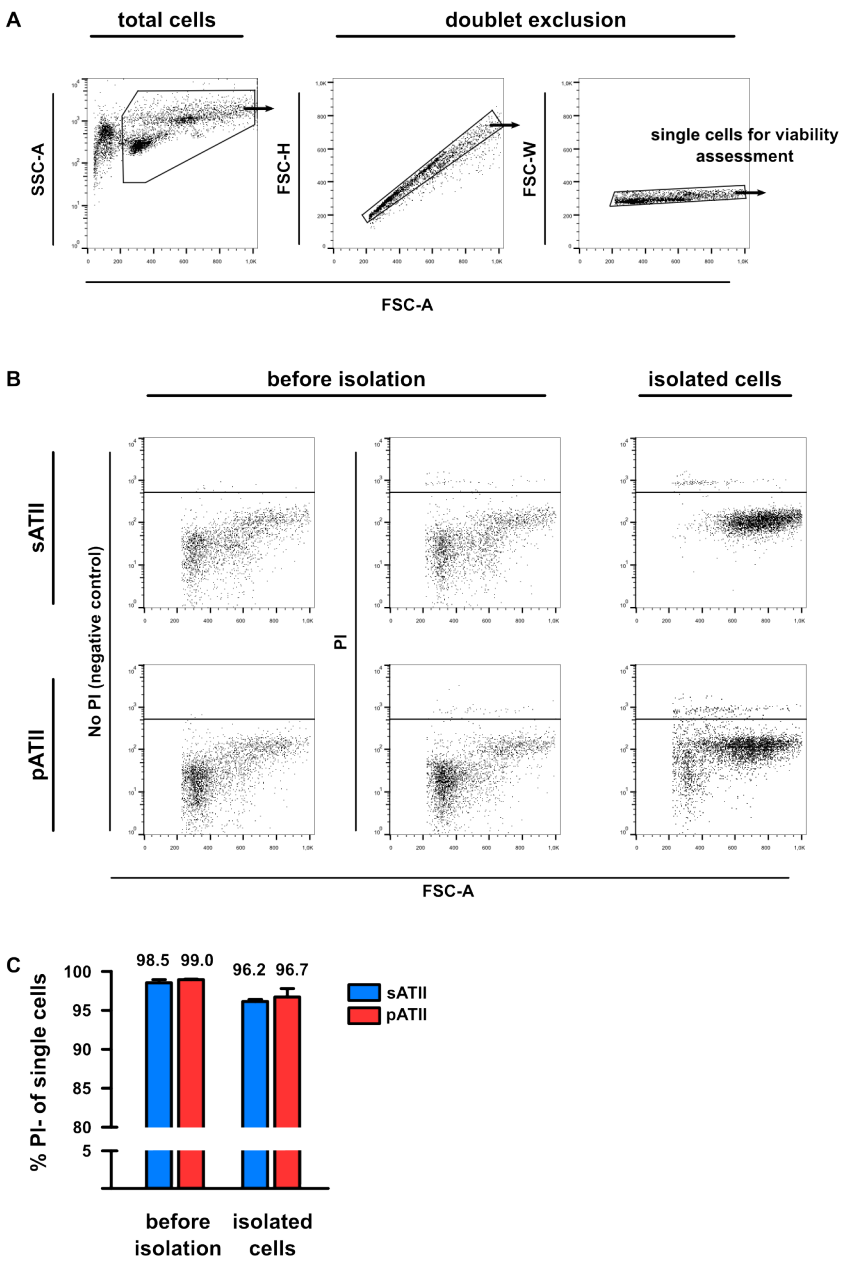

Figure 13. Flow cytometric analysis of viable cells by PI exclusion before and after sorting in the sATII and pATII cell populations. A) Debris and doublets were excluded to obtain single cells for further viability analysis. Each subsequent dot plot only displays cells that have been selected in the previous dot plot. **B)** Whole lung suspensions without PI staining were used as negative control (left panels). Viable cells were identified for sATII (upper row) and pATII (lower row) in the whole lung suspension (before isolation) and isolated cells by PI exclusion (middle and right panels). **C)** Viability of cells before and after isolation. Viable cells were defined as $PI^{negative}$ as shown in B. Each value is the mean of four independent experiments for sATII and two independent experiments for pATII. T-bars show the standard error of mean (SEM).

4.2.2 Purity of isolated cells

4.2.2.1 Expression of phenotypic markers assessed by flow cytometry

Purity of sATII and pATII was quantified by flow cytometric analysis of phenotypic markers for ATII cells and contaminating cell populations.

After exclusion of debris and doublets by FSC-characteristics (Figure 14 A, page 41), cell-specific surface molecules were examined. ATII cells have been described to express major histocompatibility complex (MHC) class II antigens on the cell surface (Cunningham et al. 1994). The MHC II-associated invariant chain CD74 has been shown to be uniformly co-expressed in proSP-C positive, freshly isolated, murine ATII cells (Marsh et al. 2009). As CD74 has also been documented to be highly expressed in primary alveolar macrophages (Takahashi et al. 2009), ATII cells in this analysis were defined as CD45-CD31-APC^{negative} and CD74-FITC^{positive} (Figure 14 B, page 41). Although CD74 is an extracellular epitope, it is quickly internalized when antibodies bind. To identify all CD74-containing cells with certainty, staining was performed intracellularly.

In order to differentiate between contaminating leukocytes and endothelial cells, cells were additionally stained with CD31-PE-antibody which recognizes a different epitope than the CD31-APC-antibody (Chacko et al. 2012). Cells not expressing CD45, CD31 or CD74 were labeled as others (see Figure 14 C, page 41).

Before sorting, the three main cell populations were leukocytes, ATII cells and endothelial cells. After isolation, sATII showed an enrichment of ATII cells from 21.0% before sorting to 98.4% in the sorted cells while pATII demonstrated an increase from 24.0% to 72.6%. Of note, endothelial cells in pATII showed a relative increase from 6.69% before sorting to 12.3% in sorted cells (data shown in Figure 14 C, page 41).

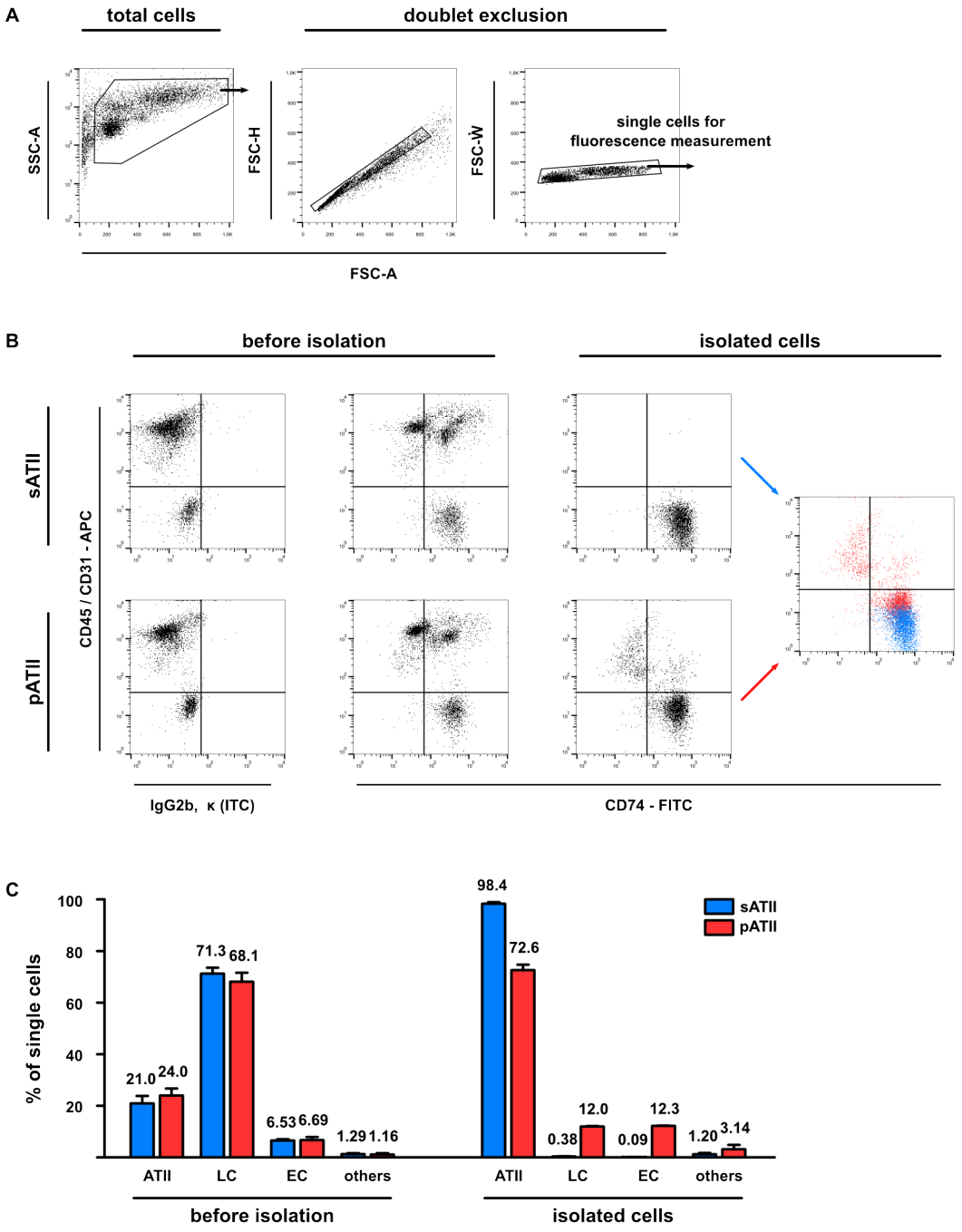

Figure 14. Flow cytometric quantification of purity in sATII and pATII preparations. **A)** Debris and doublets were excluded to obtain single cells for prospective analysis of purity. Each subsequent dot plot only displays cells that have been selected in the previous dot plot. **B)** Dot plots of cells before and after isolation stained with CD45-APC, CD31-APC and CD74-FITC-antibodies (middle and right panels) or IgG2b, κ (ITC) (left panels). Right panel shows an overlay of sATII and pATII sorted cell populations. Dot plots are representative of four independent experiments for sATII and two independent experiments for pATII. C) Cell composition before and after isolation. ATII cells were defined as CD45/CD31-APC^{negative} CD74-FITC^{positive}, leukocytes as CD45/CD31-APC^{positive} without CD31-PE^{positive} cells, endothelial cells as CD31-PE^{positive} and others as CD45/CD31-APC^{negative} and CD74-FITC^{negative}. Each value is the mean of four independent experiments for sATII and two independent experiments for pATII. T-bars show SEM.

4.2.2.2 MRNA expression of phenotypic markers assessed by qPCR

The difference in purity between sATII and pATII was further evaluated by mRNA expression levels of phenotypic markers (Figure 15). Fold changes in mRNA expression were analyzed by RT-qPCR normalized to *Hprt* and relative to the ATII cell marker *Sftpc* in the sATII population.

Both isolated cell populations showed high expression of the ATII cell marker *Sftpc* (mean Cq value of 11.6 ± 0.97 in sATII and 13.6 ± 0.45 in pATII). Likewise, markers associated with epithelial and ATII identity *Sftpa1*, *Cd74*, *Aqp5*, *Cdh1* and *Tjp1* were highly expressed in both sATII and pATII.

However, markers for the contaminating cell populations smooth muscle cells (*Acta2*), endothelial cells (*Pecam1*, protein name CD31) and leukocytes (*Ptprc*, protein name CD45) were clearly expressed at lower levels in sATII as compared to pATII.

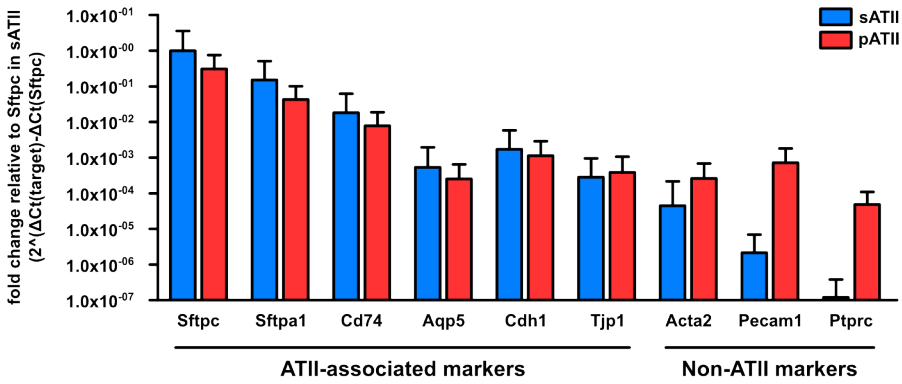

Figure 15. MRNA expression of markers associated with ATII cells and markers for non-ATII cell types. Total RNA from isolated cells by sorting (sATII, blue bars) and "panning" (pATII, red bars) was used for mRNA quantification by RT-qPCR. ATII-associated markers (*Sftpc*, *Sftpa1*, *Cd74*, *Aqp5*, *Cdh1* and *Tjp1*) as well as markers of the non-ATII cell types smooth muscle cells (*Acta2*), endothelial cells (*Pecam1*) and leukocytes (*Ptprc*) were determined. Target and *Sftpc* mRNA were normalized to *Hprt* and fold changes are displayed relative to mRNA expression of *Sftpc* in sATII. Each value is the mean of four independent experiments and two technical replicates. T-bars show the maximum expression.

4.3 MiRNA profiling of ATII cells

4.3.1 Overview

For miRNA profiling of ATII cells, a cut-set of miRNAs obtained from ATII cells isolated by the two preparation methods (sorting and "panning") was used in order to reduce potential method-related bias. Two samples of sATII and pATII, respectively, were eligible for miRNA profiling as assessed by RNA integrity and RNA quantity measurements. 111 miRNAs were expressed at similar levels (|fold difference| < 1.5) in sATII and pATII, termed ATII miRNAs. Using Ingenuity® target filter, 40 ATII miRNAs were identified with 662 previously experimentally validated mRNA targets. 38 of these

miRNAs had 343 mRNA targets in the canonical pathway library of Ingenuity®. Of note, 19 of these 38 miRNAs binding in a canonical pathway had 21 mRNA targets in the TGF-beta signaling pathway and 16 of these 19 miRNAs were expressed above median level in the ATII miRNA expression profile (see Figure 16).

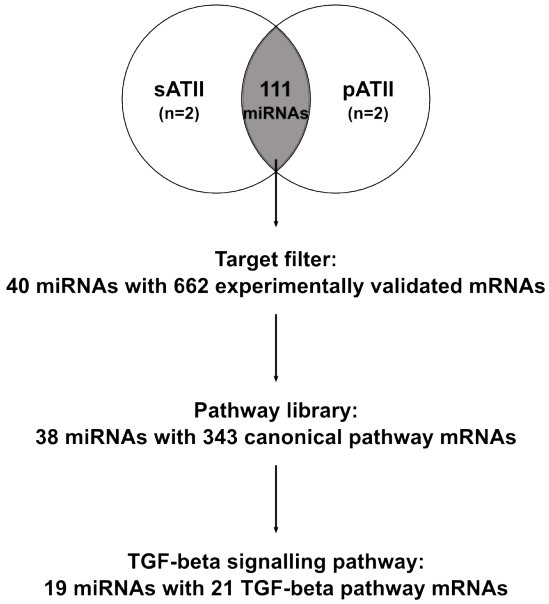

Figure 16. Overview of miRNA results. ATII miRNAs were defined as similar expressed (|fold difference| < 1.5) in sATII and pATII. Target filter and pathway library modules of Ingenuity® were used to filter ATII miRNAs with experimentally validated and canonical pathway mRNAs. Then, ATII miRNAs involved in TGF-beta signaling were identified.

4.3.2 Assessment of RNA integrity and RNA quantity

Total RNA of sATII was isolated from five samples of two independent experiments. Assessment of RNA integrity by bioanalyzer showed high quality for two samples of two independent experiments with clear ribosomal bands for the 18S and 28S subunits in the electropherogram and RIN of 8.2 (termed sATII 1) and 7.5 (termed sATII 2) (Figure 17, page 44, upper row). These two samples were further processed, while the other three sATII RNA samples were excluded due to bands of degradation products on the electropherogram and/or low RIN.

Total RNA of pATII was isolated from two samples of one experiment. Both samples passed quality control determined by electropherogram as well as RIN values of 7.3 (termed pATII 1) and 6.6 (termed pATII 2) (Figure 17, page 44, lower row).

SATII 1 / 2 and pATII 1 / 2 showed sufficient 260/280 ratios and RNA quantities above 350 ng in the spectrophotometer (Table 17, page 44). These four samples were used for reverse transcription and miRNA profiling.

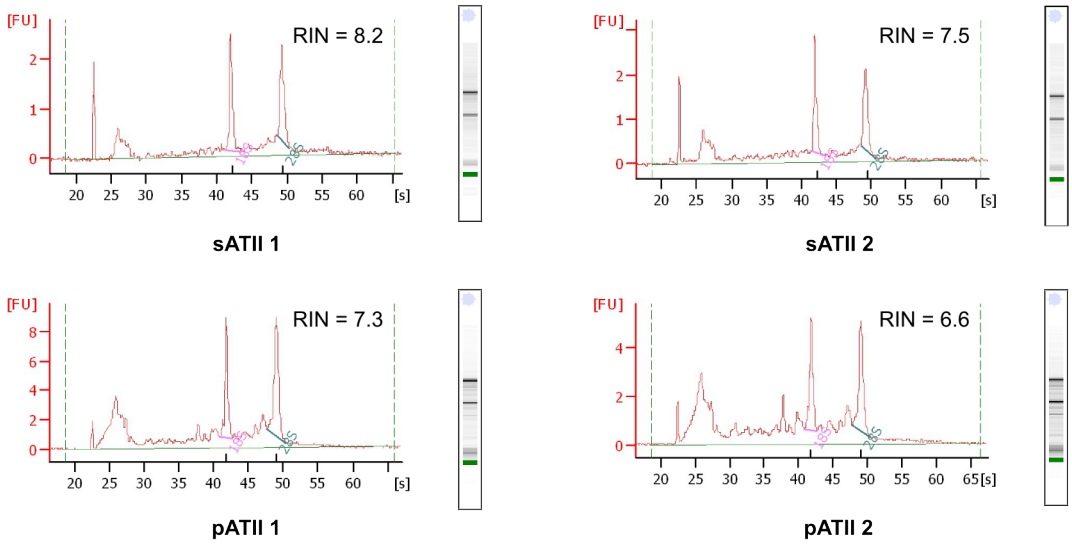

Figure 17. Electropherogram and RIN values for RNA samples used for further analysis. Total RNA of sATII and pATII samples were analyzed using bioanalyzer. Electropherogram depicts RNA bands with peaks for 18S and 28S ribosomal subunits marked in purple / green, respectively. RIN values were assessed for each sample. Shown are the four samples which were further processed. Three samples of sATII were discarded due to low RNA quality.

Table 17. RNA concentration, total RNA quantity and 260/280 ratio.

Sample	RNA concentration (ng/µl)	Total RNA quantity (ng)	260/280 ratio
sATII 1	46.05	368.40	1.87
sATII 2	46.67	373.36	1.85
pATII 1	44.34	354.72	1.92
pATII 2	44.45	355.60	1.99

4.3.3 MiRNA expression profile of ATII cells

MiRNA expression was assessed using TaqMan® MicroRNA array microfluidic cards including 641 assays for mature murine miRNAs based on miRBase v15 (miRbase 2016). A total of 316 miRNAs were expressed in sATII and/or pATII.

111 miRNAs were expressed at equal levels in sATII and pATII (|fold difference| < 1.5) and termed ATII miRNAs (Figure 18, page 45; for a list of ATII miRNAs with NRQ-values see Appendix, Table 22, page 72). Within the ATII miRNAs, 13 miRNAs were expressed at very high levels (> 20x median), 41 miRNAs were expressed at high levels (20x median > miRNA > median), 45 miRNAs were expressed at moderate levels (median > miRNA > 0.05x median) and 12 miRNAs were expressed at low levels (< 0.05x median). The 111 ATII miRNAs were used for pathway enrichment analysis.

182 miRNAs were differentially expressed in the two preparation methods (|fold difference| ≥ 1.5). 121 miRNAs were upregulated in sATII vs. pATII (fold difference ≥

1.5) and 61 miRNAs were upregulated in pATII vs. sATII (fold difference ≤ -1.5). The differentially expressed miRNAs were further analyzed using volcano plot (Figure 19, page 46). MiRNAs with |fold difference| > 4 were defined as highly differentially expressed. MiRNAs with a high probability to be differentially expressed were determined by setting the BH-adjusted p-value < 0.01. In pATII 22 miRNAs and in sATII one miRNA were highly differentially expressed. Three miRNAs of the highly differentially expressed miRNAs in pATII had a high probability to be differentially expressed: Mus musculus (mmu)-miR-126-3p, mmu-miR-10a and mmu-miR-29c (Figure 19, page 46, upper left quadrant).

Three miRNAs were only expressed in sATII and 20 miRNAs were only expressed in pATII (outlined in Table 18, page 46). MiRNAs with Ct > 32 were regarded as not expressed (compare 3.2.10.4, page 33).

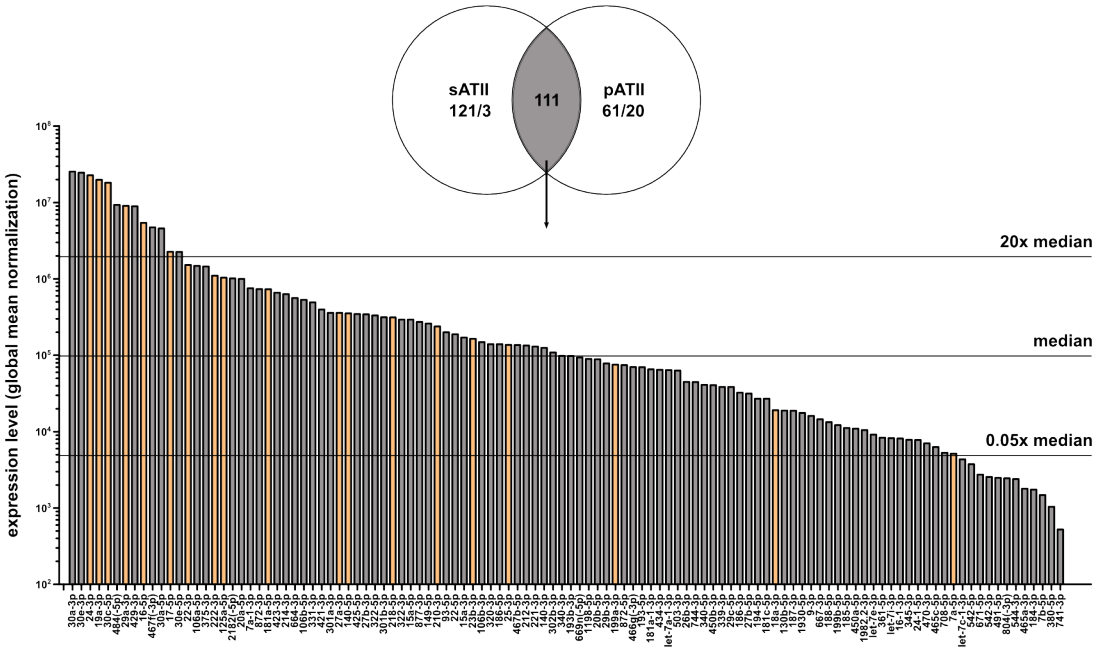

Figure 18. MiRNA expression profile of ATII cells. 111 miRNAs were expressed at similar levels (|fold difference| < 1.5) in sATII and pATII (termed ATII miRNAs). ATII miRNAs are displayed by decreasing expression level (analyzed by global mean normalization). 13 miRNAs were expressed at very high levels (> 20x median), 41 miRNAs were expressed at high levels (20x median > miRNA > median), 45 miRNAs were expressed at moderate levels (median > miRNA > 0.05x median) and 12 miRNAs were expressed at low levels (< 0.05x median). 19 miRNAs were found to target molecules within the TGF-beta signaling pathway (highlighted in yellow, discussed in 4.3.5, page 50). Only miRNA assays with complete sequence complementarity to mouse miRNAs were investigated.

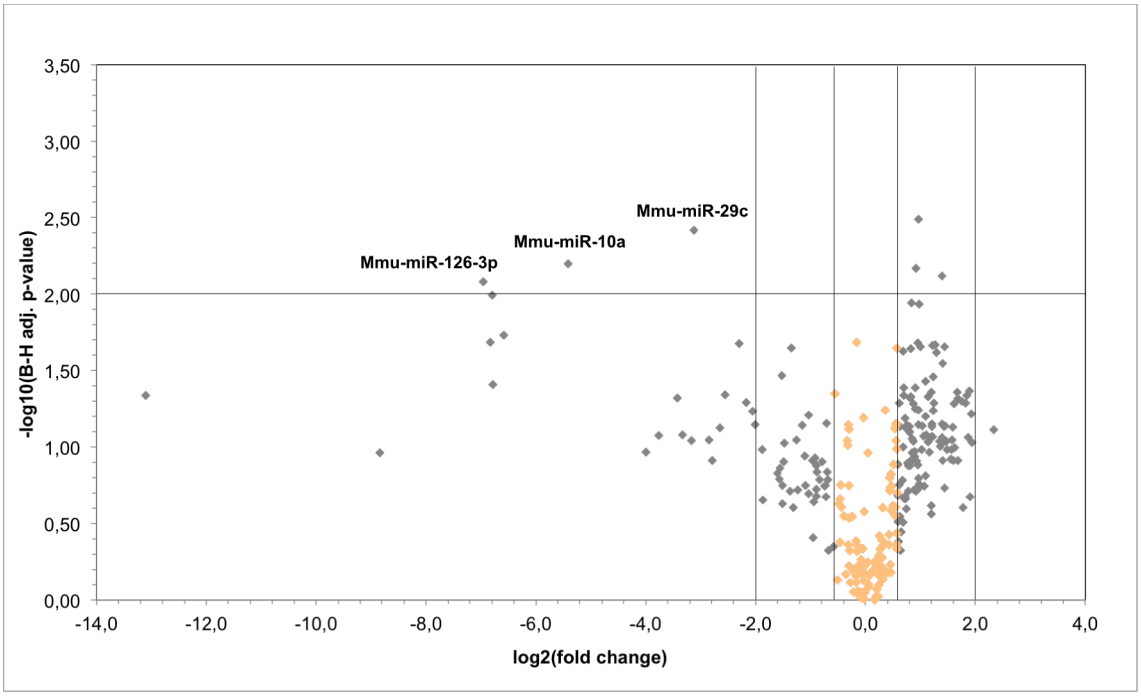

Figure 19. Volcano plot of miRNAs expressed in sATII and pATII. 182 miRNAs were differentially expressed (|fold difference| ≥ 1.5) (illustrated in grey). 121 miRNAs were upregulated in sATII (fold difference ≥ 1.5) and 61 miRNAs in pATII (fold difference ≤ -1.5). Mmu-miR-126-3p, mmu-miR-10a and mmu-miR-29c were highly differentially expressed (fold difference > -4) with a high probability to be differentially expressed (BH-adjusted p-value < 0.01). The 111 ATII miRNAs with similar expression in sATII and pATII are highlighted in yellow.

Table 18. MiRNAs only expressed in one of the isolation methods. Three miRNAs were only expressed in sATII and 20 miRNAs were only expressed in pATII.

MiRNA (mmu) only expressed in sATII	MiRNA (mmu) only expressed in pATII
mmu-miR-423-5p	mmu-miR-1903
mmu-miR-1981	mmu-miR-701
mmu-miR-376a#	mmu-miR-137
	mmu-miR-1960
	mmu-miR-135a
	mmu-miR-1194
	mmu-miR-335-3p
	mmu-miR-342-5p
	mmu-miR-511
	mmu-miR-202-3p
	mmu-miR-467c
	mmu-miR-467d
	mmu-miR-677
	mmu-miR-142-5p
	mmu-miR-1195
	mmu-miR-10b
	mmu-miR-1940
	mmu-miR-1941-5p
	mmu-miR-551b-3p
	mmu-miR-338-5p

4.3.4 MRNA target identification and pathway enrichment analysis

In the next step, miRNA-controlled pathways of ATII cell homeostasis were identified *in silico*. In order to decrease potential method-related bias, the 111 ATII miRNA expressed at similar levels in sATII and pATII were used for IPA (Ingenuity® Systems 2012). Ingenuity® microRNA target filter was restricted to experimentally validated miRNA-mRNA pairs and identified 40 miRNAs with 662 mRNA targets. In the Ingenuity® Knowledge Base, 38 of these miRNAs were associated with 343 mRNAs within the canonical pathway library (the miRNA selection strategy is outlined in Figure 16, page 43).

The pathways with significant enrichment of target mRNAs were determined by BH-adjusted p-value < 0.001. 143 signaling, but only two metabolic pathways showed significant enrichment. The top 20 signaling and the top 20 metabolic pathways are depicted in Figure 20, page 48. Of the top 20 signaling pathways nine have already been associated with fibrosis and/or EMT (Figure 20 A, page 48, yellow bars) including "G1/S checkpoint regulation in the cell cycle" (Cui et al. 2013), "cyclins and cell cycle regulation" (Cheung et al. 2015; Ju et al. 2014), "phosphoinositide 3-kinase (PI3K)/protein kinase B (AKT) signaling" (Xu et al. 2015), "p53 signaling" (Lenfert et al. 2015; X. Yang et al. 2015), "phosphatase and tensin homolog (PTEN) signaling" (H.-Y. Zhang et al. 2014), "hepatic fibrosis" (Bi et al. 2012), "Insulin-like growth factor 1 (IGF-1) signaling" (Nurwidya et al. 2014; Liao et al. 2014), "integrin-linked kinase (ILK) signaling" (J. Yang et al. 2015) and "TGF-beta signaling" (described in 1.3.4, page 13). Nine pathways were related to cancer (Figure 20 A, page 48, green bars). The pathway categories with the most significant ATII miRNA target enrichment included "cancer", "cellular growth, proliferation and development" as well as "cytokine signaling" (Table 19, page 48).

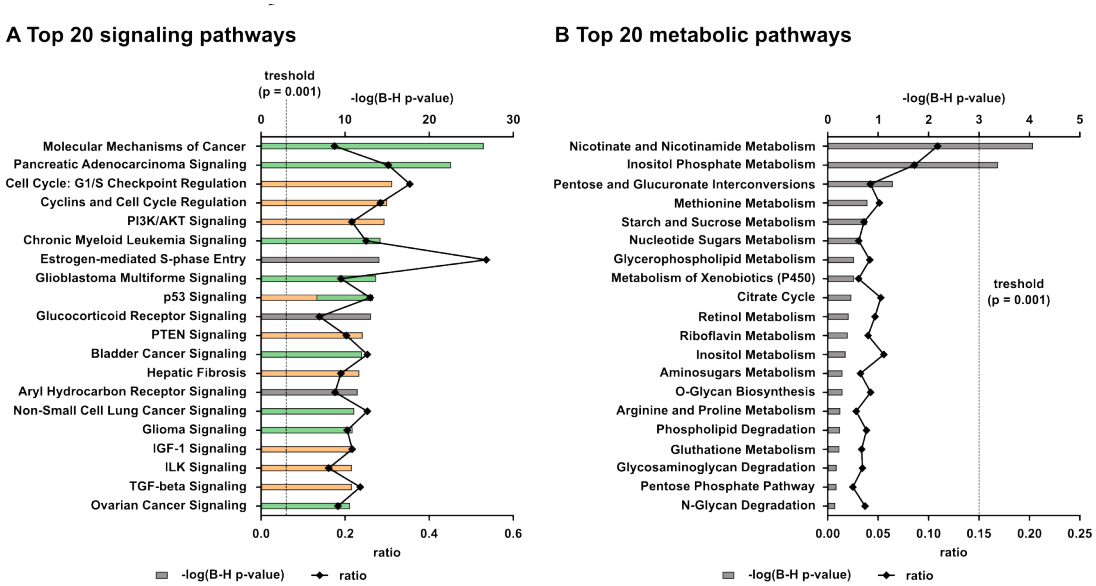

Figure 20. Top 20 canonical signaling and metabolic pathways. A) The top 20 signaling pathways are shown. Pathways associated with fibrosis and/or EMT are highlighted in yellow, pathways associated with cancer are featured in green. B) The top 20 metabolic pathways are displayed. Two markers for the significance of the association between the data set and the canonical pathway are shown. The common logarithm of the BH-adjusted p-value is depicted as bars. Threshold for significant enrichment was defined by BH-adjusted p-value < 0.001 (illustrated as a dashed line). The ratio of the number of molecules from the data set that map to the pathway divided by the total number of molecules that map to the canonical pathway is displayed as diamonds.

Table 19. Categories of pathways with significant ATII miRNA target enrichment. Classification of pathways was performed based on Ingenuity®'s pathway library.

Pathway category	Pathways per category	Examples for pathways within the category
Cancer	30	Small and non-small cell lung cancer, p53
Cellular growth, proliferation and development	28	PI3K/Akt, ILK, TGF-β, Integrin, FAK, mTOR
Cytokine signaling	27	Chemokine, IL-6, IL-8, IL-9, IL-10, IL-15, IL-17, IL-22, TNFR1
Cellular immune response	22	CXCR4, HMGB1, NF-κB, dendritic cell maturation
Growth factor signaling	21	IGF-1, EGF, GM-CSF, VEGF, FGF, PDGF
Apoptosis signaling	16	PTEN, death receptor, 14-3-3, JAK/Stat, tight junction signaling
Cell cycle regulation	13	G1/S checkpoint regulation, G2/M DNA damage checkpoint regulation
Intracellular and 2nd messenger	13	Glucocorticoid receptor, ERK/MAPK, Rac, Rho, Gα12/13, PAK
Neurotransmitters and other nervous system	13	Neuregulin, ErbB, Ephrin receptor, axonal guidance
Organismal growth and development	13	Stem cell pluripotency, HGF, BMP, Wnt/β-catenin
Disease-specific pathways	9	Hepatic fibrosis, rheumatoid arthritis,

		Huntington's disease
Cardiovascular signaling	7	Cardiac hypertrophy, atherosclerosis, thrombin signaling
Cellular stress and injury	6	HMGB1, HIF1α, p70S6K
Humoral immune response	5	CD40, IL-4, B cell receptor signaling
Nuclear receptor signaling	5	PPARα/RXRα activation, PPAR, RAR activation, VDR/RXR activation
Pathogen-influenced	3	LPS-stimulated MAPK signaling
Transcriptional regulation	2	Role of NANOG and Oct4 in mammalian embryonic stem cell pluripotency
Xenobiotic metabolism	1	Aryl hydrocarbon receptor signaling
Metabolism of cofactors and vitamins	1	Nicotinate and nicotinamide metabolism
Metabolism of complex lipids	1	Inositol phosphate metabolism

Next, upstream regulators were investigated for all 662 mRNAs that have been identified as experimentally validated targets of 40 miRNAs using Ingenuity® (Ingenuity® Systems 2012). Upstream regulators include transcription factors, miRNAs and any other molecule that affects the expression of other molecules. Thus, the biological activities controlled by the input data can be assessed. The top 20 upstream regulators are shown in Table 20. The top five consisted of three miRNAs (miR-16-5p, miR-30c-5p and miR-302d-3p) and two growth factors (TGFB1 and epithelial growth factor (EGF)). These findings are endorsed by the fact that miR-16-5p and miR-30c-5p had very high expression levels (> 20x median) in the ATII miRNA expression profile (Figure 18, page 45).

Table 20. Top 20 upstream regulators.

#	Upstream Regulator	Molecule Type	p-value of overlap
1	miR-16-5p (and other miRNAs w/seed AGCAGCA)	mature miRNA	6.62E-82
2	miR-30c-5p (and other miRNAs w/seed GUAAACA)	mature miRNA	6.88E-47
3	TGFB1	growth factor	1.70E-43
4	miR-302d-3p (and other miRNAs w/seed AAGUGCU)	mature miRNA	2.45E-41
5	EGF	growth factor	1.29E-40
6	beta-estradiol	chemical - endogenous mammalian	3.34E-38
7	TP53 (includes EG:22059)	transcription regulator	1.36E-37
8	ERBB2	kinase	2.23E-36
9	tretinoin	chemical - endogenous mammalian	3.58E-36
10	IGF1	growth factor	5.23E-36
11	TNF	cytokine	1.69E-34
12	EGFR	kinase	8.40E-34

13	FGF2	growth factor	1.53E-33
14	LY294002	chemical - kinase inhibitor	1.69E-32
15	PTEN	phosphatase	2.01E-31
16	PD98059	chemical - kinase inhibitor	7.22E-31
17	Pdgf (complex)	complex	4.67E-30
18	E2F1	transcription regulator	6.27E-30
19	HRAS	enzyme	8.22E-30
20	phorbol myristate acetate	chemical drug	1.3E-29

4.3.5 ATII miRNA regulation of the TGF-beta signaling pathway

TGF-beta signaling pathway is a canonical pathway with a crucial role in EMT (described in 1.3.4, page 13). In the present study, this pathway showed a strong regulation by the identified ATII miRNAs. 19 of the 38 ATII miRNAs binding in a canonical pathway were identified within the TGF-beta signaling pathway, of which 16 miRNAs were expressed above median level in the ATII miRNA expression profile (Figure 18, page 45, yellow bars). MiRNAs showed 21 targets on different functional levels from extracellular ligand to target genes (Figure 21 and Table 21, page 51). 10 miRNAs targeted more than one TGF-beta pathway component and 11 components were targeted by more than one miRNA with SMAD3 being targeted by four miRNAs. The important role of TGF-beta signaling is endorsed by the fact that TGF-beta is one of the top five upstream regulators.

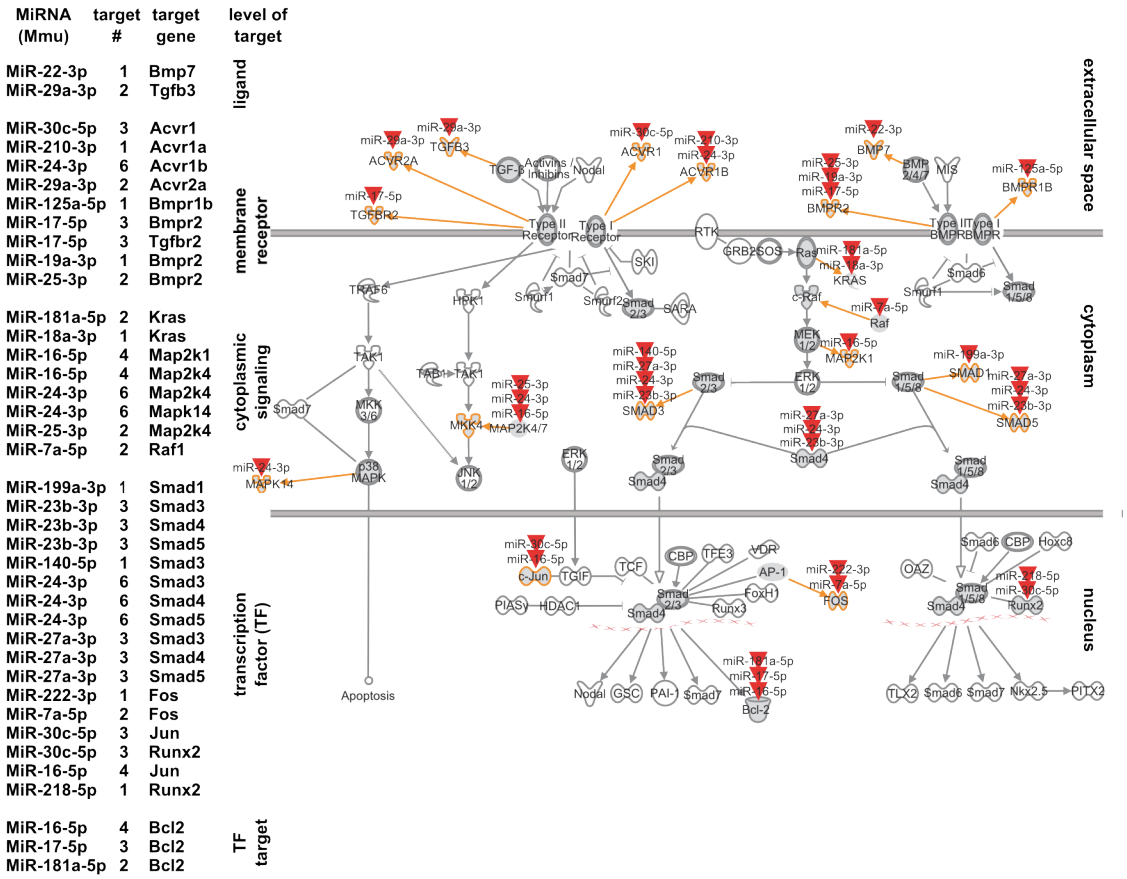

Figure 21. ATII miRNA targets within the canonical TGF-beta signaling pathway. On the right, graphical representation of the TGF-beta signaling pathway from the Ingenuity® pathway library is shown. Red arrows indicate ATII miRNAs. The pathway components are represented as nodes. Bold highlights protein families or complexes. The orange outline marks the family members or complex partners that are targeted by ATII miRNAs. The arrows show the biological relationship of the pathway components. On the left, ATII miRNAs, the number of targets, their target genes and the functional level of the target are listed. For more information see **Table 21**.

Table 21. MiRNAs targeting TGF-beta pathway components.

MiRNA name	MiRBase MIMAT ID	# of targets	Experimental observation of miRNA seed-target interaction (PMID)	Target gene	Level of target
Mmu-miR-22-3p	0000531	1	19011694	BMP7	Extracellular ligand, growth factor
Mmu-miR-29a-3p	0000535	2	19342382	TGFB3	
Mmu-miR-30c-5p	0000514	3	18258830	ACVR1	Plasma membrane receptor, kinase
Mmu-miR-24-3p	0000219	6	17906079	ACVR1B	
Mmu-miR-210-3p	0000658	1	19520079	ACVR1B	
Mmu-miR-29a-3p	0000535	2	19342382	ACVR2A	
Mmu-miR-125a-5p	0000135	1	19738052	BMPR1B	
Mmu-miR-19a-3p	0000651	1	19390056	BMPR2	

Mmu-miR-25-3p	0000652	2	19390056	BMPR2	
Mmu-miR-17-5p	0000649	3	19390056	BMPR2	
Mmu-miR-17-5p	0000649	3	20709030	TGFBR2	
Mmu-miR-18a-3p	0004626	1	19372139	KRAS	Cytoplasmic signaling, enzyme
Mmu-miR-181a-5p	0000210	2	20080834	KRAS	
Mmu-miR-16-5p	0000527	4	20065103	MAP2K1	Cytoplasmic signaling, kinase
Mmu-miR-16-5p	0000527	4	19861690	MAP2K4	
Mmu-miR-24-3p	0000219	6	19861690	MAP2K4	
Mmu-miR-25-3p	0000652	2	19861690	MAP2K4	
Mmu-miR-24-3p	0000219	6	19502786	MAPK14	
Mmu-miR-7a-5p	0000677	2	19072608	RAF1	
Mmu-miR-199a-3p	0000230	1	19251704	SMAD1	Transcription factor
Mmu-miR-23b-3p	0000125	3	19582816	SMAD3	
Mmu-miR-24-3p	0000219	6	19582816	SMAD3	
Mmu-miR-27a-3p	0000537	3	19582816	SMAD3	
Mmu-miR-140-5p	0000151	1	20071455	SMAD3	
Mmu-miR-23b-3p	0000125	3	19582816	SMAD4	
Mmu-miR-24-3p	0000219	6	19582816	SMAD4	
Mmu-miR-27a-3p	0000537	3	19582816	SMAD4	
Mmu-miR-23b-3p	0000125	3	19582816	SMAD5	
Mmu-miR-24-3p	0000219	6	19582816	SMAD5	
Mmu-miR-27a-3p	0000537	3	19582816	SMAD5	
Mmu-miR-7a-5p	0000677	2	17028171	FOS	
Mmu-miR-222-3p	0000670	1	20299489	FOS	
Mmu-miR-16-5p	0000527	4	18362358	JUN	
Mmu-miR-30c-5p	0000514	3	18668040	JUN	
Mmu-miR-30c-5p	0000514	3	21628588	RUNX2	
Mmu-miR-218-5p	0000663	1	21628588	RUNX2	
Mmu-miR-16-5p	0000527	4	18449891	BCL2	Transcription factor target, transporter
Mmu-miR-17-5p	0000649	3	19666108	BCL2	
Mmu-miR-181a-5p	0000210	2	20204284	BCL2	

5 DISCUSSION

5.1 Novel ATII cell isolation procedure by sorting based on their autofluorescence

5.1.1 Rationale for development of sorting procedure

Understanding of the pathways regulating the diverse functions of ATII cells remains highly elusive. This is hardly surprising since *in vitro* analyses of ATII cells have been so far challenging. First, no cell line exists that represents the full range of ATII cell functions. Second, primary ATII cells in culture change rapidly their phenotype. It is possible that this transformation represents their behavior *in vivo*, when changes of environmental factors occur: 1) ATII cells provide alveolar repair presumably by transforming to ATI cells (Uhal 1997; Fehrenbach 2001). 2) ATII cells differentiate to mesenchymal cells by EMT (Willis et al. 2005).

Therefore, freshly isolated, primary ATII cells are necessary to explore the full range of ATII cell functions. However, the isolation of primary cells with high viability and purity remains challenging. ATII cells were first isolated by Kikkawa and Yoneda in 1974 from rabbits using Ficoll density gradient centrifugation after barium loading of macrophages (Kikkawa & Yoneda 1974). Since then, a variety of species has been used to purify ATII cells such as rats (Mason & Williams 1977; Douglas & Farrell 1976), hamsters (Myles et al. 1989), guinea pigs (Sakamoto et al. 2001), fetal (Ballard et al. 1986) and adult human lungs (Robinson et al. 1984). From mice, ATII cells have been isolated by numerous methods (see below).

The present study focused on the isolation of ATII cells from C57BL/6 mice, because this strain is commonly used as a model animal for ATII-relevant diseases, especially IPF. Fibrotic response to bleomycin was documented to be high in C57BL/6 in contrast to a low response in BALB/c (Schrier et al. 1983).

Until today, many investigators have used variants of a common method to prepare a single cell suspension from murine lungs that optimizes prospective ATII isolation (Rice et al. 2002; Königshoff et al. 2009; Gereke et al. 2012; Messier et al. 2012). The protocol is based on the report of Corti et al. published in 1996 (Corti et al. 1996). The procedure was also used for the preparation of lung single cell suspensions in the present study with few alterations. Important steps include the perfusion of lungs for mechanical removal of blood cells, enzymatic and mechanical dissociation of parenchymal lung cells, agarose instillation and subsequent filtering.

For enzymatic digestion dispase was chosen. This enzyme specifically cleaves type IV collagen and fibronectin present within the ATII basement membrane (Stenn et al. 1989). Therefore, dispase is possibly more specific in releasing epithelial cells than other proteases while maintaining viability and cell characteristics (Corti et al. 1996). Agarose was instilled following enzyme placement to minimize Agarose-sensitive club cells (Harrison et al. 1995; Corti et al. 1996). Bronchoalveolar lavage was not performed as it could lead to dilution of dispase, diminishing enzyme activity (Corti et al. 1996), and further to lung injury with destruction and/or activation of AT II cells.

In contrast to preparation of single cell suspension, no consensus exists on a protocol for the separation of ATII cells from the other lung cell populations in mice. Until now, many different procedures have been described to isolate ATII cells from mice including magnetic bead separation (Messier et al. 2012; Corti et al. 1996), “panning” using antibody-coated cell culture dishes (Rice et al. 2002; Königshoff 2009; Königshoff et al. 2009) and FACS (Fujino, Ota, Takahashi, et al. 2012; Gereke et al. 2012). ATII cells are difficult to isolate in high purities, because, first, extracellular ATII-specific markers for mice are rare and, second, labeling could change the activation status of purified cells. A combination of epithelial cell adhesion molecule (EpCAM) and T1α protein antibody staining was used to isolate ATII cells by FACS as the $EpCAM^{high}/T1\alpha^{negative}$ subpopulation in humans with 94.0% of purified cells expressing proSP-C (Fujino, Kubo, et al. 2012). However, it is assumed that EpCAM is involved in diverse intracellular processes such as cell signaling, migration, differentiation and proliferation (Trzpis et al. 2007). Monoclonal antibodies to EpCAM were described to induce antibody-dependent cellular cytotoxicity in colorectal cancer therapy (Flieger et al. 2001). Antibody to CD74, which was recently documented as an ATII-specific marker (Marsh et al. 2009), stimulated the cleavage of the CD74 cystolic fragment inducing NF-ƙB activation (Starlets et al. 2006). Therefore, a positive selection of ATII cells carries the risk of activating cellular pathways. Gereke et al. described a negative isolation method by FACS using SSC^{high} as the distinct property of ATII cells and labeling other cell types with fluorescent antibodies (Gereke et al. 2007; Gereke et al. 2009; Gereke et al. 2012). In a recent report describing the exact isolation procedure, the purity was reported to be variable with 92 ± 5% and a viability of ~ 90% (Gereke et al. 2012). In the present study, an isolation procedure to negatively enrich “untouched” ATII cells was aimed for in order to obtain a population of highly pure and viable ATII cells for prospective miRNA profiling.

For this purpose, a new method to isolate ATII cells from mice was developed based on the autofluorescence characteristic of ATII cells. This feature has been described previously. Murine ATII cells characterized as $CD45/CD31/Sca\text{-}1/CCSP^{negative}$ and SP-

C^{positive} showed high autofluorescence (Kim et al. 2005). A population of alkaline phosphatase^{positive} and lamellar bodies^{positive} cells isolated from human lungs has been reported to display autofluorescence, which, however, is less intense than in the purified alveolar macrophage population (Cunningham et al. 1994). This is in concordance to the findings in the present study that there existed a CD45^{positive} population with slightly higher autofluorescence than the ATII cell population, which likely represented macrophages.

Autofluorescence arises from the presence of endogenous fluorophores in cells and extracellular matrix. Fluorophores are substances which emit light after absorption of light. Cellular autofluorescence emerges mainly from the metabolic coenzymes reduced nicotinamide adenine dinucleotide (NADH) and flavin adenine dinucleotide (FAD), whose natural fluorescence has been used for evaluation of metabolic activities (Heikal 2010). Further, porphyrins, which are present in hemoglobin and chlorophyll, and aromatic amino acids exhibit natural fluorescence (Monici 2005).

In ATII cells, different fluorophores could contribute. First, ATII cells have high metabolic activity due to surfactant production such that a high amount of metabolic enzymes is present in these cells (Fehrenbach 2001). Second, hemoglobin has been found in primary ATII cells isolated from normal rat and mouse lungs. The function of hemoglobin in these cells is still unknown (Bhaskaran et al. 2005; Newton et al. 2006).

Nevertheless, no study has been found in which autofluorescence has been used to isolate ATII cells previously (see 3.2.12, page 34).

5.1.2 ATII cells isolated by sorting show high viability and purity

For the isolation of primary ATII cells, the aim was to establish a preparation method that provides intact cells for prospective miRNA profiling. Therefore, the isolated cells had to have three main properties: 1) “untouched”, 2) high viability and 3) high purity.

An “untouched” cell population of ATII cells was isolated by taking advantage of the autofluorescence of this cell type and by staining of the surface markers CD45 of leukocytes and CD31 of endothelial cell. The isolated cells showed a high viability of 96.2% and purity of 98.4% analyzed by flow cytometry. Morphologic and biochemical characterization confirmed ATII phenotype of the sorted cells. Expression of CCSP, which was found in very few sorted cells, might be due to contaminating club cells. Although agarose digestion was demonstrated to nearly eliminate club cells (Corti et al. 1996), some residual cells might still be present after agarose incubation. Due to their high autofluorescence characteristic that was documented after elastase digestion and sorting (Teisanu et al. 2009), persistent club cells would be sorted in the CD45/CD31^{negative} autofluorescence^{high} population. Further, progenitor cells could have

been within the sorted ATII cell population. Bronchioalveolar stem cells (BASCs), which can develop into bronchiolar and alveolar epithelial cells, as well as club cells were shown to co-express CCSP and proSP-C (Teisanu et al. 2009; Wang et al. 2012). BASCs, however, were documented to have low autofluorescence (Teisanu et al. 2009). On the other hand, intermediate precursor cells might still express CCSP, but nonetheless be highly autofluorescent due to increasing metabolic activity. Thus, they could have contaminated the sorted cell population.

5.1.3 ATII cells isolated by sorting are superior in purity to cells isolated by "panning"

To understand the advantages and limitations of the novel sorting procedure, the newly developed method was compared to a previously published isolation method based on "panning" (Königshoff et al. 2009). Both procedures use a negative selection strategy and were compared regarding the following properties: 1) viability and 2) purity.

Both sATII and pATII showed viabilities greater than 95% throughout the study with the average viability being minimally higher in pATII than sATII (96.7% vs. 96.2%). This finding might be explained by 1) a slightly higher viability of the single cell suspension before cell isolation (99.0% vs. 98.5%) and 2) isolation by "panning" being more gentle than isolation by sorting. To improve cell viability by sorting one could increase nozzle size and/or reduce sheath pressure (Arnold & Lannigan 2010). However, increasing nozzle size will decrease the quality of droplet formation, which can lower purity. Further, reducing sheath pressure leads to fewer cells per second. In addition, the longer sorting time might reduce viability. By FACS with 100 µm nozzle size, Gereke et al. achieved a viability of ~ 90% (Gereke et al. 2012). Therefore, no larger nozzle size or lower fluid pressure were chosen.

The analysis of the single cell suspension revealed enrichment of leukocytes and ATII cells already before the isolation procedure. An enrichment of ATII cells was expected as the preparation of single cell suspension included dispase dissociation (discussed in 5.1.1, page 53).

Isolated cells showed higher purity in sATII than pATII (98.4% vs. 72.6%) as assessed by surface marker expression in flow cytometry. In sATII, the few contaminating cells were mainly within the CD45/CD31^{negative} CD74^{negative} cell population. In principle, an ATII subpopulation could exist which is negative for the CD74 cell marker. Further, contaminating cells could have included club cells, which could have been sorted in the autofluorescence^{high} population (discussed in 5.1.1, page 53). In addition, in the reanalysis after sorting before PI/CD74 staining few events appeared as autofluorescence^{low}, which was mainly attributed to cell debris. However, some

CD45/CD31^{negative} autofluorescence^{low} cells could have contaminated the cell population such as ATI cells and BASCs. Most ATI cells are expected to be destroyed by the preparation procedure of the single cell suspension.

In pATII, the contaminating cells mainly consisted of leukocytes and endothelial cells. Endothelial cells showed a relative enrichment in the isolated population (6.7% before sorting vs. 12.3% after sorting). This finding might illustrate the fact that the “panning” protocol does not use antibodies to deplete endothelial cells (described in 3.2.4, page 28). The remaining leukocyte population (12.0% after sorting), however, illustrates that even after incubation on antibody-coated dishes specific to this cell type, it is difficult to achieve a high purity by “panning”.

MRNA analysis of phenotypic markers confirmed flow cytometric data. Markers for epithelial and ATII identity were highly expressed in sATII and pATII. The water channel AQP5, which has been suggested to be ATI-specific in the distal lung of rats and humans (Nielsen et al. 1997; Kreda et al. 2001), is expressed in both alveolar cell types, ATI and ATII cells, in mice (Matsuzaki et al. 2009; Krane et al. 2001). This study confirmed this finding with sATII and pATII expressing moderate levels of *Aqp5* mRNA. Markers for the contaminating cell populations confirmed higher purity of sATII than pATII with pATII expressing moderate levels of mRNA specific for smooth muscle cells, endothelial cells and leukocytes.

5.1.4 Limitations

Taken together, these results suggest that sorting provides considerably higher purity of ATII than “panning” with similar viabilities in both methods. However, there are some limitations to this study.

Some aspects concern the comparison of sATII and pATII. 1) Considering the small sample size caution must be applied to the interpretation. The data of four independent experiments in sATII and two independent experiments in pATII might not be transferable to general differences between these methods. A greater sample size of at least three independent experiments in both study groups would be desirable. In the present study, this was not possible within the time frame of the thesis. 2) Purity of pATII can differ based on the routine of the investigator as time for cell adherence and amount of washing steps have to be judged for each experiment individually. Isolation by “panning” was performed by a trained researcher. However, experiments of at least two independent investigators would minimize person dependent variations. In the present study, only one trained researcher was available. 3) Previous data on isolated ATII cells by “panning” suggest that this method does provide purities with high percentages of greater than 90% after one incubation step (Rice et al. 2002) and 95%

± 3% after two incubation steps as it was performed in the present study (Königshoff et al. 2009). Differences between previous results and the results in the present study might be due to aspects discussed in 1) and 2). Moreover, different methods were used to assess purity in the current study compared to previous studies. Rice et al. assessed purity by modified Papanicolaou staining, electron microscopy and immunostaining (Rice et al. 2002) and Königshoff et al. quantified ATII purity by immunostaining (Königshoff et al. 2009). In the present study, purity of pATII was analyzed by flow cytometry.

Further, some limitations concern the feasibility of the sorting method itself. 1) No information was obtained on biological functionality of the cells. Sorting does stress cells. ATII cells are under high sheath pressure and have to pass the nozzle tip. 2) It is unclear how ATII cells obtained from a murine disease model e.g. for IPF would react to the isolation procedure. ATII cells of pathologic lungs could be more easily affected by the sorting procedure, resulting in a lower viability. ATII cells isolated by FACS from mice infected with influenza A virus made up a smaller proportion of all lung cells due to influx of immune cells (Gereke et al. 2012) and on day three postinfection the absolute number of isolated ATII cells was reduced (Stegemann-Koniszewski et al. 2016, supplemental data). However, the authors did not report whether the viability of ATII cells isolated from influenza A infected mice was lower compared to cells from uninfected mice (Gereke et al. 2012; Stegemann-Koniszewski et al. 2016). 3) A recent workshop on IPF of the National Heart, Lung and Blood Institute (NHLBI) of the United States claimed to focus in future studies on profiling models that most closely represent human IPF (Blackwell et al. 2014). Autofluorescence in human ATII cells, however, has been described as low compared to alveolar macrophages (Cunningham et al. 1994). It therefore remains open whether the established method using unchallenged C57BL/6 mice could be applied to different species, especially human lungs.

In addition, ATII cells are not a uniform population (Fehrenbach 2001). In every isolation procedure chosen, there is the possibility that a subtype of the ATII population is preferentially isolated over other subpopulations. The subsequently studied ATII functions *in vitro* may not be representative for all ATII cells *in vivo*. For these reasons, in the present study a cut-set of miRNAs obtained from ATII cells isolated by two different methods was chosen for miRNA profiling (see 5.2.1).

5.2 Functional role of miRNAs in ATII cells under healthy conditions

5.2.1 Rationale for the profiling strategy

Several studies have linked aberrant miRNA expression to ATII-associated diseases (as described in 1.3.4, page 13). Until now, profiling of miRNAs in pulmonary diseases

and healthy controls has been mainly performed in cell lines and human whole lung samples. Few studies have analyzed miRNAs in primary ATII cells. Let-7d and miR-15b expression in ATII was documented by *in situ* hybridization (Pandit et al. 2010; Ezzie et al. 2012) and levels of miR-21 in sorted ATII cells were compared between saline- vs. bleomycin-treated mice and IPF vs. control patients (Yamada et al. 2013). However, as far as known, a comprehensive miRNA profile of primary ATII cells remains unaccounted.

Therefore, the aim of the present study was to generate a thorough miRNA expression profile in primary, "untouched" ATII cells of healthy mice. Further, the regulated pathways of the target mRNAs were investigated. This provides insight into the role of miRNAs in ATII cells in a healthy state.

A cut-set of miRNAs from ATII cells isolated by the novel sorting method and a previously published method was used for further pathway analysis. This approach was chosen, because 1) it reduces miRNAs from contaminating cell types present in cell samples from one of the isolation methods, 2) it identifies miRNAs which are common to the whole ATII cell population and not restricted to a subpopulation that is enriched by one of the isolation methods and 3) it minimizes changes in miRNA expression due to activation of pathways during specific isolation steps.

5.2.2 Differentially expressed miRNAs support purity of sATII over pATII

Out of the 316 identified miRNAs, 42 miRNAs were highly differentially expressed or only expressed in pATII compared to only four miRNAs in sATII. Mmu-miR-126-3p, mmu-miR-10a and mmu-miR-29c were the most significant miRNAs with increased expression based on the BH-adjusted p-values. All of them were upregulated in pATII.

MiR-126-3p was expressed in endothelial cells, controlling the response to vascular endothelial growth factor (VEGF) (Fish et al. 2008; Harris et al. 2008), and platelets (Gatsiou et al. 2012). MiR-10a has been mainly found in lung, kidney, muscle and liver (Beuvink et al. 2007; Landgraf et al. 2007). Within the lung, miR-10a was reported to be the most abundant miRNA in primary human smooth muscle cells. It showed cellular specificity within the lung with >30x higher expression in smooth muscle cells than in alveolar epithelial cells (Hu et al. 2014). This miRNA induced smooth muscle differentiation and proliferation (Huang et al. 2010; Hu et al. 2014). MiR-29c is part of the miR-29-family (miR-29a, miR-29b, miR-29c). All three members were found in murine fibroblasts of healthy lungs (Xiao et al. 2012). MiR-29 showed high expression in two mouse fibroblast cell lines compared to low expression in an ATII-like epithelial cell line (Cushing et al. 2011). Thus, a preferential expression in mesenchymal cells was suggested (Cushing et al. 2011).

Taken together, the great amount of highly differentially or only expressed miRNAs in pATII compared to sATII and the fact that the miRNAs with the most significant increased expression in pATII are those that have been described in non-ATII cell types support the results of a higher purity in sATII than pATII.

5.2.3 Similarly expressed miRNAs give insight into miRNA regulated ATII pathways

To identify potential pathways of ATII cell homeostasis regulated by miRNAs, the 111 ATII miRNAs were used for pathway enrichment analysis. 143 pathways with significant enrichment were classified as signaling pathways and only two pathways regulate metabolic processes. This suggests that miRNAs may not play an important role in regulation of metabolic pathways in ATII cells under normal conditions. From the top 20 signaling pathways nine were related to cancer and nine were related to fibrosis and/or EMT.

This role of miRNAs was confirmed by the analysis of the pathway categories: The top pathway categories revealed involvement of ATII miRNAs in pathways linked to “cancer” and to “cellular growth, proliferation and development”. Recently, these pathways have been elucidated as major pathways in ATII cells. Fujino et al. showed by gene enrichment analysis that “positive regulation of cell differentiation” and “lung development” are among the four highest enriched gene ontology terms in ATII cells isolated from human lungs and ATII-like cells derived from alveolar epithelial progenitor cells, following “transcription” and “RNA splicing”. Further, genes that downregulate EMT pathway were upregulated in mature ATII cells (Fujino, Ota, Suzuki, et al. 2012).

The miRNA-regulated pathways and pathway categories suggest that miRNAs in ATII cells play an important role for cell differentiation and proliferation. In this context, EMT is a key mechanism and the TFG-beta superfamily signaling pathway is a crucial regulator for maintaining epithelial homeostasis (see 1.3.4, page 13). In the present study, several findings revealed strong miRNA-regulation of TGF-beta signaling pathway in ATII cells at normal conditions: 1) The growth factors TGF-beta and EGF were identified within the top five upstream regulators. 2) 19 miRNAs of which 16 miRNAs were expressed above median levels in the isolated ATII cells have targets in the canonical TGF-beta signaling pathway. 3) Two of these miRNAs were within the top five upstream regulators.

In the present study, TGF-beta 1 and EGF were found to be within the top five upstream regulators. Like TGF-beta, the EGF family promotes EMT by stimulation of alveolar epithelial cell proliferation and migration (Crosby & Waters 2010). A close cross-talk between EGF and TGF-beta signaling pathways had a synergistic effect on

EMT in pancreatic cancer (Ouyang et al. 2014; Deharvengt et al. 2012) and renal fibrosis (Tian et al. 2007). In breast cancer cells, miR-21 repressed SMAD7, an inhibitor of the TGF-beta signaling pathway, which enhanced TGF- and EGF-dependent cancer cell invasion and migration (Han et al. 2016). This suggests that both growth factors interact within the TGF-beta signaling pathway. However, the exact mechanism of the interplay remains to be elucidated.

MiR-30a-3p/5p, miR-30c-5p and miR-30e-3p/5p were amongst the 13 very high expressed miRNAs. MiR-30a-3p and miR-30e-3p were the most abundant miRNAs while miR-30c-5p has three targets within the TGF-beta signaling pathway and was one of the top five upstream regulators. The miR-30 family-members (miR-30a, miR-30b, miR-30c, miR-30d, miR-30e) all contain the same seed sequence at the 5'-terminus, potentially regulating similar targets. MiR-30c was downregulated in human lung biopsies of patients with IPF and NSCLC compared to healthy controls (Pandit et al. 2010; Zhong et al. 2014). Besides suppression of TGF-beta-mediated EMT, miR-30 family directly inhibited the EMT-inducing transcription factor SNAIL1 in human hepatocytes (Zhang et al. 2012). Thus, the high abundance of three miR-30 family-members in the present study suggests that this family plays an important role in suppressing EMT in ATII cells at normal, physiological conditions.

The miR-200 family-member miR-429 was also expressed at high levels. The miR-200 family consists of five members (miR-200a, miR-200b, miR-200c, miR-141 and miR-429). The family can be divided into two groups by two different criteria. The first is by their gene localization in two clusters on chromosome 1 (miR-200a, miR-200b and miR-429) and chromosome 12 (miR-200c, miR-141). The second is by their function differing in one nucleotide of the seed sequence in the first group (miR-200a, miR-141) compared to the second group (miR-200b, miR-200c, miR-429) (Park et al. 2008). The miR-200 family is a well-known inhibitor of EMT. An increasing body of literature suggests that many, maybe even all, epithelial cell types contain a high abundance of the miR-200 family-members (Hill et al. 2013). Low expression of the miR-200 family-members in tumor cells has been associated with poor prognosis in ovarian cancer, gastric cancer, spindle cell carcinoma of the head and neck, thyroid carcinoma and many more (Hu et al. 2009; Kurashige et al. 2012; Zidar et al. 2011; Braun et al. 2010). In immortalized human bronchial epithelial cells, miR-200 family-members were repressed during EMT induced by tobacco carcinogens (Tellez et al. 2011) and by arsenic exposure (Z. Wang et al. 2011). In a lung adenocarcinoma mouse model, miR-200 family overexpression restricted the cancer cells to an epithelial phenotype and stopped metastases (Gibbons et al. 2009). Functional studies showed that inhibition of miR-200 induced EMT and overexpression of miR-200 provoked MET and suppressed

cancer cell motility by direct repression of ZEB1 and ZEB2 (Park et al. 2008; Korpal et al. 2008; Gregory et al. 2008). Both transcription factors were involved in the TGF-beta signaling pathway (see 1.3.3, page 11) forming a negative feedback loop with miR-200. In addition to the high expression of miR-30 family-members, the presence of a miR-200 family-member reinforces the concept of ATII miRNAs playing an important role in maintaining epithelial homeostasis.

Interestingly, members of the polycistronic miR-17-92 cluster and its two mammalian paralogs miR-106a-363 cluster and miR-106b-25 cluster were highly represented in the ATII miRNAs. These clusters contain four seed families: miR-17, miR-18, miR-19 and miR-92 (Concepcion et al. 2012). In the present study, four miR-17-92 cluster members (miR-19a, miR-17, miR-20a, miR-18a) were detected. MiR-19a and miR-17-5p were expressed at high levels with miR-17-5p having three targets within the canonical TGF-beta signaling pathway. Further, miR-106a from the miR-106a-363 cluster and all three members of miR-106b-25 cluster (miR-25, miR-93, miR-106b) were expressed at moderate levels. MiR-20b of the miR-106a-363 cluster was found at low level. So far, most studies have described the main role of the miR-17-92 cluster and its paralogs as oncogenes with upregulation in hematopoietic and solid cancers (Concepcion et al. 2012). However, there is growing evidence on its physiological function in normal development with loss of function of miR-17-92 cluster leading to early postnatal death (Ventura et al. 2008) and its potential role in tumor suppression. TGF-beta type II transmembrane receptor was directly inhibited by miR-17, miR-20a and miR-20b and these miRNAs were upregulated in A549 with cisplatin sensitivity compared to cisplatin resistance (Jiang et al. 2014). Further, in oral squamous cell carcinoma miR-17 and miR-20a repressed tumor migration (Chang et al. 2013). Of special interest for the present study, in lung development miR-17, miR-20a and miR-106b controlled E-cadherin expression and distribution, thus, provoking an epithelial phenotype. MiR-17 and miR-20a were expressed more highly during lung development than in adult lung, while miR-106b had even higher levels in adult lungs (Carraro et al. 2009). In the present study, miR-17, miR-20a and miR-106b were expressed above median levels in ATII cells in adult, healthy mice. These data suggest that not only during lung development, but also in adult mice all three miRNAs have a physiological role in maintaining epithelial homeostasis.

Further, the data in the current study suggest that miR-16-5p has a crucial role in ATII homeostasis. The miRNA was expressed at a very high level, was the top upstream regulator and showed four targets within the TGF-beta signaling pathway. The other member of its family, miR-15, was also expressed at a high level. The two miRNAs are located as a cluster on chromosome 14. The miR-15 family has been described as a

tumor suppressor in nasopharyngeal carcinoma, pituitary tumors, glioma and NSCLC (Jiang et al. 2016; Renjie & Haiqian 2015; Wang et al. 2014; Bandi et al. 2009). Within the EMT-pathway, miR-16 and miR-15 were documented to repress activating protein-4 (AP4). This transcription factor promoted EMT by upregulation of E-cadherin and SNAIL (Shi et al. 2014). MiR-16 and miR-15 were induced by p53, which was also confirmed for the miR-200 family (Shi et al. 2014). P53 is a tumor suppressor and downregulation of p53 led to EMT-associated stem cell phenotypes (De Craene & Berx 2013). This suggests that miRNAs in normal ATII cells are regulators of p53-controlled epithelial phenotype.

These data enforce the findings that the highly expressed miRNAs found in healthy ATII cells in the present study are important for guarding the maintenance of the ATII cell phenotype while protecting from fibrotic changes and cancer progression.

5.2.4 Limitations

In summary, the pathway enrichment analysis of ATII miRNAs suggests a strong role of miRNAs in homeostasis and during proliferation and differentiation, and in particular within the TGF-beta signaling pathway. However, there are limitations to the present study.

1) Two samples of each preparation method were used for miRNA profiling. Due to the small sample size the result for similarly expressed miRNAs might not represent the general miRNAs present in ATII cells in a healthy state. At least three samples of each isolation method would be desirable for analysis. 2) Some aspects account for exclusion of some miRNA-mRNA target interactions: a) The applied microRNA arrays do not include all known miRNAs. b) For pathway enrichment analysis the 111 miRNAs detected at similar levels in sATII and pATII were restricted to 40 miRNAs with 662 experimentally validated targets. c) By using a cut-set of two different preparation methods the identified miRNAs exclude miRNAs which might have been present in a subgroup selectively enriched by one of the isolation methods. Therefore, further miRNA-mRNA target interactions might play a relevant role, which were not listed in the database so far or were excluded by the study design. 3) No functional characterization was performed to link the changes in miRNAs to target gene expression.

In the present study, these issues could not be addressed within the time frame of the thesis. Hence, the findings should be supported by further research analyzing the miRNA effect on downstream effects. Moreover, additional pathways regulated by miRNAs might be elucidated in the future.

6 CONCLUSIONS AND OUTLOOK

ATII cells are important regulators in lung homeostasis. Alterations in this cell type by EMT contribute to various lung diseases, the main groups being developmental, fibrotic and malignant diseases. However, diagnostic and therapeutic options affecting this cell type remain highly elusive. One aspect is the difficulty to obtain ATII cells that can be used for analysis and functional studies including miRNA analysis.

In this work, three main findings contribute to the research field of ATII cells in regard to the goals defined at the beginning of this study (see 2, page 15):

1. By this work a new method was established to gain highly pure and viable “untouched” ATII cells from healthy mice at day 0 (day of isolation). This isolation method is superior to a previously published isolation method (“panning”) in regard to the purity of the freshly isolated cells with similar viability. The newly developed method can be used for future studies on primary ATII cells.
2. For the first time a coherent ATII miRNA profile of healthy mice was established. The profile was obtained from a cut-set of miRNAs isolated by two different methods. This is the basis for further studies comparing ATII miRNA profiles of healthy mice to mouse models of lung diseases. Thereby, changes in miRNA expression profile during pathogenesis of diseases can be identified.
3. TGF-beta signaling pathway was identified as a key target for miRNAs in ATII cells regulating homeostasis. Distinct miRNAs depicted in the present study as regulators of the TGF-beta signaling pathway can be used for specific miRNA analysis in fibrotic and/or cancer models compared to healthy mice.

Identification of dysregulated miRNAs in ATII cells will have potential use in human diseases as 1) biomarkers and 2) therapeutic targets. MiRNAs have been studied in various diseases as biomarkers for diagnosis, patient stratification, treatment monitoring and prognosis of diseases (Mishra 2014). MiRNAs have several characteristics that make them ideal biomarkers. They are stable in biological fluids such as plasma, serum, urine and saliva (Chen et al. 2008; Mitchell et al. 2008; Mall et al. 2013; Park et al. 2009). They are easy to measure and alteration of miRNA profiles does correlate with disease manifestation, status and prognosis in a variety of diseases such as malignancies (Shen et al. 2013; Cortez et al. 2011), cardiovascular diseases (Rawal et al. 2014; Siasos et al. 2013), neurologic/psychiatric diseases (Maciotta et al. 2013; Rao et al. 2013) and autoinflammatory diseases (Ma et al. 2014; Chen et al.

2014). Further, identified miRNAs could be used as therapeutic targets in the future (Moreno-Moya et al. 2014).

However, there are limitations to the study, which could not be addressed within the time frame of the thesis, indicating that further research has to be performed in the future. 1) The newly developed isolation procedure has not been used for functional studies. Therefore, the biological functionality of the cells and their potential use for functional studies remain to be investigated. 2) On behalf of the identified ATII miRNAs, their role in ATII cells was analyzed using a bioinformatic prediction program. However, functional studies linking the identified miRNAs to changes in target mRNAs need to be performed. 3) In the present study, further analyses of the ATII miRNA regulated pathways focused on EMT. Today, many more pathways such as Wnt signaling have been described contributing to lung diseases including fibrosis and malignancies (Bartis et al. 2014). Further, contradictory studies suggest that mesenchymal cells in fibrotic disease do not originate from epithelial cells (Rock et al. 2011). Therefore, whether EMT contributes to lung disease and if so, which pathways are accountable for lung disease, needs to be understood in the future.

7 SUMMARY

7.1 Summary

Alveolar epithelial type II (ATII) cells play an important role in the maintenance of alveolar homeostasis. During injury, loss or dysregulation, however, ATII cells can lead to lung fibrosis and cancer by epithelial-to-mesenchymal transition (EMT). The complex regulatory networks that maintain ATII cells under physiologic condition are still little understood. MicroRNAs (miRNAs) are important regulators of gene expression at the posttranscriptional level. Hence, the goal of this study was to identify miRNAs expressed by murine ATII cells under normal, non-pathologic conditions and to elucidate potential miRNA-controlled pathways of ATII cell homeostasis.

A new protocol was established to isolate “untouched” murine ATII cells by Fluorescence Activated Cell Sorting (FACS) based on their autofluorescence (termed sATII). The purity and viability of sATII were compared to ATII cells obtained by the previously published isolation method “panning” (termed pATII). MiRNA profiles were obtained of both sATII and pATII using TaqMan® MicroRNA Arrays. MiRNAs with similar expression levels in sATII and pATII (|fold difference| < 1.5; termed ATII miRNAs) were used for Ingenuity® Pathway Analysis (IPA) with restriction to experimentally observed miRNA-mRNA interactions and canonical pathways.

Isolated sATII showed a higher purity than pATII (98.4% vs. 72.6%) with a similar viability in sATII and pATII (96.2% vs. 96.7%). 111 miRNAs were expressed at similar levels in ATII cells obtained by the novel sorting method and the previously published method. In the Ingenuity® pathway enrichment analysis, nine pathways were associated with fibrosis and/or EMT and nine pathways were related to cancer within the top 20 signaling pathways. The transforming growth factor beta (TGF-beta) signaling pathway was identified as a key pathway regulated by 19 ATII miRNAs targeting 21 TGF-beta pathway components.

This work contributes to the research field of ATII cells with three main findings. First, the newly developed isolation protocol can be used for future studies on primary murine ATII cells with the need for “untouched” cells with high purity and viability at the day of isolation. Second, for the first time a coherent ATII miRNA profile of healthy mice was obtained. Third, the identified ATII miRNAs seem to play an important role in the regulation of fibrosis/EMT, especially within the TGF-beta signaling pathway. Future studies investigating miRNAs in mouse models of lung diseases e.g. pulmonary fibrosis can compare their findings with the ATII miRNA profile of healthy mice of the present study and, thus, identify miRNA changes during pathogenesis of diseases.

7.2 Zusammenfassung

Alveolarepithel-Typ II (ATII) Zellen spielen eine wichtige Rolle in der Erhaltung der alveolaren Homöostase. Bei Verletzung, Verlust oder Dysregulation können ATII Zellen jedoch zu Lungenfibrose und malignen Erkrankungen durch epithelial-mesenchymale Transition (EMT) führen. Die komplexen Signalnetzwerke, die den physiologischen Zustand der ATII Zellen aufrechterhalten, sind bislang nur wenig verstanden. MicroRNAs (miRNAs) sind wichtige Regulatoren der Genexpression auf posttranskriptionaler Ebene. Das Ziel dieser Arbeit war die Identifikation von miRNAs, die von ATII Zellen unter physiologischen Bedingungen exprimiert werden, und die Ermittlung potentieller miRNA-regulierter Signalwege der ATII Zell-Homöostase.

Ein neues Protokoll wurde für die Isolation von „unberührten“ murinen ATII Zellen mittels Fluorescence Activated Cell Sorting (FACS) basierend auf deren Autofluoreszenz entwickelt (bezeichnet als sATII). Die Reinheit und Viabilität der sATII wurden mit ATII Zellen, die durch die bereits publizierte Methode „Panning“ isoliert wurden (bezeichnet als pATII), verglichen. MiRNA Profile wurden von sATII und pATII mittels TaqMan® MicroRNA Arrays erstellt. Die ähnlich exprimierten miRNAs in sATII und pATII (|fold difference| < 1.5; bezeichnet als ATII miRNAs) wurden für Ingenuity® Signalweganalysen mit Beschränkung auf experimentell bestätigte miRNA-mRNA Interaktionen und kanonische Signalwege verwendet.

Die isolierten sATII zeigten eine höhere Reinheit im Vergleich zu pATII (98.4% vs. 72.6%) bei ähnlicher Viabilität von sATII und pATII (96.2% vs. 96.7%). 111 miRNAs wiesen eine ähnliche Expression in ATII Zellen aus beiden Isolationsmethoden auf. In der Ingenuity® Signalweganalyse waren innerhalb der 20 häufigsten Signalwege neun mit Fibrose und/oder EMT und neun mit malignen Erkrankungen assoziiert. Der transforming growth factor beta (TGF-beta) Signalweg wurde mit 19 ATII miRNAs, die 21 TGF-beta Signalwegkomponenten regulieren, als ein zentraler Signalweg ermittelt.

Die vorliegende Arbeit trägt drei wesentliche Erkenntnisse zu dem Forschungsgebiet der ATII Zellen bei. Erstens kann das neu etablierte Isolationsprotokoll für zukünftige Studien verwendet werden, die „unberührte“ murine ATII Zellen mit hoher Reinheit und Viabilität am Tag der Isolation benötigen. Zweitens wurde erstmalig ein umfassendes ATII miRNA Profil von gesunden Mäusen erstellt. Drittens scheinen die identifizierten ATII miRNAs eine wichtige Rolle in der Regulation von Fibrose/EMT, insbesondere im TGF-beta Signalweg, zu spielen. Zukünftige Studien, die ATII miRNAs in Mausmodellen von Lungenerkrankungen untersuchen, können diese mit dem Expressionsprofil gesunder Mäuse aus dieser Arbeit vergleichen und dadurch miRNA Veränderungen während der Pathogenese von Erkrankungen identifizieren.

8 APPENDIX

8.1 Abbreviations

2’ OH	2’ hydroxyl group
α-SMA	α-smooth muscle actin
AAAA(n)	3’ poly(A) tail
Acta2	actin, alpha 2, smooth muscle, aorta
Ago	Argonaute
AKT	protein kinase B
AP4	activating protein-4
APC	allophycocyanin
Aqp5	aquaporin 5
ATI	alveolar epithelial type I
ATII	alveolar epithelial type II
ATPase	adenosine triphosphatase
BASC	bronchioalveolar stem cell
BH	Benjamini-Hochberg
BMP	bone morphogenetic protein
BSA	bovine serum albumin
CCSP	club cell secretory protein
Cd74	CD74 antigen
Cdh1	cadherin 1 (E-cadherin)
cDNA	complementary DNA
COPD	chronic obstructive pulmonary disease
Cq	raw cycle threshold
DAPI	4',6-diamidino-2-phenylindole
DGCR-8	DiGeorge syndrome critical region 8
DMEM	Dulbecco’s Modified Eagle Medium
DNase	deoxyribonuclease
dNTP	deoxyribonucleoside triphosphate

dsRNA	double-stranded RNA
dTTP	deoxythymidine triphosphate
E-cadherin	epithelial cadherin
EGF	epithelial growth factor
eIF4GI	eukaryotic translation initiation factor 4GI
EMT	epithelial-to-mesenchymal transition
ENaC	apical epithelial sodium channel
EpCAM	epithelial cell adhesion molecule
FACS	Fluorescence Activated Cell Sorting
FAD	flavin adenine dinucleotide
FBS	fetal bovine serum
FITC	fluorescein isothiocyanate
FSC	forward scatter
FSC-A	forward scatter-area
FSC-H	forward scatter-height
FSC-W	forward scatter-width
FSP1	fibroblast specific protein 1
GDF	growth and differentiation factor
HCV	Hepatitis C virus
Hprt	hypoxanthine guanine phosphoribosyl transferase
HSC70	heat shock cognate protein 70
HSP90	heat shock protein 90
Ig	immunoglobulin
IGF-1	Insulin-like growth factor 1
IL	interleukin
ILK	integrin-linked kinase
INF-γ	interferon-γ
IPA	Ingenuity® Pathway Analysis
IPF	idiopathic pulmonary fibrosis
ITC	isotype control

m7Gppp	7-methylguanosine cap
MAD	mothers against decapentaplegic
MET	mesenchymal-to-epithelial transition
MHC	major histocompatibility complex
miRISC	miRNA-containing RNA-induced silencing complex
miRNA	microRNA
mmu	Mus musculus
mRNA	messenger RNA
N-cadherin	neural cadherin
NADH	reduced nicotinamide adenine dinucleotide
ncRNA	non-coding RNA
NHLBI	National Heart, Lung and Blood Institute
NRQ	normalized relative quantity
NSCLC	non-small cell lung cancer
nt	nucleotides
NTC	no template control
ORF	open reading frame
PACT	protein kinase R-activating protein
Par6	partitioning-defective protein 6
pATII	ATII cells isolated by “panning”
PAZ	Piwi-Argonaute-Zwille
PBS	phosphate buffered saline
PCR	polymerase chain reaction
PE	phycoerythrin
Pecam1	platelet/endothelial cell adhesion molecule 1 (protein: CD31)
PFA	paraformaldehyde
PI	propidium iodide
PI3K	phosphoinositide 3-kinase
piRNA	piwi-interacting RNA
Piwi	P-element induced wimpy testis

Pol	RNA polymerase
pre-miRNA	precursor miRNA
pri-miRNA	primary miRNA
proSP-C	prosurfactant protein C
PTEN	phosphatase and tensin homolog
Ptprc	protein tyrosine phosphatase, receptor type, C (protein: CD45)
Ran-GTP	ras-related nuclear protein guanosine triphosphate
RIN	RNA Integrity Number
RISC	RNA-induced silencing complex
RNA	ribonucleic acid
RNAi	RNA interference
RNase	ribonuclease
rRNA	ribosomal RNA
RT	reverse transcription
RT-qPCR	Real-time quantitative PCR
S	standard deviation
sATII	ATII cells isolated by sorting
SBE	SMAD binding element
SDS	Sequence Detection Software
SEM	standard error of mean
Sftpa1	surfactant associated protein A1
Sftpc	surfactant associated protein C
siRNA	small interfering RNA
SMAD	acronym combined from SMA and MAD
snoRNA	small nucleolar RNA
snRNA	small nuclear RNA
SP	surfactant protein
SPF	specific pathogen-free
SSC-A	side scatter-area
ssRNA	single-stranded RNA

TGF-beta	transforming growth factor beta
Tjp1	tight junction protein 1
TNF-α	tumor necrosis factor-α
TRBP	transactivation response RNA binding protein
tRNA	transfer RNA
UTR	untranslated region
VEGF	vascular endothelial growth factor
vs.	versus
ZEB	zinc-finger E-box binding factor

8.2 List of miRNAs similarly expressed in sATII and pATII

Table 22. MiRNAs similarly expressed in sATII and pATII. 111 miRNAs were expressed at similar levels (|fold difference| < 1.5) in sATII and pATII (termed ATII miRNAs). Mean NRQ was determined of NRQ of sATII and pATII. 13 miRNAs were expressed at very high levels (> 20x median), 41 miRNAs were expressed at high levels (20x median > miRNA > median), 45 miRNAs were expressed at moderate levels (median > miRNA > 0.05x median) and 12 miRNAs were expressed at low levels (< 0.05x median).

Index	Detector (ABI)	MiRNA	MiRNA (mmu)	MiRBase accession	Mean NRQ	log10 NRQ
1	hsa-miR-30a-3p-000416	hsa-miR-30a-3p	mmu-miR-30a-3p	MIMAT0000129	25498116	7.41
2	hsa-miR-30e-3p-000422	hsa-miR-30e-3p	mmu-miR-30e-3p	MIMAT0000249	24660029	7.39
3	mmu-miR-24-4373072	mmu-miR-24	mmu-miR-24-3p	MIMAT0000219	22745232	7.36
4	mmu-miR-19a-4373099	mmu-miR-19a	mmu-miR-19a-3p	MIMAT0000651	19888530	7.30
5	mmu-miR-30c-4373060	mmu-miR-30c	mmu-miR-30c-5p	MIMAT0000514	18189872	7.26
6	mmu-miR-484-4381032	mmu-miR-484	mmu-miR-484(-5p)	MIMAT0003127	9335209	6.97
7	mmu-miR-29a-4395223	mmu-miR-29a	mmu-miR-29a-3p	MIMAT0000535	9059648	6.96
8	mmu-miR-429-4373355	mmu-miR-429	mmu-miR-429-3p	MIMAT0001537	8918566	6.95
9	mmu-miR-16-4373121	mmu-miR-16	mmu-miR-16-5p	MIMAT0000527	5425638	6.73
10	mmu-miR-467F-002886	mmu-miR-467F	mmu-miR-467f(-3p)	MIMAT0005846	4732664	6.68
11	mmu-miR-30a-4373061	mmu-miR-30a	mmu-miR-30a-5p	MIMAT0000128	4572894	6.66
12	mmu-miR-17-4395419	mmu-miR-17	mmu-miR-17-5p	MIMAT0000649	2267710	6.36
13	mmu-miR-30e-4395334	mmu-miR-30e	mmu-miR-30e-5p	MIMAT0000248	2261515	6.35
14	hsa-miR-22-000398	hsa-miR-22	mmu-miR-22-3p	MIMAT0000531	1521069	6.18
15	mmu-miR-	mmu-miR-	mmu-miR-	MIMAT0000385	1488258	6.17

	106a-4395589	106a	106a-5p			
16	mmu-miR-375-4373027	mmu-miR-375	mmu-miR-375-3p	MIMAT0000739	1453573	6.16
17	mmu-miR-222-4395387	mmu-miR-222	mmu-miR-222-3p	MIMAT0000670	1101376	6.04
18	mmu-miR-125a-5p-4395309	mmu-miR-125a-5p	mmu-miR-125a-5p	MIMAT0000135	1039820	6.02
19	mmu-miR-2182-241119_mat	mmu-miR-2182	mmu-miR-2182(-5p)	MIMAT0011286	1013419	6.01
20	mmu-miR-20a-4373286	mmu-miR-20a	mmu-miR-20a-5p	MIMAT0000529	999774	6.00
21	rno-miR-7#-001338	rno-miR-7*	mmu-miR-7a-1-3p	MIMAT0004670	755796	5.88
22	mmu-miR-872#-002542	mmu-miR-872*	mmu-miR-872-3p	MIMAT0004935	736923	5.87
23	mmu-miR-181a-4373117	mmu-miR-181a	mmu-miR-181a-5p	MIMAT0000210	731896	5.86
24	hsa-miR-423-3P-002626	hsa-miR-423-3P	mmu-miR-423-3p	MIMAT0003454	662507	5.82
25	rno-miR-664-001323	rno-miR-664	mmu-miR-664-3p	MIMAT0012774	562810	5.75
26	mmu-miR-106b-4373155	mmu-miR-106b	mmu-miR-106b-5p	MIMAT0000386	534359	5.73
27	mmu-miR-331-3p-4373046	mmu-miR-331-3p	mmu-miR-331-3p	MIMAT0000571	492723	5.69
28	hsa-miR-421-002700	hsa-miR-421	mmu-miR-421-3p	MIMAT0004869	397700	5.60
29	mmu-miR-301a-4373064	mmu-miR-301a	mmu-miR-301a-3p	MIMAT0000379	359723	5.56
30	mmu-miR-27a-4373287	mmu-miR-27a	mmu-miR-27a-3p	MIMAT0000537	359594	5.56
31	mmu-miR-140-4373374	mmu-miR-140	mmu-miR-140-5p	MIMAT0000151	353672	5.55
32	mmu-miR-425-4380926	mmu-miR-425	mmu-miR-425-5p	MIMAT0004750	347158	5.54
33	mmu-miR-27b-4373068	mmu-miR-27b	mmu-miR-27b-3p	MIMAT0000126	343986	5.54
34	mmu-miR-322-4378107	mmu-miR-322	mmu-miR-322-5p	MIMAT0000548	332636	5.52
35	mmu-miR-301b-4395730	mmu-miR-301b	mmu-miR-301b-3p	MIMAT0004186	315728	5.50
36	mmu-miR-218-4373081	mmu-miR-218	mmu-miR-218-5p	MIMAT0000663	313732	5.50
37	mmu-miR-322-001059	mmu-miR-322	mmu-miR-322-3p	MIMAT0000549	294531	5.47
38	mmu-miR-15a-4373123	mmu-miR-15a	mmu-miR-15a-5p	MIMAT0000526	294464	5.47
39	mmu-miR-877#-002548	mmu-miR-877*	mmu-miR-877-3p	MIMAT0004862	272988	5.44
40	hsa-miR-149-002255	hsa-miR-149	mmu-miR-149-5p	MIMAT0000159	260557	5.42
41	mmu-miR-210-4373089	mmu-miR-210	mmu-miR-210-3p	MIMAT0000658	238402	5.38
42	mmu-miR-93-4373302	mmu-miR-93	mmu-miR-93-5p	MIMAT0000540	200408	5.30
43	hsa-miR-22#-002301	hsa-miR-22*	mmu-miR-22-5p	MIMAT0004629	189242	5.28
44	mmu-miR-15a#-002488	mmu-miR-15a*	mmu-miR-15a-3p	MIMAT0004624	171640	5.23

45	mmu-miR-23b-4373073	mmu-miR-23b	mmu-miR-23b-3p	MIMAT0000125	164476	5.22
46	hsa-miR-106b#-002380	hsa-miR-106b*	mmu-miR-106b-3p	MIMAT0004582	148777	5.17
47	mmu-miR-320-4395388	mmu-miR-320	mmu-miR-320-3p	MIMAT0000666	139481	5.14
48	mmu-miR-186-4395396	mmu-miR-186	mmu-miR-186-5p	MIMAT0000215	139369	5.14
49	mmu-miR-25-4373071	mmu-miR-25	mmu-miR-25-3p	MIMAT0000652	137232	5.14
50	mmu-miR-467b-001684	mmu-miR-467b	mmu-miR-467b-5p	MIMAT0003478	136262	5.13
51	mmu-miR-212-002551	mmu-miR-212	mmu-miR-212-3p	MIMAT0000659	134387	5.13
52	mmu-miR-221-4373077	mmu-miR-221	mmu-miR-221-3p	MIMAT0000669	130551	5.12
53	hsa-miR-140-3p-002234	hsa-miR-140-3p	mmu-miR-140-3p	MIMAT0000152	125211	5.10
54	mmu-miR-302b-4378071	mmu-miR-302b	mmu-miR-302b-3p	MIMAT0003374	108824	5.04
55	mmu-miR-193b-4395597	mmu-miR-193b	mmu-miR-193b-3p	MIMAT0004859	97676	4.99
56	mmu-miR-669n-197143_mat	mmu-miR-669n	mmu-miR-669n(-5p)	MIMAT0009427	93714	4.97
57	mmu-miR-1198-002780	mmu-miR-1198	mmu-miR-1198-5p	MIMAT0005859	89614	4.95
58	mmu-miR-20b-4373263	mmu-miR-20b	mmu-miR-20b-5p	MIMAT0003187	88621	4.95
59	mmu-miR-29b-4373288	mmu-miR-29b	mmu-miR-29b-3p	MIMAT0000127	78207	4.89
60	mmu-miR-214-4395417	mmu-miR-214	mmu-miR-214-3p	MIMAT0000661	76485	4.88
61	mmu-miR-199a-3p-4395415	mmu-miR-199a-3p	mmu-miR-199a-3p	MIMAT0000230	75574	4.88
62	mmu-miR-872-4395375	mmu-miR-872	mmu-miR-872-5p	MIMAT0004934	74360	4.87
63	mmu-miR-466g-241015_mat	mmu-miR-466g	mmu-miR-466g(-3p)	MIMAT0004883	70096	4.85
64	mmu-miR-193#-002577	mmu-miR-193*	mmu-miR-193-5p	MIMAT0004544	69717	4.84
65	hsa-miR-213-000516	hsa-miR-213	mmu-miR-181a-1-3p	MIMAT0000660	65495	4.82
66	mmu-miR-434-3p-4395734	mmu-miR-434-3p	mmu-miR-434-3p	MIMAT0001422	64543	4.81
67	mmu-let-7a#-002478	mmu-let-7a*	mmu-let-7a-1-3p	MIMAT0004620	64136	4.81
68	mmu-miR-503#-002536	mmu-miR-503*	mmu-miR-503-3p	MIMAT0004790	63231	4.80
69	hsa-miR-26b#-002444	hsa-miR-26b*	mmu-miR-26b-3p	MIMAT0004630	44764	4.65
70	hsa-miR-744#-002325	hsa-miR-744*	mmu-miR-744-3p	MIMAT0004820	44587	4.65
71	mmu-miR-340-5p-4395369	mmu-miR-340-5p	mmu-miR-340-5p	MIMAT0004651	41069	4.61
72	mmu-miR-450B-3P-002632	mmu-miR-450B-3P	mmu-miR-450b-3p	MIMAT0003512	40759	4.61
73	mmu-miR-339-	mmu-miR-	mmu-miR-	MIMAT0004649	38532	4.59

	3p-4395663	339-3p	339-3p			
74	rno-miR-29c#-001818	rno-miR-29c*	mmu-miR-29c-5p	MIMAT0004632	38463	4.59
75	mmu-miR-186#-002574	mmu-miR-186*	mmu-miR-186-3p	MIMAT0004540	32461	4.51
76	hsa-miR-27b#-002174	hsa-miR-27b*	mmu-miR-27b-5p	MIMAT0004522	31512	4.50
77	mmu-miR-194-4373106	mmu-miR-194	mmu-miR-194-5p	MIMAT0000224	27064	4.43
78	mmu-miR-181c-4373115	mmu-miR-181c	mmu-miR-181c-5p	MIMAT0000674	27051	4.43
79	mmu-miR-340-3p-4395370	mmu-miR-340-3p	mmu-miR-340-3p	MIMAT0000586	25986	4.41
80	mmu-miR-18a#-002490	mmu-miR-18a*	mmu-miR-18a-3p	MIMAT0004626	19116	4.28
81	mmu-miR-130b#-002460	mmu-miR-130b*	mmu-miR-130b-5p	MIMAT0004583	18917	4.28
82	mmu-miR-187-4373307	mmu-miR-187	mmu-miR-187-3p	MIMAT0000216	18814	4.27
83	mmu-miR-1930-121201_mat	mmu-miR-1930	mmu-miR-1930-5p	MIMAT0009393	17619	4.25
84	hsa-miR-9#-002231	hsa-miR-9*	mmu-miR-9-3p	MIMAT0000143	16097	4.21
85	mmu-miR-667-4386769	mmu-miR-667	mmu-miR-667-3p	MIMAT0003734	14574	4.16
86	mmu-miR-188-5p-4395431	mmu-miR-188-5p	mmu-miR-188-5p	MIMAT0000217	13323	4.12
87	mmu-miR-199b-001131	mmu-miR-199b	mmu-miR-199b-5p	MIMAT0000672	12203	4.09
88	mmu-miR-185-4395382	mmu-miR-185	mmu-miR-185-5p	MIMAT0000214	11161	4.05
89	mmu-miR-450a-5p-4395414	mmu-miR-450a-5p	mmu-miR-450a-5p	MIMAT0001546	10939	4.04
90	mmu-miR-1982.2-121154_mat	mmu-miR-1982.2	mmu-miR-1982.2-3p	MIMAT0009461	10472	4.02
91	hsa-let-7e#-002407	hsa-let-7e*	mmu-let-7e-3p	MIMAT0017016	9156	3.96
92	mmu-miR-361-4373035	mmu-miR-361	mmu-miR-361-5p	MIMAT0000704	8352	3.92
93	hsa-let-7i#-002172	hsa-let-7i*	mmu-let-7i-3p	MIMAT0004520	8216	3.91
94	mmu-miR-16#-002489	mmu-miR-16*	mmu-miR-16-1-3p	MIMAT0004625	8141	3.91
95	hsa-miR-189-000488	hsa-miR-189	mmu-miR-24-1-5p	MIMAT0000218	7800	3.89
96	mmu-miR-470#-002589	mmu-miR-470*	mmu-miR-470-3p	MIMAT0004760	7050	3.85
97	mmu-miR-465C-5P-002654	mmu-miR-465C-5P	mmu-miR-465c-5p	MIMAT0004873	6280	3.80
98	mmu-miR-708-4395452	mmu-miR-708	mmu-miR-708-5p	MIMAT0004828	5314	3.73
99	mmu-miR-7a-4378130	mmu-miR-7a	mmu-miR-7a-5p	MIMAT0000677	5149	3.71
100	mmu-let-7c-1#-002479	mmu-let-7c-1*	mmu-let-7c-1-3p	MIMAT0004622	4334	3.64
101	mmu-miR-542-5p-4395693	mmu-miR-542-5p	mmu-miR-542-5p	MIMAT0003171	3745	3.57

102	hsa-miR-671-5p-197646_mat	hsa-miR-671-5p	mmu-miR-671-5p	MIMAT0003731	2745	3.44
103	mmu-miR-542-3p-4378101	mmu-miR-542-3p	mmu-miR-542-3p	MIMAT0003172	2546	3.41
104	mmu-miR-491-4381053	mmu-miR-491	mmu-miR-491-5p	MIMAT0003486	2493	3.40
105	mmu-miR-804-002044	mmu-miR-804	mmu-miR-804(-3p)	MIMAT0004210	2457	3.39
106	mmu-miR-544-4395680	mmu-miR-544	mmu-miR-544-3p	MIMAT0004941	2396	3.38
107	mmu-miR-465a-3p-4395574	mmu-miR-465a-3p	mmu-miR-465a-3p	MIMAT0004217	1795	3.25
108	mmu-miR-184-4373113	mmu-miR-184	mmu-miR-184-3p	MIMAT0000213	1745	3.24
109	mmu-miR-7b-4395685	mmu-miR-7b	mmu-miR-7b-5p	MIMAT0000678	1479	3.17
110	mmu-miR-380-5p-4395731	mmu-miR-380-5p	mmu-miR-380-5p	MIMAT0000744	1043	3.02
111	mmu-miR-741-4395587	mmu-miR-741	mmu-miR-741-3p	MIMAT0004236	524	2.72

9 REFERENCES

Abell, A.N. & Johnson, G.L., 2014. Implications of Mesenchymal Cells in Cancer Stem Cell Populations: Relevance to EMT. *Current Pathobiology Reports*, 2(1), pp.21–26.

Adams, B.D. et al., 2017. Targeting noncoding RNAs in disease. *The Journal of Clinical Investigation*, 127(3), pp.761–71.

Agarwal, A. et al., 2001. Two-photon laser scanning microscopy of epithelial cell-modulated collagen density in engineered human lung tissue. *Tissue Engineering*, 7(2), pp.191–202.

Ameres, S.L. & Zamore, P.D., 2013. Diversifying microRNA sequence and function. *Nature Reviews Molecular Cell Biology*, 14(8), pp.475–88.

Applied Biosystems Life Technologies, 2010. TaqMan® Array Rodent MicroRNA Cards. Available at: http://tools.lifetechnologies.com/content/sfs/brochures/cms_054743.pdf [Accessed February 26, 2014].

Aravin, A. et al., 2006. A novel class of small RNAs bind to MILI protein in mouse testes. *Nature*, 442(7099), pp.203–7.

Ariki, S., Nishitani, C. & Kuroki, Y., 2012. Diverse functions of pulmonary collectins in host defense of the lung. *Journal of Biomedicine and Biotechnology*, 2012, pp.1–7.

Arnold, L.W. & Lannigan, J., 2010. Practical issues in high-speed cell sorting. *Current Protocols in Cytometry*, Chapter 1(24), pp.1–30.

Aumüller, G. et al., 2007. Duale Reihe Anatomie. *Georg Thieme Verlag*, p.533.

Bai, W.-D. et al., 2014. MiR-200c suppresses TGF-β signaling and counteracts trastuzumab resistance and metastasis by targeting ZNF217 and ZEB1 in breast cancer. *International Journal of Cancer*, 135(6), pp.1356–68.

Baker, R. et al., 1992. Quantitation of alveolar distribution of liposome-entrapped antioxidant enzymes. *American Journal of Physiology*, 263(5 Pt 1), pp.L585–94.

Ballard, P.L. et al., 1986. Isolation and characterization of differentiated alveolar type II cells from fetal human lung. *Biochimica et Biophysica Acta*, 883(2), pp.335–44.

Bandi, N. et al., 2009. miR-15a and miR-16 are implicated in cell cycle regulation in a Rb-dependent manner and are frequently deleted or down-regulated in non-small cell lung cancer. *Cancer Research*, 69(13), pp.5553–9.

Barkauskas, C.E. et al., 2013. Type 2 alveolar cells are stem cells in adult lung. *The Journal of Clinical Investigation*, 123(7), pp.3025–36.

Bartel, D.P., 2004. MicroRNAs: genomics, biogenesis, mechanism, and function. *Cell*, 116(2), pp.281–97.

Bartel, D.P., 2009. MicroRNAs: target recognition and regulatory functions. *Cell*, 136(2), pp.215–33.

Bartis, D. et al., 2014. Epithelial-mesenchymal transition in lung development and disease: does it exist and is it important? *Thorax*, 69(8), pp.760–5.

Bastid, J., 2012. EMT in carcinoma progression and dissemination: facts, unanswered questions, and clinical considerations. *Cancer and Metastasis Reviews*, 31(1-2), pp.277–83.

BD Biosciences, 2009. BD FACSAria II User's Guide. Available at: https://www.bdbiosciences.com/documents/BD_FACSAria_II_User_Guide.pdf [Accessed November 14, 2013].

Benjamini, Y. & Hochberg, Y., 1995. Controlling the false discovery rate: a practical and powerful approach to multiple testing. *Journal of the Royal Statistical Society. Series B (Methodological)*, 57(1), pp.298–300.

Beuvink, I. et al., 2007. A novel microarray approach reveals new tissue-specific signatures of known and predicted mammalian microRNAs. *Nucleic Acids Research*, 35(7), pp.1–11.

Bhaskaran, M. et al., 2005. Hemoglobin is expressed in alveolar epithelial type II cells. *Biochemical and Biophysical Research Communications*, 333(4), pp.1348–52.

Bi, W.-R., Yang, C.-Q. & Shi, Q., 2012. Transforming growth factor-β1 induced epithelial-mesenchymal transition in hepatic fibrosis. *Hepato-Gastroenterology*, 59(118), pp.1960–3.

Blackwell, T.S. et al., 2014. Future Directions in Idiopathic Pulmonary Fibrosis Research: An NHLBI Workshop Report. *American Journal of Respiratory and Critical Care Medicine*, 189(2), pp.214–22.

Borchert, G.M., Lanier, W. & Davidson, B.L., 2006. RNA polymerase III transcribes human microRNAs. *Nature Structural & Molecular Biology*, 13(12), pp.1097–101.

Borok, Z. et al., 1998. Modulation of t1alpha expression with alveolar epithelial cell phenotype in vitro. *The American Journal of Physiology*, 275(1 Pt 1), pp.L155–64.

Brabletz, T., 2012. To differentiate or not - routes towards metastasis. *Nature Reviews Cancer*, 12(6), pp.425–436.

Braun, J. et al., 2010. Downregulation of microRNAs directs the EMT and invasive potential of anaplastic thyroid carcinomas. *Oncogene*, 29(29), pp.4237–44.

Braun, J.E. et al., 2011. GW182 proteins directly recruit cytoplasmic deadenylase complexes to miRNA targets. *Molecular Cell*, 44(1), pp.120–33.

Brown, T., 2007. Genomes 3. *Garland Science Publishing*, p.436.

Brushart, T.M., 2011. Nerve Repair. *Oxford University Press*, Chapter 9, pp.250–352.

Butz, H. et al., 2012. Crosstalk between TGF-β signaling and the microRNA machinery. *Trends in Pharmacological Sciences*, 33(7), pp.382–93.

Carraro, G. et al., 2009. miR-17 family of microRNAs controls FGF10-mediated embryonic lung epithelial branching morphogenesis through MAPK14 and STAT3 regulation of E-Cadherin distribution. *Developmental Biology*, 333(2), pp.238–50.

Carthew, R.W. & Sontheimer, E.J., 2009. Origins and Mechanisms of miRNAs and siRNAs. *Cell*, 136(4), pp.642–55.

Ceppi, P. et al., 2010. Loss of miR-200c expression induces an aggressive, invasive, and chemoresistant phenotype in non-small cell lung cancer. *Molecular Cancer Research*, 8(9), pp.1207–16.

Chacko, A.-M. et al., 2012. Collaborative enhancement of antibody binding to distinct PECAM-1 epitopes modulates endothelial targeting. *PLoS One*, 7(4), pp.1–11.

Chang, C.-C. et al., 2013. MicroRNA-17/20a functions to inhibit cell migration and can be used a prognostic marker in oral squamous cell carcinoma. *Oral Oncology*, 49(9), pp.923–31.

Cheek, J.M., Evans, M.J. & Crandall, E.D., 1989. Type I cell-like morphology in tight alveolar epithelial monolayers. *Experimental Cell Research*, 184(2), pp.375–87.

Chekulaeva, M. et al., 2011. miRNA repression involves GW182-mediated recruitment of CCR4-NOT through conserved W-containing motifs. *Nature Structural & Molecular Biology*, 18(11), pp.1218–26.

Chen, M. et al., 2015. MiR-23b controls TGF-β1 induced airway smooth muscle cell proliferation via TGFβR2/p-Smad3 signals. *Molecular Immunology*, 70, pp.84–93.

Chen, W.-X., Ren, L.-H. & Shi, R.-H., 2014. Implication of miRNAs for inflammatory bowel disease treatment: Systematic review. *World Journal of Gastrointestinal Pathophysiology*, 5(2), pp.63–70.

Chen, X. et al., 2008. Characterization of microRNAs in serum: a novel class of biomarkers for diagnosis of cancer and other diseases. *Cell Research*, 18(10), pp.997–1006.

Chendrimada, T.P. et al., 2005. TRBP recruits the Dicer complex to Ago2 for microRNA processing and gene silencing. *Nature*, 436(7051), pp.740–4.

Cheung, C.T. et al., 2015. Cyclin A2 modulates EMT via β-catenin and phospholipase C pathways. *Carcinogenesis*, 36(8), pp.914–24.

Chiang, H.R. et al., 2010. Mammalian microRNAs: experimental evaluation of novel and previously annotated genes. *Genes & Development*, 24(10), pp.992–1009.

Cho, J.-H. et al., 2011. Systems biology of interstitial lung diseases: integration of mRNA and microRNA expression changes. *BMC Medical Genomics*, 4, pp.1–20.

Concepcion, C.P., Bonetti, C. & Ventura, A., 2012. The microRNA-17-92 family of microRNA clusters in development and disease. *The Cancer Journal*, 18(3), pp.262–7.

Cortez, M.A. et al., 2011. MicroRNAs in body fluids-the mix of hormones and biomarkers. *Nature Reviews Clinical Oncology*, 8(8), pp.467–77.

Corti, M., Brody, A.R. & Harrison, J.H., 1996. Isolation and primary culture of murine alveolar type II cells. *American Journal of Respiratory Cell and Molecular Biology*, 14(4), pp.309–15.

De Craene, B. & Berx, G., 2013. Regulatory networks defining EMT during cancer initiation and progression. *Nature Reviews Cancer*, 13(2), pp.97–110.

Crapo, J.D. et al., 1982. Cell number and cell characteristics of the normal human lung. *The American Review of Respiratory Disease*, 126(2), pp.332–7.

Crosby, L.M. & Waters, C.M., 2010. Epithelial repair mechanisms in the lung. *American Journal of Physiology. Lung Cellular and Molecular Physiology*, 298(6), pp.L715–31.

Cui, J. et al., 2013. Regulation of EMT by KLF4 in gastrointestinal cancer. *Current Cancer Drug Targets*, 13(9), pp.986–95.

Cunningham, A.C. et al., 1994. Constitutive expression of MHC and adhesion molecules by alveolar epithelial cells (type II pneumocytes) isolated from human lung and comparison with immunocytochemical findings. *Journal of Cell Science*, 107(Pt 2), pp.443–9.

Cushing, L. et al., 2011. miR-29 is a major regulator of genes associated with pulmonary fibrosis. *American Journal of Respiratory Cell and Molecular Biology*, 45(2), pp.287–94.

Dalmay, T., 2013. Mechanism of miRNA-mediated repression of mRNA translation. *Essays in Biochemistry*, 54, pp.29–38.

Das, S. et al., 2014. MicroRNA-326 regulates profibrotic functions of transforming growth factor-β in pulmonary fibrosis. *American Journal of Respiratory Cell and Molecular Biology*, 50(5), pp.882–92.

Davies, L. et al., 2007. Identification of transfected cell types following non-viral gene transfer to the murine lung. *Journal of Gene Medicine*, 9(3), pp.184–96.

Davis-Dusenbery, B.N. & Hata, A., 2010. Mechanisms of control of microRNA biogenesis. *Journal of Biochemistry*, 148(4), pp.381–92.

Davis, B.N. et al., 2010. Smad proteins bind a conserved RNA sequence to promote microRNA maturation by Drosha. *Molecular Cell*, 39(3), pp.373–84.

Degryse, A.L. et al., 2010. Repetitive intratracheal bleomycin models several features of idiopathic pulmonary fibrosis. *American Journal of Physiology. Lung Cellular and Molecular Physiology*, 299(4), pp.L442–52.

Deharvengt, S., Marmarelis, M. & Korc, M., 2012. Concomitant targeting of EGF receptor, TGF-beta and SRC points to a novel therapeutic approach in pancreatic cancer. *PLoS One*, 7(6), pp.1–11.

Dellagi, K. et al., 1983. Alteration of vimentin intermediate filament expression during differentiation of human hemopoietic cells. *The EMBO Journal*, 2(9), pp.1509–14.

Demaio, L. et al., 2009. Characterization of mouse alveolar epithelial cell monolayers. *American Journal of Physiology. Lung Cellular and Molecular Physiology*, 296(6), pp.L1051–8.

Denli, A.M. et al., 2004. Processing of primary microRNAs by the Microprocessor complex. *Nature*, 432(7014), pp.231–5.

Ding, X.C. & Grosshans, H., 2009. Repression of C. elegans microRNA targets at the initiation level of translation requires GW182 proteins. *The EMBO Journal*, 28(3), pp.213–22.

Dobbs, L.G., 1990. Isolation and culture of alveolar type II cells. *The American Journal of Physiology*, 258(4 Pt 1), pp.L134–47.

Douglas, W.H. & Farrell, P.M., 1976. Isolation of cells that retain differentiated functions in vitro: properties of clonally isolated type II alveolar pneymonocytes. *Environmental Health Perspectives*, 16, pp.83–8.

Eaton, D.C. et al., 2004. Regulation of Na+ channels in lung alveolar type II epithelial cells. *Proceedings of the American Thoracic Society*, 1(1), pp.10–6.

Eckes, B. et al., 1998. Impaired mechanical stability, migration and contractile capacity in vimentin-deficient fibroblasts. *Journal of Cell Science*, 111(Pt 13), pp.1897–907.

Elbashir, S.M., Harborth, J., et al., 2001. Duplexes of 21-nucleotide RNAs mediate RNA interference in cultured mammalian cells. *Nature*, 411(6836), pp.494–8.

Elbashir, S.M., Lendeckel, W. & Tuschl, T., 2001. RNA interference is mediated by 21- and 22-nucleotide RNAs. *Genes & Development*, 15(2), pp.188–200.

Esteban, M.A. et al., 2012. The mesenchymal-to-epithelial transition in somatic cell reprogramming. *Current Opinion in Genetics & Development*, 22(5), pp.423–8.

Evans, M.J. et al., 1975. Transformation of alveolar type 2 cells to type 1 cells following exposure to NO2. *Experimental and Molecular Pathology*, 22(1), pp.142–50.

Ezzie, M.E. et al., 2012. Gene expression networks in COPD: microRNA and mRNA regulation. *Thorax*, 67(2), pp.122–31.

Fabian, M.R. et al., 2011. miRNA-mediated deadenylation is orchestrated by GW182 through two conserved motifs that interact with CCR4-NOT. *Nature Structural & Molecular Biology*, 18(11), pp.1211–7.

Fang, X. et al., 2006. Contribution of CFTR to apical-basolateral fluid transport in cultured human alveolar epithelial type II cells. *American Journal of Physiology. Lung Cellular and Molecular Physiology*, 290(2), pp.L242–9.

Fehrenbach, H., 2001. Alveolar epithelial type II cell: defender of the alveolus revisited. *Respiratory Research*, 2(1), pp.33–46.

Felton, V.M., Borok, Z. & Willis, B.C., 2009. N-acetylcysteine inhibits alveolar epithelial-mesenchymal transition. *American Journal of Physiology. Lung Cellular and Molecular Physiology*, 297(5), pp.L805–12.

Fire, A. et al., 1998. Potent and specific genetic interference by double-stranded RNA in Caenorhabditis elegans. *Nature*, 391(6669), pp.806–11.

Fish, J.E. et al., 2008. miR-126 regulates angiogenic signaling and vascular integrity. *Developmental Cell*, 15(2), pp.272–84.

Flieger, D. et al., 2001. Influence of cytokines, monoclonal antibodies and chemotherapeutic drugs on epithelial cell adhesion molecule (EpCAM) and LewisY antigen expression. *Clinical and Experimental Immunology*, 123(1), pp.9–14.

Franke, W.W. et al., 1978. Different intermediate-sized filaments distinguished by immunofluorescence microscopy. *Proceedings of the National Academy of Sciences of the United States of America*, 75(10), pp.5034–8.

Friedman, R.C. et al., 2009. Most mammalian mRNAs are conserved targets of microRNAs. *Genome Research*, 19(1), pp.92–105.

Fuchs, S. et al., 2003. Differentiation of human alveolar epithelial cells in primary culture: morphological characterization and synthesis of caveolin-1 and surfactant protein-C. *Cell and Tissue Research*, 311(1), pp.31–45.

Fujino, N., Kubo, H., et al., 2012. A novel method for isolating individual cellular components from the adult human distal lung. *American Journal of Respiratory Cell and Molecular Biology*, 46(4), pp.422–30.

Fujino, N., Ota, C., Suzuki, T., et al., 2012. Analysis of gene expression profiles in alveolar epithelial type II-like cells differentiated from human alveolar epithelial progenitor cells. *Respiratory Investigation*, 50(3), pp.110–6.

Fujino, N., Ota, C., Takahashi, T., et al., 2012. Gene expression profiles of alveolar type II cells of chronic obstructive pulmonary disease: a case-control study. *BMJ open*, 2(6), pp.1–10.

Gatsiou, A. et al., 2012. MicroRNAs in platelet biogenesis and function: implications in vascular homeostasis and inflammation. *Current Vascular Pharmacology*, 10(5), pp.524–31.

Gaunsbaek, M.Q. et al., 2013. Lung surfactant protein D (SP-D) response and regulation during acute and chronic lung injury. *Lung*, 191(3), pp.295–303.

Gereke, M. et al., 2009. Alveolar type II epithelial cells present antigen to CD4(+) T cells and induce Foxp3(+) regulatory T cells. *American Journal of Respiratory and Critical Care Medicine*, 179(5), pp.344–55.

Gereke, M. et al., 2012. Flow cytometric isolation of primary murine type II alveolar epithelial cells for functional and molecular studies. *Journal of Visualized Experiments: JoVE*, 70, pp.1–7.

Gereke, M. et al., 2007. Phenotypic alterations in type II alveolar epithelial cells in CD4+ T cell mediated lung inflammation. *Respiratory Research*, 8(47), pp.1–13.

Ghildiyal, M. & Zamore, P.D., 2009. Small silencing RNAs: an expanding universe. *Nature Reviews Genetics*, 10(2), pp.94–108.

Giannoni, E. et al., 2006. Surfactant proteins A and D enhance pulmonary clearance of Pseudomonas aeruginosa. *American Journal of Respiratory Cell and Molecular Biology*, 34(6), pp.704–10.

Gibbons, D.L. et al., 2009. Contextual extracellular cues promote tumor cell EMT and metastasis by regulating miR-200 family expression. *Genes & Development*, 23(18), pp.2140–51.

Girard, A. et al., 2006. A germline-specific class of small RNAs binds mammalian Piwi

proteins. *Nature*, 442(7099), pp.199–202.

Gordon, K.J. & Blobe, G.C., 2008. Role of transforming growth factor-beta superfamily signaling pathways in human disease. *Biochimica et Biophysica Acta*, 1782(4), pp.197–228.

Greene, C.M. & Gaughan, K.P., 2013. microRNAs in asthma: potential therapeutic targets. *Current Opinion in Pulmonary Medicine*, 19(1), pp.66–72.

Gregory, P.A. et al., 2008. The miR-200 family and miR-205 regulate epithelial to mesenchymal transition by targeting ZEB1 and SIP1. *Nature Cell Biology*, 10(5), pp.593–601.

Gregory, R.I. et al., 2004. The Microprocessor complex mediates the genesis of microRNAs. *Nature*, 432(7014), pp.235–40.

Griese, M., 1999. Pulmonary surfactant in health and human lung diseases: state of the art. *The European Respiratory Journal*, 13(6), pp.1455–76.

Griese, M. et al., 2001. Uptake of a natural surfactant and increased delivery of small organic anions into type II pneumocytes. *American Journal of Physiology. Lung Cellular and Molecular Physiology*, 281(1), pp.L144–54.

Grivna, S.T. et al., 2006. A novel class of small RNAs in mouse spermatogenic cells. *Genes & Development*, 20(13), pp.1709–14.

Guo, H. et al., 2010. Mammalian microRNAs predominantly act to decrease target mRNA levels. *Nature*, 466(7308), pp.835–40.

Gwizdek, C. et al., 2003. Exportin-5 mediates nuclear export of minihelix-containing RNAs. *The Journal of Biological Chemistry*, 278(8), pp.5505–8.

Ha, M. & Kim, V.N., 2014. Regulation of microRNA biogenesis. *Nature Reviews Molecular Cell Biology*, 15(8), pp.509–24.

Hagimoto, N. et al., 1997. Induction of apoptosis and pulmonary fibrosis in mice in response to ligation of Fas antigen. *American Journal of Respiratory Cell and Molecular Biology*, 17(3), pp.272–8.

Hammond, S.M., 2015. An overview of microRNAs. *Advanced Drug Delivery Reviews*, 87, pp.3–14.

Han, J. et al., 2006. Molecular basis for the recognition of primary microRNAs by the Drosha-DGCR8 complex. *Cell*, 125(5), pp.887–901.

Han, J. et al., 2004. The Drosha-DGCR8 complex in primary microRNA processing. *Genes & Development*, 18(24), pp.3016–27.

Han, M. et al., 2016. MicroRNA-21 induces breast cancer cell invasion and migration by suppressing smad7 via EGF and TGF-β pathways. *Oncology Reports*, 35(1), pp.73–80.

Harris, T.A. et al., 2008. MicroRNA-126 regulates endothelial expression of vascular cell adhesion molecule 1. *Proceedings of the National Academy of Sciences of the United States of America*, 105(5), pp.1516–21.

Harrison, J.H., Porretta, C.P. & Leming, K., 1995. Purification of murine pulmonary type II cells for flow cytometric cell cycle analysis. *Experimental Lung Research*, 21(3), pp.407–21.

Hassan, F. et al., 2012. MiR-101 and miR-144 regulate the expression of the CFTR chloride channel in the lung. *PLoS One*, 7(11), pp.1–11.

He, L. & Hannon, G.J., 2004. MicroRNAs: small RNAs with a big role in gene regulation. *Nature Reviews Genetics*, 5(7), pp.522–31.

Heikal, A.A., 2010. Intracellular coenzymes as natural biomarkers for metabolic activities and mitochondrial anomalies. *Biomarkers in Medicine*, 4(2), pp.241–63.

Henke, J.I. et al., 2008. microRNA-122 stimulates translation of hepatitis C virus RNA. *The EMBO Journal*, 27(24), pp.3300–10.

Hill, L., Browne, G. & Tulchinsky, E., 2013. ZEB/miR-200 feedback loop: at the crossroads of signal transduction in cancer. *International Journal of Cancer*, 132(4), pp.745–54.

Houtz, B., Trotter, J. & Sasaki, D., 2004. BD FACSAria Sorting. *BD FACServiceTM Technotes*, 9(4), pp.4–9.

Hu, R. et al., 2014. MicroRNA-10a controls airway smooth muscle cell proliferation via direct targeting of the PI3 kinase pathway. *The FASEB Journal*, 28(5), pp.2347–57.

Hu, X. et al., 2009. A miR-200 microRNA cluster as prognostic marker in advanced ovarian cancer. *Gynecologic Oncology*, 114(3), pp.457–464.

Huang, H. et al., 2010. miR-10a contributes to retinoid acid-induced smooth muscle cell differentiation. *The Journal of Biological Chemistry*, 285(13), pp.9383–9.

Hugo, H. et al., 2007. Epithelial-mesenchymal and mesenchymal-epithelial transitions in carcinoma progression. *Journal of Cellular Physiology*, 213(2), pp.374–83.

Humphreys, D.T. et al., 2005. MicroRNAs control translation initiation by inhibiting eukaryotic initiation factor 4E/cap and poly(A) tail function. *Proceedings of the National Academy of Sciences of the United States of America*, 102(47),

pp.16961–6.

Huntzinger, E. & Izaurralde, E., 2011. Gene silencing by microRNAs: contributions of translational repression and mRNA decay. *Nature Reviews Genetics*, 12(2), pp.99–110.

Ingenuity® Systems, 2012. Summer release 2012. Available at: www.ingenuity.com [Accessed January 14, 2014].

Inui, M., Martello, G. & Piccolo, S., 2010. MicroRNA control of signal transduction. *Nature Reviews Molecular Cell Biology*, 11(4), pp.252–63.

Itoh, S. & Itoh, F., 2011. Inhibitory machinery for the TGF-β family signaling pathway. *Growth Factors*, 29(5), pp.163–73.

Iwasaki, S. & Tomari, Y., 2009. Argonaute-mediated translational repression (and activation). *Fly*, 3(3), pp.204–6.

Jiang, Q. et al., 2016. miR-16 induction after CDK4 knockdown is mediated by c-Myc suppression and inhibits cell growth as well as sensitizes nasopharyngeal carcinoma cells to chemotherapy. *Tumor Biology*, 37(2), pp.2425–33.

Jiang, Z. et al., 2014. MiRNA 17 family regulates cisplatin-resistant and metastasis by targeting TGFbetaR2 in NSCLC. *PLoS One*, 9(4), pp.1–9.

Jimenez-Mateos, E.M. & Henshall, D.C., 2013. Epilepsy and microRNA. *Neuroscience*, 238, pp.218–29.

Jopling, C.L., Norman, K.L. & Sarnow, P., 2006. Positive and negative modulation of viral and cellular mRNAs by liver-specific microRNA miR-122. *Cold Spring Harbor Symposia on Quantitative Biology*, 71, pp.369–76.

Ju, X. et al., 2014. Identification of a cyclin D1 network in prostate cancer that antagonizes epithelial-mesenchymal restraint. *Cancer Research*, 74(2), pp.508–19.

Kalluri, R. & Neilson, E.G., 2003. Epithelial-mesenchymal transition and its implications for fibrosis. *The Journal of Clinical Investigation*, 112(12), pp.1776–84.

Kalluri, R. & Weinberg, R.A., 2009. The basics of epithelial-mesenchymal transition. *The Journal of Clinical Investigation*, 119(6), pp.1420–8.

Kantyka, T. et al., 2013. Staphylococcus aureus proteases degrade lung surfactant protein A potentially impairing innate immunity of the lung. *Journal of Innate Immunity*, 5(3), pp.251–60.

Kikkawa, Y. & Yoneda, K., 1974. The type II epithelial cell of the lung. I. Method of isolation. *Laboratory Investigation*, 30(1), pp.76–84.

Kim, C.F.B. et al., 2005. Identification of bronchioalveolar stem cells in normal lung and lung cancer. *Cell*, 121(6), pp.823–35.

Kim, K.K. et al., 2006. Alveolar epithelial cell mesenchymal transition develops in vivo during pulmonary fibrosis and is regulated by the extracellular matrix. *Proceedings of the National Academy of Sciences of the United States of America*, 103(35), pp.13180–5.

Kim, K.K. et al., 2009. Epithelial cell alpha3beta1 integrin links beta-catenin and Smad signaling to promote myofibroblast formation and pulmonary fibrosis. *The Journal of Clinical Investigation*, 119(1), pp.213–24.

Kim, V.N., Han, J. & Siomi, M.C., 2009. Biogenesis of small RNAs in animals. *Nature Reviews Molecular Cell Biology*, 10(2), pp.126–39.

Königshoff, M., 2009. *The WNT1 induced signalling protein 1 is a novel mediator of impaired epithelial-mesenchymal interactions in lung fibrosis [Dissertation]*. Giessen: Faculty of Medicine of the Justus Liebig University Giessen.

Königshoff, M. et al., 2009. WNT1-inducible signaling protein-1 mediates pulmonary fibrosis in mice and is upregulated in humans with idiopathic pulmonary fibrosis. *The Journal of Clinical Investigation*, 119(4), pp.772–87.

Königshoff, M. & Eickelberg, O., 2011. Inhibitors of Glycogen Synthase Kinase 3 for Use in Therapeutic Methods and Screening Method Relating Thereto. *World Intellectual Property Organization*, Patent No.(WO 2011/113586 A1).

Korpal, M. et al., 2008. The miR-200 family inhibits epithelial-mesenchymal transition and cancer cell migration by direct targeting of E-cadherin transcriptional repressors ZEB1 and ZEB2. *The Journal of Biological Chemistry*, 283(22), pp.14910–4.

Kotton, D., Fabian, A. & Mulligan, R., 2005. Failure of bone marrow to reconstitute lung epithelium. *American Journal of Respiratory Cell and Molecular Biology*, 33(4), pp.328–34.

Kozomara, A. & Griffiths-Jones, S., 2014. miRBase: annotating high confidence microRNAs using deep sequencing data. *Nucleic Acids Research*, 42(1), pp.D68–73.

Krane, C.M. et al., 2001. Aquaporin 5-deficient mouse lungs are hyperresponsive to cholinergic stimulation. *Proceedings of the National Academy of Sciences of the United States of America*, 98(24), pp.14114–9.

Kreda, S.M. et al., 2001. Expression and localization of epithelial aquaporins in the adult human lung. *American Journal of Respiratory Cell and Molecular Biology*,

24(3), pp.224–34.

Kurashige, J. et al., 2012. MicroRNA-200b regulates cell proliferation, invasion, and migration by directly targeting ZEB2 in gastric carcinoma. *Annals of Surgical Oncology*, 19 Suppl 3, pp.S656–64.

Lagos-Quintana, M. et al., 2001. Identification of novel genes coding for small expressed RNAs. *Science*, 294(5543), pp.853–8.

Lamouille, S. et al., 2013. Regulation of epithelial-mesenchymal and mesenchymal-epithelial transitions by microRNAs. *Current Opinion in Cell Biology*, 25(2), pp.200–7.

Lamouille, S., Xu, J. & Derynck, R., 2014. Molecular mechanisms of epithelial-mesenchymal transition. *Nature Reviews Molecular Cell Biology*, 15(3), pp.178–96.

Landgraf, P. et al., 2007. A mammalian microRNA expression atlas based on small RNA library sequencing. *Cell*, 129(7), pp.1401–14.

Landthaler, M., Yalcin, A. & Tuschl, T., 2004. The human DiGeorge syndrome critical region gene 8 and Its D. melanogaster homolog are required for miRNA biogenesis. *Current Biology*, 14(23), pp.2162–7.

Lau, N.C. et al., 2001. An abundant class of tiny RNAs with probable regulatory roles in Caenorhabditis elegans. *Science*, 294(5543), pp.858–62.

Lau, N.C. et al., 2006. Characterization of the piRNA complex from rat testes. *Science*, 313(5785), pp.363–7.

LeBleu, V.S. et al., 2013. Origin and function of myofibroblasts in kidney fibrosis. *Nature Medicine*, 19(8), pp.1047–53.

Lee, D. et al., 2015. DJ-1 regulates the expression of renal (pro)renin receptor via reactive oxygen species-mediated epigenetic modification. *Biochimica et Biophysica Acta*, 1850(2), pp.426–34.

Lee, R.C. & Ambros, V., 2001. An extensive class of small RNAs in Caenorhabditis elegans. *Science*, 294(5543), pp.862–4.

Lee, R.C., Feinbaum, R.L. & Ambros, V., 1993. The C. elegans heterochronic gene lin-4 encodes small RNAs with antisense complementarity to lin-14. *Cell*, 75(5), pp.843–54.

Lee, Y. et al., 2004. MicroRNA genes are transcribed by RNA polymerase II. *The EMBO Journal*, 23(20), pp.4051–60.

Lee, Y. et al., 2006. The role of PACT in the RNA silencing pathway. *The EMBO*

Journal, 25(3), pp.522–32.

Lenfert, E. et al., 2015. Mutant p53 promotes epithelial-mesenchymal plasticity and enhances metastasis in mammary carcinomas of WAP-T mice. *International Journal of Cancer*, 136(6), pp.E521–33.

Li, R. et al., 2010. A mesenchymal-to-epithelial transition initiates and is required for the nuclear reprogramming of mouse fibroblasts. *Cell Stem Cell*, 7(1), pp.51–63.

Liao, G. et al., 2014. IGF-1-induced epithelial-mesenchymal transition in MCF-7 cells is mediated by MUC1. *Cellular Signalling*, 26(10), pp.2131–7.

Liu, G. et al., 2010. miR-21 mediates fibrogenic activation of pulmonary fibroblasts and lung fibrosis. *The Journal of Experimental Medicine*, 207(8), pp.1589–97.

Liu, X. et al., 2013. Regulation of microRNAs by epigenetics and their interplay involved in cancer. *Journal of Experimental & Clinical Cancer Research*, 32(96), pp.1–8.

Livak, K.J. & Schmittgen, T.D., 2001. Analysis of relative gene expression data using real-time quantitative PCR and the 2(-Delta Delta C(T)) Method. *Methods*, 25(4), pp.402–8.

Loh, K. et al., 2006. A comparison study of cerebral protection using Ginkgo biloba extract and Losartan on stroked rats. *Neuroscience Letters*, 398(1-2), pp.28–33.

Ma, X. et al., 2014. Expression, Regulation and Function of MicroRNAs in Multiple Sclerosis. *International Journal of Medical Sciences*, 11(8), pp.810–818.

Maciotta, S., Meregalli, M. & Torrente, Y., 2013. The involvement of microRNAs in neurodegenerative diseases. *Frontiers in Cellular Neuroscience*, 7, pp.1–17.

Mall, C. et al., 2013. Stability of miRNA in human urine supports its biomarker potential. *Biomarkers in Medicine*, 7(4), pp.623–31.

Maroney, P.A. et al., 2006. Evidence that microRNAs are associated with translating messenger RNAs in human cells. *Nature Structural & Molecular Biology*, 13(12), pp.1102–7.

Marsh, L.M. et al., 2009. Surface expression of CD74 by type II alveolar epithelial cells: a potential mechanism for macrophage migration inhibitory factor-induced epithelial repair. *American Journal of Physiology. Lung Cellular and Molecular Physiology*, 296(3), pp.L442–52.

Mason, R.J., 2006. Biology of alveolar type II cells. *Respirology*, 11 Suppl, pp.S12–5.

Mason, R.J. & Williams, M.C., 1977. Type II alveolar cell. Defender of the alveolus. *The American Review of Respiratory Disease*, 115(6 Pt 2), pp.81–91.

Massagué, J., 1998. TGF-beta signal transduction. *Annual Review of Biochemistry*, 67, pp.753–91.

Massagué, J., 2012. TGFβ signalling in context. *Nature Reviews Molecular Cell Biology*, 13(10), pp.616–30.

Matsuzaki, T. et al., 2009. Immunohistochemical localization of the aquaporins AQP1, AQP3, AQP4, and AQP5 in the mouse respiratory system. *Acta Histochemica et Cytochemica*, 42(6), pp.159–69.

Mattick, J.S. & Makunin, I. V, 2006. Non-coding RNA. *Human Molecular Genetics*, 15 Suppl 1, pp.R17–29.

Meister, G. et al., 2004. Human Argonaute2 mediates RNA cleavage targeted by miRNAs and siRNAs. *Molecular Cell*, 15(2), pp.185–97.

Messier, E.M., Mason, R.J. & Kosmider, B., 2012. Efficient and rapid isolation and purification of mouse alveolar type II epithelial cells. *Experimental Lung Research*, 38(7), pp.363–73.

miRbase, 2016. miRBase. Available at: http://www.mirbase.org/ [Accessed February 26, 2016].

Mishra, P.J., 2014. MicroRNAs as promising biomarkers in cancer diagnostics. *Biomarker Research*, 2, pp.1–4.

Mitchell, P.S. et al., 2008. Circulating microRNAs as stable blood-based markers for cancer detection. *Proceedings of the National Academy of Sciences of the United States of America*, 105(30), pp.10513–8.

Mittal, V., 2016. Epithelial Mesenchymal Transition in Aggressive Lung Cancers. *Advances in Experimental Medicine and Biology*, 890, pp.37–56.

Monici, M., 2005. Cell and tissue autofluorescence research and diagnostic applications. *Biotechnology Annual Review*, 11, pp.227–56.

Moreno-Moya, J.M., Vilella, F. & Simón, C., 2014. MicroRNA: key gene expression regulators. *Fertility and Sterility*, 101(6), pp.1516–23.

Moustakas, A. & Heldin, C.-H., 2009. The regulation of TGFbeta signal transduction. *Development*, 136(22), pp.3699–714.

Mueller, O., Lightfoot, S. & Schroeder, A., 2004. RNA Integrity Number (RIN) – Standardization of RNA Quality Control Application. *Agilent Application Note*. Available at: https://www.agilent.com/cs/library/applications/5989-1165EN.pdf [Accessed November 15, 2013].

Mutze, K. et al., 2015. Enolase 1 (ENO1) and protein disulfide-isomerase associated 3

(PDIA3) regulate Wnt/β-catenin-driven trans-differentiation of murine alveolar epithelial cells. *Disease Models & Mechanisms*, 8(8), pp.877–90.

Myles, J.E., Geddes, B.A. & Massey, T.E., 1989. Biotransformation activities in Clara and alveolar type II cells isolated from hamster lungs. *Research Communications in Chemical Pathology and Pharmacology*, 66(2), pp.297–309.

Natarajan, S.K. et al., 2013. MicroRNA Function in Human Diseases. *Medical Epigenetics*, 1(1), pp.106–115.

NCBI, 2016. Home - PubMed - NCBI. Available at: http://www.ncbi.nlm.nih.gov/pubmed/ [Accessed July 2, 2016].

Newton, D. a et al., 2006. Hemoglobin is expressed by alveolar epithelial cells. *The Journal of Biological Chemistry*, 281(9), pp.5668–76.

Nielsen, S. et al., 1997. Aquaporins in complex tissues. II. Subcellular distribution in respiratory and glandular tissues of rat. *The American Journal of Physiology*, 273(5 Pt 1), pp.C1549–61.

Nottrott, S., Simard, M.J. & Richter, J.D., 2006. Human let-7a miRNA blocks protein production on actively translating polyribosomes. *Nature Structural & Molecular Biology*, 13(12), pp.1108–14.

Nurwidya, F. et al., 2014. Treatment with insulin-like growth factor 1 receptor inhibitor reverses hypoxia-induced epithelial-mesenchymal transition in non-small cell lung cancer. *Biochemical and Biophysical Research Communications*, 455(3-4), pp.332–8.

Ørom, U.A., Nielsen, F.C. & Lund, A.H., 2008. MicroRNA-10a binds the 5'UTR of ribosomal protein mRNAs and enhances their translation. *Molecular Cell*, 30(4), pp.460–71.

Ouyang, H. et al., 2014. microRNA-10b enhances pancreatic cancer cell invasion by suppressing TIP30 expression and promoting EGF and TGF-β actions. *Oncogene*, 33(38), pp.4664–74.

Ozdamar, B. et al., 2005. Regulation of the polarity protein Par6 by TGFbeta receptors controls epithelial cell plasticity. *Science*, 307(5715), pp.1603–9.

Pandit, K. V et al., 2010. Inhibition and role of let-7d in idiopathic pulmonary fibrosis. *American Journal of Respiratory and Critical Care Medicine*, 182(2), pp.220–9.

Park, N.J. et al., 2009. Salivary microRNA: discovery, characterization, and clinical utility for oral cancer detection. *Clinical Cancer Research*, 15(17), pp.5473–7.

Park, S.-M. et al., 2008. The miR-200 family determines the epithelial phenotype of

cancer cells by targeting the E-cadherin repressors ZEB1 and ZEB2. *Genes & Development*, 22(7), pp.894–907.

Pataki, G. et al., 1996. Quantitation of the alveolar distribution of surfactant mixtures in normal and injured lungs. *American Journal of Respiratory Cell and Molecular Biology*, 15(4), pp.451–9.

Perry, M.M. et al., 2014. Airway smooth muscle hyperproliferation is regulated by microRNA-221 in severe asthma. *American Journal of Respiratory Cell and Molecular Biology*, 50(1), pp.7–17.

Petersen, C.P. et al., 2006. Short RNAs repress translation after initiation in mammalian cells. *Molecular Cell*, 21(4), pp.533–42.

Postigo, A.A., 2003. Opposing functions of ZEB proteins in the regulation of the TGFbeta/BMP signaling pathway. *The EMBO Journal*, 22(10), pp.2443–52.

Pottelberge, G.R. Van et al., 2011. MicroRNA expression in induced sputum of smokers and patients with chronic obstructive pulmonary disease. *American Journal of Respiratory and Critical Care Medicine*, 183(7), pp.898–906.

Prudkin, L. et al., 2009. Epithelial-to-mesenchymal transition in the development and progression of adenocarcinoma and squamous cell carcinoma of the lung. *Modern Pathology*, 22(5), pp.668–78.

Puisieux, A., Brabletz, T. & Caramel, J., 2014. Oncogenic roles of EMT-inducing transcription factors. *Nature Cell Biology*, 16(6), pp.488–94.

Rao, P., Benito, E. & Fischer, A., 2013. MicroRNAs as biomarkers for CNS disease. *Frontiers in Molecular Neuroscience*, 6, pp.1–13.

Ravasio, A. et al., 2010. Lamellar bodies form solid three-dimensional films at the respiratory air-liquid interface. *The Journal of Biological Chemistry*, 285(36), pp.28174–82.

Rawal, S., Manning, P. & Katare, R., 2014. Cardiovascular microRNAs: as modulators and diagnostic biomarkers of diabetic heart disease. *Cardiovascular Diabetology*, 13, pp.1–24.

Reinhart, B.J. et al., 2000. The 21-nucleotide let-7 RNA regulates developmental timing in Caenorhabditis elegans. *Nature*, 403(6772), pp.901–6.

Renjie, W. & Haiqian, L., 2015. MiR-132, miR-15a and miR-16 synergistically inhibit pituitary tumor cell proliferation, invasion and migration by targeting Sox5. *Cancer Letters*, 356(2 Pt B), pp.568–78.

Rice, W.R. et al., 2002. Maintenance of the mouse type II cell phenotype in vitro.

American Journal of Physiology. Lung Cellular and Molecular Physiology, 283(2), pp.L256–64.

Robinson, P.C., Voelker, D.R. & Mason, R.J., 1984. Isolation and culture of human alveolar type II epithelial cells. Characterization of their phospholipid secretion. *The American Review of Respiratory Disease*, 130(6), pp.1156–60.

Rochat, T.R., Casale, J.M. & Hunninghake, G.W., 1988. Characterization of type II alveolar epithelial cells by flow cytometry and fluorescent markers. *The Journal of Laboratory and Clinical Medicine*, 112(4), pp.418–25.

Rock, J.R. et al., 2011. Multiple stromal populations contribute to pulmonary fibrosis without evidence for epithelial to mesenchymal transition. *Proceedings of the National Academy of Sciences of the United States of America*, 108(52), pp.E1475–83.

Rockey, D.C., Bell, P.D. & Hill, J.A., 2015. Fibrosis-a common pathway to organ injury and failure. *The New England Journal of Medicine*, 372(12), pp.1138–49.

Ross, R.J., Weiner, M.M. & Lin, H., 2014. PIWI proteins and PIWI-interacting RNAs in the soma. *Nature*, 505(7483), pp.353–9.

Ryu, I. et al., 2013. eIF4GI facilitates the MicroRNA-mediated gene silencing. *PLoS One*, 8(2), pp.1–13.

Sakamoto, T. et al., 2001. Maintenance of the differentiated type II cell characteristics by culture on an acellular human amnion membrane. *In Vitro Cellular & Developmental Biology - Animal*, 37(8), pp.471–9.

Samavarchi-Tehrani, P. et al., 2010. Functional genomics reveals a BMP-driven mesenchymal-to-epithelial transition in the initiation of somatic cell reprogramming. *Cell Stem Cell*, 7(1), pp.64–77.

Sato, T. et al., 2010. Reduced miR-146a increases prostaglandin E_2 in chronic obstructive pulmonary disease fibroblasts. *American Journal of Respiratory and Critical Care Medicine*, 182(8), pp.1020–9.

Schrier, D.J., Kunkel, R.G. & Phan, S.H., 1983. The role of strain variation in murine bleomycin-induced pulmonary fibrosis. *The American Review of Respiratory Disease*, 127(1), pp.63–6.

Schwarz, D.S. et al., 2003. Asymmetry in the assembly of the RNAi enzyme complex. *Cell*, 115(2), pp.199–208.

Selbach, M. et al., 2008. Widespread changes in protein synthesis induced by microRNAs. *Nature*, 455(7209), pp.58–63.

Shen, J., Stass, S.A. & Jiang, F., 2013. MicroRNAs as potential biomarkers in human solid tumors. *Cancer Letters*, 329(2), pp.125–36.

Shi, L. et al., 2014. p53-induced miR-15a/16-1 and AP4 form a double-negative feedback loop to regulate epithelial-mesenchymal transition and metastasis in colorectal cancer. *Cancer Research*, 74(2), pp.532–42.

Siasos, G. et al., 2013. MicroRNAs: Novel diagnostic and prognostic biomarkers in atherosclerosis. *Current Topics in Medicinal Chemistry*, 13(13), pp.1503–17.

Siomi, M.C. et al., 2011. PIWI-interacting small RNAs: the vanguard of genome defence. *Nature Reviews Molecular Cell Biology*, 12(4), pp.246–58.

Soltermann, A., 2012. Epithelial-mesenchymale Transition beim nichtkleinzelligen Bronchialkarzinom. *Der Pathologe*, 33 Suppl 2, pp.311–7.

Starlets, D. et al., 2006. Cell-surface CD74 initiates a signaling cascade leading to cell proliferation and survival. *Blood*, 107(12), pp.4807–16.

Stegemann-Koniszewski, S. et al., 2016. Alveolar Type II Epithelial Cells Contribute to the Anti-Influenza A Virus Response in the Lung by Integrating Pathogen- and Microenvironment-Derived Signals. *mBio*, 7(3), pp.1–11.

Stenn, K.S. et al., 1989. Dispase, a neutral protease from Bacillus polymyxa, is a powerful fibronectinase and type IV collagenase. *The Journal of Investigative Dermatology*, 93(2), pp.287–90.

Takahashi, K. et al., 2009. Macrophage CD74 contributes to MIF-induced pulmonary inflammation. *Respiratory Research*, 10(1), p.33.

Tang, D. et al., 2013. Identification of plasma microRNAs as novel noninvasive biomarkers for early detection of lung cancer. *European Journal of Cancer Prevention*, 22(6), pp.540–8.

Tanjore, H. et al., 2011. Alveolar epithelial cells undergo epithelial-to-mesenchymal transition in response to endoplasmic reticulum stress. *The Journal of Biological Chemistry*, 286(35), pp.30972–80.

Tanjore, H. et al., 2009. Contribution of epithelial-derived fibroblasts to bleomycin-induced lung fibrosis. *American Journal of Respiratory and Critical Care Medicine*, 180(7), pp.657–65.

Teisanu, R.M. et al., 2009. Prospective isolation of bronchiolar stem cells based upon immunophenotypic and autofluorescence characteristics. *Stem Cells*, 27(3), pp.612–22.

Tellez, C.S. et al., 2011. EMT and stem cell-like properties associated with miR-205

and miR-200 epigenetic silencing are early manifestations during carcinogen-induced transformation of human lung epithelial cells. *Cancer Research*, 71(8), pp.3087–97.

Thiery, J.P. et al., 2009. Epithelial-mesenchymal transitions in development and disease. *Cell*, 139(5), pp.871–90.

Thomson, J.M., 2006. Extensive post-transcriptional regulation of microRNAs and its implications for cancer. *Genes & Development*, 20(16), pp.2202–7.

Tian, Y.-C. et al., 2007. Epidermal growth factor and transforming growth factor-beta1 enhance HK-2 cell migration through a synergistic increase of matrix metalloproteinase and sustained activation of ERK signaling pathway. *Experimental Cell Research*, 313(11), pp.2367–77.

Trzpis, M. et al., 2007. Epithelial Cell Adhesion Molecule. *The American Journal of Pathology*, 171(2), pp.386–95.

Uhal, B.D. et al., 1998. Alveolar epithelial cell death adjacent to underlying myofibroblasts in advanced fibrotic human lung. *The American Journal of Physiology*, 275(6 Pt 1), pp.L1192–9.

Uhal, B.D., 1997. Cell cycle kinetics in the alveolar epithelium. *The American Journal of Physiology*, 272(6 Pt 1), pp.L1031–45.

Uhal, B.D. et al., 1995. Fibroblasts isolated after fibrotic lung injury induce apoptosis of alveolar epithelial cells in vitro. *The American Journal of Physiology*, 269(6 Pt 1), pp.L819–28.

Vasudevan, S., 2011. Posttranscriptional upregulation by microRNAs. *Wiley Interdisciplinary Reviews: RNA*, 3(3), pp.311–30.

Vasudevan, S., Tong, Y. & Steitz, J.A., 2007. Switching from repression to activation: microRNAs can up-regulate translation. *Science*, 318(5858), pp.1931–4.

Ventura, A. et al., 2008. Targeted deletion reveals essential and overlapping functions of the miR-17 through 92 family of miRNA clusters. *Cell*, 132(5), pp.875–86.

Vickers, K.C., Rye, K.-A. & Tabet, F., 2014. MicroRNAs in the onset and development of cardiovascular disease. *Clinical Science*, 126(3), pp.183–94.

Wakiyama, M. et al., 2007. Let-7 microRNA-mediated mRNA deadenylation and translational repression in a mammalian cell-free system. *Genes & Development*, 21(15), pp.1857–62.

Wang, B. et al., 2011. miR-200a Prevents renal fibrogenesis through repression of TGF-β2 expression. *Diabetes*, 60(1), pp.280–7.

Wang, B. et al., 2006. Recapitulation of short RNA-directed translational gene silencing in vitro. *Molecular Cell*, 22(4), pp.553–60.

Wang, Q. et al., 2014. MicroRNA-16 suppresses epithelial-mesenchymal transition-related gene expression in human glioma. *Molecular Medicine Reports*, 10(6), pp.3310–4.

Wang, X.-Y. et al., 2012. Novel method for isolation of murine clara cell secretory protein-expressing cells with traces of stemness. *PLoS One*, 7(8), pp.1–10.

Wang, Z. et al., 2011. Reversal and prevention of arsenic-induced human bronchial epithelial cell malignant transformation by microRNA-200b. *Toxicological Sciences*, 121(1), pp.110–22.

Watanabe, T. et al., 2006. Identification and characterization of two novel classes of small RNAs in the mouse germline: retrotransposon-derived siRNAs in oocytes and germline small RNAs in testes. *Genes & Development*, 20(13), pp.1732–43.

Weiss, A. & Attisano, L., 2013. The TGFbeta Superfamily Signaling Pathway. *Wiley Interdisciplinary Reviews: Developmental Biology*, 2(1), pp.47–63.

Willis, B.C. et al., 2005. Induction of Epithelial-Mesenchymal Transition in Alveolar Epithelial Cells by Transforming Growth Factor-β1. *The American Journal of Pathology*, 166(5), pp.1321–32.

Willis, B.C. & Borok, Z., 2007. TGF-beta-induced EMT: mechanisms and implications for fibrotic lung disease. *American Journal of Physiology. Lung Cellular and Molecular Physiology*, 293(3), pp.L525–34.

Winter, J. et al., 2009. Many roads to maturity: microRNA biogenesis pathways and their regulation. *Nature Cell Biology*, 11(3), pp.228–34.

Wu, T. et al., 2013. Tracking the engraftment and regenerative capabilities of transplanted lung stem cells using fluorescent nanodiamonds. *Nature Nanotechnology*, 8(9), pp.682–9.

Xiao, J. et al., 2012. miR-29 inhibits bleomycin-induced pulmonary fibrosis in mice. *Molecular Therapy*, 20(6), pp.1251–60.

Xu, J. et al., 2014. A novel “Turn-On” fluorescent probe for F(-) detection in aqueous solution and its application in live-cell imaging. *Analytica Chimica Acta*, 849, pp.36–42.

Xu, W., Yang, Z. & Lu, N., 2015. A new role for the PI3K/Akt signaling pathway in the epithelial-mesenchymal transition. *Cell Adhesion & Migration*, 9(4), pp.317–24.

Yamada, M. et al., 2008. Dual-immunohistochemistry provides little evidence for

epithelial-mesenchymal transition in pulmonary fibrosis. *Histochemistry and Cell Biology*, 129(4), pp.453–62.

Yamada, M. et al., 2013. The increase of microRNA-21 during lung fibrosis and its contribution to epithelial-mesenchymal transition in pulmonary epithelial cells. *Respiratory Research*, 14, pp.1–13.

Yang, J. et al., 2015. Twist induces epithelial-mesenchymal transition and cell motility in breast cancer via ITGB1-FAK/ILK signaling axis and its associated downstream network. *The International Journal of Biochemistry & Cell Biology*, 71, pp.62–71.

Yang, S. et al., 2012. Participation of miR-200 in pulmonary fibrosis. *The American Journal of Pathology*, 180(2), pp.484–93.

Yang, X. et al., 2015. Downregulation of p53 promotes in vitro perineural invasive activity of human salivary adenoid cystic carcinoma cells through epithelial-mesenchymal transition-like changes. *Oncology Reports*, 33(4), pp.1650–6.

Yilmaz, M. & Christofori, G., 2009. EMT, the cytoskeleton, and cancer cell invasion. *Cancer and Metastasis Reviews*, 28(1-2), pp.15–33.

Yu, J. et al., 2014. miR-300 inhibits epithelial to mesenchymal transition and metastasis by targeting Twist in human epithelial cancer. *Molecular Cancer*, 13, pp.1–12.

Yu, L. et al., 2010. Early detection of lung adenocarcinoma in sputum by a panel of microRNA markers. *International Journal of Cancer*, 127(12), pp.2870–8.

Zander, D. et al., 2006. Donor-derived type II pneumocytes are rare in the lungs of allogeneic hematopoietic cell transplant recipients. *Annals of Clinical and Laboratory Science*, 36(1), pp.47–52.

Zandvoort, A. et al., 2006. Altered expression of the Smad signalling pathway: implications for COPD pathogenesis. *The European Respiratory Journal*, 28(3), pp.533–41.

Zeisberg, M. & Neilson, E.G., 2009. Biomarkers for epithelial-mesenchymal transitions. *The Journal of Clinical Investigation*, 119(6), pp.1429–37.

Zeng, Y., Yi, R. & Cullen, B.R., 2005. Recognition and cleavage of primary microRNA precursors by the nuclear processing enzyme Drosha. *The EMBO Journal*, 24(1), pp.138–48.

Zhang, H.-Y. et al., 2014. Transforming growth factor-β1-induced epithelial-mesenchymal transition in human esophageal squamous cell carcinoma via the PTEN/PI3K signaling pathway. *Oncology Reports*, 32(5), pp.2134–42.

Zhang, J. et al., 2012. miR-30 inhibits TGF-β1-induced epithelial-to-mesenchymal transition in hepatocyte by targeting Snail1. *Biochemical and Biophysical Research Communications*, 417(3), pp.1100–5.

Zhang, Y. et al., 2014. Nicotine upregulates microRNA-21 and promotes TGF-β-dependent epithelial-mesenchymal transition of esophageal cancer cells. *Tumor Biology*, 35(7), pp.7063–72.

Zhong, Z. et al., 2014. Low expression of microRNA-30c promotes invasion by inducing epithelial mesenchymal transition in non-small cell lung cancer. *Molecular Medicine Reports*, 10(5), pp.2575–9.

Zidar, N. et al., 2011. Down-regulation of microRNAs of the miR-200 family and miR-205, and an altered expression of classic and desmosomal cadherins in spindle cell carcinoma of the head and neck—hallmark of epithelial-mesenchymal transition. *Human Pathology*, 42(4), pp.482–8.

10 EIDESSTATTLICHE VERSICHERUNG

Ich, Katharina Julia Singer, erkläre hiermit an Eides statt, dass ich die vorliegende Dissertation mit dem Thema “MicroRNA profiling of purified alveolar epithelial type II cells from normal mice” selbstständig verfasst, mich außer der angegebenen keiner weiteren Hilfsmittel bedient und alle Erkenntnisse, die aus dem Schrifttum ganz oder annähernd übernommen sind, als solche kenntlich gemacht und nach ihrer Herkunft unter Bezeichnung der Fundstelle einzeln nachgewiesen habe.

Ich erkläre des Weiteren, dass die hier vorgelegte Dissertation nicht in gleicher oder in ähnlicher Form bei einer anderen Stelle zur Erlangung eines akademischen Grades eingereicht wurde.

München, 05.07.2018	Katharina Singer
Ort, Datum	Unterschrift

11 DANKSAGUNG

Diese Arbeit wurde unter der Betreuung von Frau Prof. Dr. Susanne Krauss-Etschmann am Comprehensive Pneumology Center erstellt. Ich bedanke mich herzlich für die Überlassung dieses interessanten und vielseitigen Themas. Dadurch hatte ich die Möglichkeit, mich in verschiedene experimentelle Methoden von Fluorescence Activated Cell Sorting bis hin zu microRNA Arrays und *in silico* Signalweganalysen einzuarbeiten. Ich danke Frau Prof. Dr. Susanne Krauss-Etschmann für das mir entgegengebrachte Vertrauen und für die Möglichkeit, meine Ideen einzubringen und unter ihrer Betreuung umzusetzen. Danke für die Gelegenheit mit Kollegen aus anderen Arbeitsgruppen zusammenzuarbeiten und meine Ergebnisse auf Kongressen mit hochrangigen internationalen Wissenschaftlern zu diskutieren. Ich habe die immer positive und konstruktive Zusammenarbeit sehr geschätzt und bedanke mich für die langjährige Begleitung bis hin zur Unterstützung bei meinem Berufsweg.

Einen großen Beitrag zu meiner Doktorarbeit leistete Herr Dr. Stefan Dehmel. Vielen Dank für das große Engagement für das Projekt, insbesondere in der Arbeit mit microRNA Arrays und Ingenuity®, und für die Bereitschaft das Wissen und die Erfahrungen an mich weiterzugeben. Ich bin sehr dankbar für die umfassende und langjährige Unterstützung bis hin zur Korrektur meiner Doktorarbeit.

Die praktische Ausführung der zeitintensiven Experimente war nur durch die tatkräftige Unterstützung der Technischen Assistentin Rabea Imker möglich. Danke für die Flexibilität, die Ausdauer und auch die emotionale Unterstützung. Natürlich auch ein besonderer Dank an die weiteren Mitarbeiter der Arbeitsgruppe: Nikola Schulz für die Unterstützung bei der RNA Arbeit, Manish Aneja für die Einführung in die Mauspräparation und allen anderen für die fachliche und persönliche Unterstützung: Inge Kepert, Theresa Käuferle, Sabine Bartel, Petra Nathan, Yingyan Yu, Eva Brudy, Birte Konrad, Cornelia Dalibor und Gabriele Heilig.

Weiterhin bedanke ich mich bei Herrn Prof. Dr. Oliver Eickelberg für die Möglichkeit, die Arbeit am Comprehensive Pneumology Center durchzuführen und für die umfassende wissenschaftiche Ausbildung, die ich durch Seminare, Journal Clubs und die fachliche Hilfestellung jedes einzelnen Mitarbeiters erhalten habe. Vielen Dank an Frau Dr. Dr. Melanie Königshoff und ihrer Arbeitsgruppe, insbesondere an Herrn Dr. Jens Callegari, für die Einarbeitung in die Präparation der Lungeneinzelzellsuspension, das „Panning“ und die Unterstützung und Weitergabe ihrer Erfahrungen bei den weiteren Experimenten mit ATII Zellen. Ebenso bedanke ich mich bei Frau Dr. Marion Frankenberger für die Einführung in die Durchflusszytometrie und Fluorescence

Activated Cell Sorting sowie bei Herrn Dr. Gerald Burgstaller für die Unterstützung bei der Mikroskopie.

Herzlichen Dank an Herrn Prof. Dr. Dr. Heesemann für die finanzielle und ideelle Unterstützung der Arbeit im Rahmen des Förderprogramms für Forschung und Lehre (FöFoLe) der Medizinischen Fakultät der Ludwig-Maximilians-Universität München.

Weiterhin bedanke ich mich bei denjenigen, die meine Arbeit korrigiert haben.

Besonders danken möchte ich meiner Familie, meinem Partner und meinen Freunden. Ich schätze sehr die umfassende Unterstützung und den großen Rückhalt bei meinem beruflichen und privaten Weg.